The Pennsylvania State University

The Graduate School

College of Engineering

USING OCCUPANT FEEDBACK IN MODEL PREDICTIVE CONTROL FOR INDOOR THERMAL COMFORT AND ENERGY OPTIMIZATION

A Dissertation in

Mechanical Engineering

by

Xiao Chen

Submitted in Partial Fulfillment
of the Requirements
for the Degree of

Doctor of Philosophy

December 2015

The dissertation of Xiao Chen was reviewed and approved* by the following:

Qian Wang
Professor of Mechanical Engineering
Dissertation Advisor
Chair of Committee

Alok Sinha
Professor of Mechanical Engineering

Bo Cheng
Assistant Professor of Mechanical Engineering

Stephen Treado
Associate Professor of Architectural Engineering

Jelena Srebric
Professor of Mechanical Engineering

Karen A. Thole
Professor of Mechanical Engineering
Department Head of Mechanical and Nuclear Engineering

*Signatures are on file in the Graduate School

ABSTRACT

Buildings are our society's biggest energy users. Reducing building energy consumption and creating a better indoor thermal environment have becoming a more and more important topic among policy makers, building scientists/engineers, and the masses. To achieve this target, great efforts have been made in several aspects including but not limited to using better thermal insulation materials, integrating renewable power sources, developing intelligent buildings, and creating better and more efficient building climate control systems.

With the ever increasing computation power, advancements in building modeling and simulation, and accurate weather forecast, model predictive control (MPC) reveals its power as one of the best control methods in building climate control to save energy and maintain high level of indoor comfort. Although many researchers have investigated extensively on how to use building's active or passive thermal storage along with accurate weather forecast and occupants' schedule prediction to reduce energy consumption or shift loads, not much research has been done on how a better thermal comfort model used in MPC would help reducing energy usage and improve comfort level. Furthermore, unlike lighting control in which occupants have plenty of opportunities to adjust lights and blinds so that visual comfort can be improved, centralized and automated building thermal control systems take away users' ability to intervene the control system directly.

In this dissertation, we study occupant augmented MPC control design in which feedback information from occupants is used to adaptively update the prediction given by a data-driven dynamic thermal sensation model. It is demonstrated both in simulation and chamber experiment that including users directly in the feedback loop of MPC control design provides opportunity to significantly save energy and still maintain thermal comfort.

We propose a data-driven state-space dynamic thermal sensation (DTS) model based on data collected in a chamber experiment. The developed model takes air temperature as input, and the occupant actual mean thermal sensation vote as an output. To account for cases in which indoor environmental or occupant associated conditions deviate from the nominal condition conducted in the chamber experiment, a time-varying offset parameter in the model is adaptively estimated by an extended Kalman filter using feedback information from occupants.

We develop two different MPC controls based on the proposed DTS model: a certainty equivalence MPC and a chance constrained MPC. By using this thermal comfort model in the MPC design, users are included directly in the feedback loop. We compare the DTS model based MPC with predicted mean vote (PMV) model based MPC. Simulation results demonstrate that an MPC based on occupant feedback can be expected to produce better energy and thermal comfort outcomes than an MPC based on PMV model. The proposed chance-constrained MPC is designed to allow specifying the probability of violation of thermal comfort constraint, so that a balance between energy saving and thermal comfort can be achieved.

The DTS model based MPC is evaluated in chamber experiment. A hierarchical control strategy is used. On the high level, MPC calculates optimal supply air temperature of the chamber's HVAC system. On the low level, the actual supply air temperature of the HVAC system is controlled by the chiller and heater using PI control to achieve the optimal level set by the high level. Results from experiments show that the DTS-based MPC with occupant feedback provides the opportunity to reduce energy consumption significantly while maintain occupant thermal comfort.

TABLE OF CONTENTS

LIST OF FIGURES

LIST OF TABLES

ACKNOWLEDGEMENTS

This dissertation is dedicated to my family and many people who helped me, especially

- To my parents, Jian Chen and Ping Huang, for their unconditional love and support,
- To my wife, Linye Wei, for the encouragement, happy, and joy brought to my life,
- To my advisor, Dr. Qian Wang, for her guidance and patience throughout my study,
- To Dr. Jelena Srebric and her research group for the valuable advice and help,
- To Dr. Alok Sinha, Dr. Bo Cheng, and Dr. Stephen Treado for their insightful commentary.

Chapter 1

Introduction

1.1 Motivation

Building sector consumes about 40% of primary energy consumption worldwide. According to US department of energy, space heating, water heating, space cooling are the top three end uses and they account for 37%, 12% and 10% of building energy consumption respectively. Improving the heating, ventilation, and air conditioning (HVAC) system is one of the most promising ways to reduce energy usage. Creating a better indoor thermal environment not only helps to reduce emission rate and thus increase the sustainability, but also keeps people more productive at work, and keeps them away from building health related problems.

Since building is such a complex system, it is difficult to improve the performance and it requires a wide range of expertise from different areas. Efforts have been made in the following several aspects. When building designers construct new buildings or refurbish old ones, they increase building envelope insulation by using better materials and double windows [1]-[2]. Window placement and building orientation are optimized [3] so they are more 'climate appropriate' for the building. Renewable energy including solar, wind, geothermal has been applied to building systems [4]. The waste of energy due to occupants' behavior should not be ignored either. For example, making people aware of potential savings by simply turning off air conditioners and other equipment that are not needed is important [5]-[6]. Most importantly, engineers are trying to come up with different solutions to design or improve HVAC systems so that they use energy more efficiently. Developing models, creating simulation tools, improving

existing control algorithms and developing new algorithms are among the most active areas of building research.

Another challenge to reduce building energy usage arises from the fact that thermal comfort and energy consumption are usually on the opposite ends of the spectrum. Control engineers are trying to find solutions that bring down energy consumption without sacrificing thermal comfort. Various advanced control techniques including optimal control [7]-[8], fuzzy logic control [9]-[10], controls with computational intelligence such as genetic algorithms and artificial neural networks [11]-[12], and agent-based intelligent control [13]-[14] have been applied to building systems. A lot of these advanced techniques can be combined to create new solutions [15]-[16]. Many of these control methods have shown vast performance improvement over conventional control. Among all these advanced control methods, model predictive control (MPC) is one of the most promising techniques.

1.2 Background and Literature Review

1.2.1 MPC in Building Thermal Control

Compared to traditional building control algorithms including PID control, on-off control and other advanced control techniques, one of the biggest advantages of model predictive control is that it has the ability to take control action at the current time according to the prediction of the system states in the future while satisfies the constraints which can be formulated explicitly. A brief description of MPC is given as follows. At current time step, the dynamic model predicts the states and outputs of the system in the next N future time steps called prediction horizon. So a sequence of control inputs along the horizon can be calculated that minimize a cost function and keep all the constraints satisfied. However, at each time step only the first control action in the

sequence is implemented. At the next time step the previous procedure is repeated and for this reason model predictive control is also called receding horizon control. The details of MPC control can be found in [17].

A. Using passive or active thermal storage

There exist opportunities for both energy saving and thermal comfort improvement by applying MPC to building temperature regulation. Buildings have large thermal mass that can store energy and thus the response time is large. Lots of research on building MPC control takes advantage of either passive or active thermal storage [18]-[22]. Passive thermal storage refers to buildings with heavy mass of concrete walls, floors, ceilings and furniture. Buildings with active thermal storage are those equipped with reservoir (water tank or ice storage) or battery that can be controlled to charge or discharge energy.

Early in 1990 Braun investigated the cooling energy cost savings by using thermal mass to shift cooling load from daytime to nighttime [7]-[8]. The saving could be achieved in the following several aspects: Firstly the buildings can be preconditioned by the "free" cooling at night at lower ambient temperatures; Secondly the electricity rate is cheaper at off-peak time or night, so shifting the cooling load to night reduces electricity bill; And in the end, efficiency of a mechanical system varies as the actual load of plant changes, so by manipulating the load cooling system could work more efficiently.

Kummert et al. [18], [20] explored applying MPC control of heating system to a passive solar building. He emphasized the importance of anticipation of solar gain and internal gain to save energy and avoid thermal comfort violation. Simulation results were shown for a typical sunny mid-season day, in which heating is needed in the morning but over heating (or cooling) might occur in the afternoon due to solar gain and internal gain. In contrast to MPC control, which was able to foresee the possible outcome due to disturbance from outdoor and indoor and

thus take the appropriate control action to maintain the comfort, traditional thermostatic control failed to keep the zone temperature within the comfort range for a large fraction of the entire simulation time [18]. One obvious difference between cooling and heating applications is that free cooling is available at night but there is no free heating at night. However, night setback can be utilized to save energy for many buildings. Usually the temperature could be set at a lower than comfort level at night when the building is not occupied. To find the optimal time to start the heating such that by the time people arrive in the morning they would not complain temperature to be too low, MPC controller needs to access the ambient temperature forecast [20].

Henze et al. [21] took advantage of both active and passive building thermal storage in a cooling application. Time-of-day electricity rate is used to reduce utility cost. In their optimization problem, the optimal cooling load profile related to passive storage is solved first and then the optimal control inputs for the active storage are calculated according to the cooling load. Ma et al. [22] also investigated MPC control using both passive and active thermal storage.

Gwerder et al. [23] pointed out that a wider comfort temperature band could lead to a larger energy and cost saving since the range in which thermal capacitance can be operated is larger. For example, the thermal capacitance in a typical concrete ceiling is more than 1kWh/m2 given a 5K comfort temperature width.

Renewable energy such as solar, wind, geothermal energy has been used more and more in buildings since they have a much less impact on environment. Many countries make policies to subsidize clean energy. However, most of the renewable energy could not serve as a stable energy resource alone and usually there is an energy storage system associated with them. Along with energy storage, renewable energy supplements the electric power. MPC can utilize the power storage to shift the peak-load and save electric bills [24]-[25]. Ma et al. [24] investigated using MPC in a MicroGrid with distributed energy resources to achieve higher level of penetration of renewable energy.

B. MPC control for real buildings

Privara et al. [26] demonstrated the superiority of MPC control over a weather compensated control by testing on a real building. Even though the weather condition was used in the weather compensated control, the knowledge of building dynamics was not taken into consideration. It was shown in their experiment that a saving of 17-24% was achieved depending on different building blocks. Aswani et al. [27] examined the MPC control for a heat pump cooling system. In their research, they estimated the internal gain level and used MPC control scheme to compensate for occupancy variation. Compared to traditional on-off control, MPC was able to achieve 30-70% reduction in energy consumption based on test results collected from a computer lab. Ferreira et al. [29] conducted their experiment in a classroom equipped with computers, and showed that at least 30% saving can be achieved both in winter and summer. Another very important experiment of MPC control for real building is from Ma et al. [22]. For a cooling plant with active thermal storage tank, it was found that performance improvement can be achieved by load shifting and optimization of HVAC components. They compared MPC control and a base line control logic, which was set according to building manager's experience, with application to the active thermal storage and found that the coefficient of performance was improved by 19% equivalent to $1280 weekly saving in terms of energy bill. In summary, MPC has demonstrated great energy saving potential while still be able to maintain a relatively high level of thermal comfort.

C. Flexibility of MPC problem formulation

Model predictive control is flexible in terms of both problem formulation and types of mechanical cooling/heating systems it can be applied to. The cost function is often defined in terms of energy consumption or utility cost. For example, if time of day rate is used and peak energy reduction is desired then the cost function in MPC can be formulated in such a way that

the building thermal mass can be utilized to reduce the electricity bill [7], [21]-[22]. The comfort level is either set as a constraint since MPC treats constraints explicitly, or it is incorporated in the cost function. The dynamics constraints usually include building dynamics. The inequality constraints include upper or lower bound on thermal comfort and limitations of physical system such as maximum output of an actuator. When the comfort level and energy consumption are both considered in the cost function, a tunable weighting factor is often used to balance the tradeoff between energy and comfort. In [20] a Pareto frontier was plotted to show performance of MPC as value of weighting factor varied. Freire et al. proposed five different schemes of MPC formulation in [19]. These formulations were based on two different thermal comfort models: effective temperature defined from a psychrometric chart and Fanger's predictive mean vote model (PMV) [30]. In some of these formulations, only energy consumption was included in the cost function with either effective temperature or PMV formulated in constraint on comfort level. In other formulations, the cost contained terms related to both energy and comfort. Castilla et al. [31] also considered PMV in the cost function. Besides these two papers mentioned above, there are not many papers that included comfort level as part of their cost function. The unique strength of MPC in handling constraints makes it natural to consider comfort in a constraint and most researchers adopted this formulation.

D. Different control architecture

MPC is also flexible in control architecture. In one of these different architectures, the MPC works as a high level controller that determines the optimal set-point of the system such as indoor air temperature [19], [21], [29], [32]. In the lower level simple PID or on-off controls are applied to the fan, coil, damper and other components of a HVAC system so that the set-point received from the high level could be achieved. In other works [22], [31], [33], the low-level components were also considered in the MPC problem formulation and they were orchestrated by

a high level MPC controller. With the former control architecture, savings associated with thermal storage can be achieved with accurate estimation on weather and occupancy level. The latter architecture further explored saving potential by coordinating all components together to achieve a higher level of system efficiency [22]. In [31] these two architectures were compared and it was shown that the latter strategy saved more energy but was required to solve higher dimensional problem, which often could be computation intensive for large and complex buildings. Another difference is that the first architecture can be applied to different system without modification/retrofit of the existing HVAC systems, while the second one requires more embedded sensors, which might lead to a prohibiting cost.

E. Factors that affect MPC performance

Energy consumption and thermal comfort level are two indices used to evaluate the performance of MPC building thermal control. Simulations are usually conducted for a long term performance evaluation. Whereas real building tests are usually done for a short time. In real life, the performance of a building is largely dependent on the experience of building managers. Comparison of controller performance in real building is difficult since there are too many uncontrolled factors. For example, it is almost impossible to find the same weather conditions for different days. The occupancy level is not fixed either. Reported performance improvement over conventional controls in both simulations and real building tests could vary drastically. As it was discussed in [7], [21], there are several important factors that could affect the performance of a MPC controller such as weather conditions, occupant schedule (internal gain), utility structure, building characteristics and mechanical systems. Weather conditions including ambient temperature, solar radiation and humidity are among these many limiting factors. Occupant schedules could be different for different types of buildings. Buildings such as large office buildings or shopping centers have strict schedules. Other buildings such as hospitals or

apartments have occupants 24 hours so the opportunity to use "free cooling" is almost impossible. Utility structure, which represents demand charge, time of day rate, and the ratio of peak and off peak hours, also greatly affects the load shifting plan. In addition, building characteristics, which refer to the properties related to thermal storage such as thermal mass and thermal coupling, are vital for the MPC performance as well.

1.2.2 Thermal Comfort Models

The most influential thermal comfort model was developed by Fanger [30], which was later adopted by ASHRAE 55 and ISO 7730. Based on the energy balance of a human body, Fanger developed the predicted mean vote (PMV) model. This model describes the mean thermal sensation for a large group of occupants as a function of thermal environmental variables (such as air temperature, velocity, humidity and mean radiant temperature), activities (measured by metabolic rate), and clothing insulation. Then based on PMV, the predicted percentage of people dissatisfied (PPD) can be determined. Since 1970 when Fanger's model was introduced, HVAC engineers, building designers and indoor air researchers have applied it in many applications. Practice has shown values of the model in the area of air conditioned buildings where thermal comfort and neutral, slightly cool or warm thermal conditions are maintained well.

However, whether the thermal comfort and the preferred temperature in naturally ventilated buildings could be predicted by the PMV model is still under debate. Many field studies have shown the discrepancy between survey votes and PMV calculations [34]-[38]. In addition, researchers found a different relationship between PMV and PPD than the one given by Fanger [39]. As a result, another thermal comfort model, the so-called adaptive thermal comfort model, was proposed by de Dear and Brager [40] to relate the indoor neutral temperature to the monthly average outdoor temperature. It was pointed out by de Dear and his coworkers that

several factors such as thermal adaptations through behavioral adjustment, acclimatization and especially expectation are important to affect thermal comfort in naturally ventilated buildings [38], [40]. The adaptive thermal comfort model was incorporated into the ASHRAE Standard 55 in 2004 as an optional method. Fanger also extended his PMV model to naturally ventilated buildings in a warm climate by adding an expectancy factor [41].

Both these aforementioned models are generally used in a steady state condition. However, people in real life often encounter non-uniform or transient conditions. In recent years, there has been increasing interest in studying dynamic thermal sensation models in transient conditions [42]-[44]. By regression analysis of data obtained from experiments in the literature and from simulation of a physiological model of human thermoregulation, Fiala et al. developed a model for dynamic thermal sensation as a function of mean skin temperature and its rate of change [42]. It was suggested by Fiala et al. in that sudden decrease in air temperature could induce an almost immediate cold sensation overshoot. However, they indicated that it could take more time to develop the warm sensation in response to an increase in air temperature. The response of human body to transient temperature changes via warm or cold cutaneous thermo-receptors was examined by De Dear et al. [43], where a model of thermo-receptor impulse frequency was proposed as a function of skin temperature and its derivative. Zhang et al. studied local thermal sensation of individual body parts under non-uniform and transient environments, as well as their impact on the whole body sensation and comfort [44].

F. Thermal Comfort Models Used in Existing MPC

There are mainly 3 different thermal comfort models used in existing MPC control for buildings. In conventional building control, thermal comfort is provided by enforcing the indoor temperature within a temperature band specified by the heating set-point and cooling set-point. Most researchers adopt this simplest model [22], [27], [28], [32], [33], [45]. The second one is

called effective temperature model, in which thermal comfort is enforced by restricting the temperature and humidity in a comfort zone within a psychrometric chart [19]. The third one is the PMV model. Even though PMV is a more accurate index and using it in the control design could potentially save energy and improve comfort [11], it was only adopted by a small number of researchers [19], [29], [31] mainly due to the additional computational burden, added cost of sensing, and possible discrepancy between model prediction and actual sensation votes. In this study, we develop a new control oriented model. Unlike other models that try to approximate PMV index, our model improves its accuracy of prediction by receiving real time feedback from occupants.

1.2.3 Building Models in MPC

One of the major differences between MPC control and other advanced building control techniques such as fuzzy logic is the use of a building model. In the past MPC building control did not draw much attention among control community due to the following reasons: 1) each building has a unique model and it is difficult and costly to obtain a good building model; 2) the cost of energy was not a big concern; and 3) the computation power was limited. However, the urge to save energy has motivated researchers to look into MPC which has been widely used by chemical and mechanical engineers in the past several decades. The recent development in the building modeling and its simulation tools, the improved accuracy in weather forecast, and the ever increasing computation power together have made MPC applicable for building applications [45].

Existing building models can be divided into three categories: physics-based models, black box models, and grey box models (see [49] for detail). Physics-based models are commonly derived based on the energy conservation. In terms of the computation complexity of the models,

they can be further divided into Computer Fluid Dynamic model (CFD), zonal model, and nodal model (thermal network model) [50]-[51]. Due to its simplicity, the nodal building model is the most widely used one in MPC control. Liu et al. [52] investigated the impact of modeling accuracy of internal dominated buildings on MPC control. They found that deviation of building geometry and zoning from the reference building could only affect optimal control inputs marginally, while building materials and other construction characteristics need to be modeled accurately in order to achieve the energy saving potential. A nodal model is considered to be well balanced between the model complexity and capability of capturing building dynamics without losing the energy saving potential. Black box models are those identified by statistical method including regression models, neural network models and so on. For example in [19], an auto-regression with exogenous input (ARX) model was used to describe a building coupled to a HVAC system and in [29], a neural network was utilized to predict indoor room temperature and humidity. Each type of model has its advantages and disadvantages. Physical models are usually hard to derive. Statistical model does not give any physical insight of the system and a large number of data points are needed to generate a good model. A grey model (or hybrid model) is able to incorporate some good features from the physical and statistical models and overcome some of the limitations. An example of grey models can be found in [22], [28] in which the author used measured data to estimate values of parameters of the physical models.

1.2.4 Uncertainty in MPC Building Control

The uncertainties of a building control system come from both outside and inside the building. The outside weather condition is essentially stochastic. The predicted weather conditions including temperature, humidity, and solar radiation are generally obtained by downloading data from national weather service, through dedicated meteorological station for

some buildings or using weather forecasting models. For example in [29], nonlinear auto-regressive models were used for weather prediction, where internal disturbance or internal load was estimated according to occupant schedule or data received from sensors. A simple occupant level estimation based on temperate measurement was presented in [27]. In [53], authors used an agent-based model to simulate occupant behavior. In [54], researchers developed an intelligent counting algorithm using video cameras to estimate occupancy level. A network of sensors including video, sound, CO2, and passive infrared sensors was used and it was shown that the estimation accuracy was greatly improved [55].

To account for the stochastic disturbance in weather conditions or occupancy level, a robust MPC and a stochastic MPC control were developed [32], [33], [45], [56], [57]. By assuming the weather disturbance to be normally distributed, Oldewurtel et al. formulated a chance constrained problem [32], [45], [56]. A chance constrained stochastic control is difficult to solve since it is generally non-convex. When disturbance in weather or occupancy level has a Gaussian distribution, the chance constraint can be transformed into a deterministic second order cone constraint [58]. A closed loop robust MPC with disturbance feedback was then formulated and solved by sequential linear programming. The authors examined the energy usage versus probability of constraint violation. It was demonstrated that energy consumption could be reduced at the cost of thermal comfort violation for a certain amount of time. Maasoumy et al. [57] compared the performance among regular MPC (which did not account for disturbance), open loop robust MPC (OL-Robust MPC) and closed loop robust MPC (CL-Robust MPC). The disturbances were assumed to be bounded due to the imperfect predictions of internal and external heat gains. It was found in simulations that CL-Robust MPC out performed OL-Robust MPC by using less energy. Ma et al. [33] presented a nonlinear stochastic MPC for the application of building temperature regulation. A tailored fast sequential quadratic programming was used to solve the nonlinear programming problem.

1.3 Contributions and Outline

In this dissertation we explored the benefit of using a novel thermal sensation model in MPC problem formulation. Using this unique control oriented thermal sensation model, our MPC controller provides a mechanism/interface for occupants to interact with the thermal control system. With the user feedback information, the designed controller can adapt to occupants' perceptions about their environment. It has been shown both in simulation and chamber experiment that MPC design based on this unique thermal sensation model could potentially save more energy while maintain a satisfactory level of comfort.

The main contributions of this dissertation lie in the following three aspects:

- We developed a data-driven state-space Wiener model to characterize the dynamic relation between ambient temperature changes and the resulting occupant thermal sensation. In the proposed state-space model, the mean thermal sensation state variable is governed by a linear dynamic equation driven by changes of ambient temperature and process noise. The output variable, corresponding to occupant actual mean vote, is modeled to be a static nonlinearity of the thermal sensation state corrupted by sensor noise. A chamber experiment was conducted and the collected thermal data and occupants' thermal sensation votes were used to estimate model coefficients. Then the performance of the proposed Wiener model was evaluated and compared to existing thermal sensation models. In addition, an Extended Kalman Filter (EKF) was applied to use the real-time feedback from occupants to estimate a Wiener model with a time-varying offset parameter, which can be used to adapt the model prediction to environmental and/or occupant variability.
- We developed two MPC algorithms, a certainty-equivalence MPC and a chance-constrained MPC, for indoor thermal control to minimize energy consumption while

maintaining occupant thermal comfort. It is assumed that occupant perceptions of thermal sensation can be continually collected and fed back to calibrate the proposed Wiener model and to update the MPC. The performance of the proposed MPCs based on Actual Mean Vote (AMV) was compared to an MPC using PMV as the thermal comfort index. Simulation results demonstrated that when the PMV gives an accurate prediction of occupants' AMV, the proposed MPCs achieve a comparable level of energy consumption and thermal comfort, while it reduces the demand on continually sensing environmental and occupant parameters used by the PMV model. Simulation results also showed that when there is a discrepancy between the PMV and AMV, the proposed MPC controllers based on AMV is expected to outperform the PMV based MPC by providing a better outcome in indoor thermal comfort and energy consumption. In addition, we proposed a chance-constrained MPC which offers an opportunity to adjust the probability of satisfying the thermal comfort constraint to achieve a balance between energy consumption and thermal comfort.

- We evaluated the certainty-equivalence MPC in chamber experiment. The original MPC formulation was modified for the chamber experiment. A hierarchical control structure was adopted in the experiment. One the high level, the MPC controller calculates optimal supply air temperature of chamber HVAC system with the real time feedback information from participants. On the low level, the actual supply air temperature is controlled by chiller/heater using PI control. The chamber experiment validated that inclusion of occupants in the MPC control is a promising research direction in building thermal control.

This dissertation is organized as follows.

In Chapter, 2 a new data-driven state-space dynamic thermal sensation (DTS) model is developed. In section 2.1, the novel model with Wiener structure is presented. We discuss the

assumptions, inputs, output, states, and parameters of this model. A chamber experiment designed for the identification of the model is presented in section 2.2. In section 2.3, the modeling results are presented. The identified model is compared with existing thermal sensation models including Fanger's PMV model and Fiala's model. We then consider a time-varying offset parameter in the identified model. This offset parameter is estimated in real time via an extended Kalman filter using occupant feedback. Simulation results are presented to show how model prediction can be improved using feedback from occupants.

In Chapter 3, two MPC algorithms based on the DTS model proposed in Chapter 2, a certainty-equivalence MPC (CEMPC-DTS) and a chance-constrained MPC (CCMPC-DTS) are developed. The performances of the MPCs are demonstrated in simulation results. In section 3.1, the thermal transport model of a single zone building is introduced. This model serves as a highly simplified building simulation model. In section 3.2, CEMPC-DTS and CCMPC-DTS are formulated. Another MPC, which uses PMV as the thermal comfort index and is denoted as MPC-PMV, is used to compare to the two aforementioned MPCs. A rule-based PI control denoted as RuleBased-PI is also presented as a baseline controller in this section. In section 3.3, simulation results are presented. Performance metrics are defined and their values for different controllers under different weather conditions and simulation scenarios are reported.

In Chapter 4, result of MPCs applied to chamber experiment is presented. In section 4.1, the chamber model is identified using a linear regression model. The chamber model is then validated by comparing its prediction with collected data. In section 4.2, the certainty equivalence MPC proposed in Chapter 3 is reformulated by replacing the building model with chamber model and by taking the constraints of the actual HVAC system of the chamber into the problem formulation. In section 4.3, we describe the control experiment design. In section 4.4, experiment results are presented and analyzed.

In chapter 5, conclusions about this research are provided and ideals for future study are given.

Chapter 2

A Data-driven State-space Dynamic Thermal Sensation Model

One of the problems with current automated building climate control is that users do not have the opportunity to interact with the control system. It was found out that users' awareness of opportunities to control their environment could affect their perceptions of comfort [59]-[60]. In fact, sometimes occupants could be more forgiving in buildings that provide control opportunities to users [61]. In field surveys, occupants have expressed their wishes to intervene the automated control system [62]. Since occupants have more controls over visual comfort by adjusting electric lighting, window, blind, and awning, light intervention has been investigated by many researchers [63]-[65]. Giving occupants full control of opening/closing windows or adjusting blinds not only affects their visual comfort but also thermal comfort [65]-[66]. Nevertheless, there is not much research on occupant intervention in thermal control. This is because automatic building controllers are designed to use energy efficiently in the first place. If users were granted to have the control over the temperature set-point or ventilation rate, the whole building's performance might deteriorate and thus result in a higher level of energy consumption. So instead of allowing people to directly tune the valve on heating/cooling or adjust the fan speed, it is better to let occupants express their "wishes" to the system. When the building control system sees the need to adjust the control parameters to better accommodate occupants, it can do so in a more energy efficient way with a MPC working as a high level controller that orchestrates the low level subsystems all together.

In this chapter, we developed a data-driven state-space thermal sensation model that can use the feedback from occupants to adaptively update its prediction. The model was identified

using the data collected from a chamber experiment. Compared with other model such as PMV model, the proposed model has such a form that is more suitable for the design of model based control. Using this model in the control design, occupants are included directly into the feedback control loop. Simulation results of the model using feedback from occupants are presented in this chapter.

2.1 Data-driven State-space Model

2.1.1 Assumptions

This study considered the air temperature change as the only control input to the proposed thermal sensation model, and also used it as the sole control variable in building thermal control. The only heat source in the chamber came from the heating or cooling supply and thus that the mean radiant temperature (MRT) followed the air temperature closely. The available humidifier was not used in the chamber experiment to simulate the indoor environmental conditions typical for buildings without humidification. The study did not explicitly evaluate how the change of humidity, air velocity, and occupant activity and clothing levels affect occupant thermal sensation as it would explode the number of experimental conditions. But instead, the study assumed that the aggregate effect of aforementioned significant factors on occupant thermal sensation was captured by an offset parameter in the proposed state-space Wiener model with a logistic output function. Other thermal or non-thermal factors were considered as process and sensor noise in the proposed state-space model.

Note that even though the MRT changed during the conducted step-up and step-down experiments by 9K and 7K respectively (see Figure 2.1), these changes were gradual and applicable to all chamber surfaces. Therefore, it should be noted that the model is not applicable

to chambers and indoor spaces with highly asymmetric radiant surfaces, recognized to influence the thermal sensation of human subjects. Nevertheless, the model and data-collection methodology can be extended to indoor spaces with highly asymmetric radiant surfaces that typically use hydronic systems, such as chilled ceilings and radiant heating elements. This extension would require additional experiments for data collection to calibrate the proposed state-space model for thermal sensation.

2.1.2 Model Structure

The dynamic thermal sensation driven by ambient temperature changes is essentially nonlinear. Thermal sensation could approximately be considered as linear around the neutral region. However, it gets saturated when it reaches hot or cold conditions. Consequently, this study considered a dynamic state-space model of a Hammerstein-Wiener structure, specifically a Wiener model for thermal sensation. The advantage of adopting a Wiener model is that the thermal sensation dynamic responses can be decomposed into a linear state equation and a nonlinear output equation. Logistic functions, which have an "S' shape, are particularly suitable for modeling the nonlinear output function for thermal sensation.

Consider a discrete time dynamic model defined as follows,

$$x(k+1) = \sum_{i=1}^{n} f_i \times x(k+1-i) + \sum_{j=1}^{m} g_j \times u(k+1-j-p) + e(k) \tag{2.1}$$

where *k* denotes the discrete-valued time index for which the sampling time should be chosen long enough to allow detection of physiological response, *x(k)* denotes the mean thermal sensation state at time index *k*, *u(k)* denotes the ambient temperature, *p* denotes input delay, and *e(k)* denotes the process noise entering the state equation. It should be noted that the thermal sensation state defined in the empirical model (2.1) should correlate, but not necessarily coincide

with the physiological thermal state of a human body. The parameter *n* and *m* determine the order of the auto-regression and dynamic regression, respectively, and the parameters f_i and g_j denote the corresponding auto-regression and dynamic linear regression coefficients. For any nonzero order *n* and *m*, the thermal sensation state *x(k)* is assumed to depend on the previous history.

The measurement of the mean thermal sensation by occupants, the subject actual mean vote y(k), is then modeled as

$$y(k) = \frac{a}{\exp\left[-c - b \times (x(k) - r)\right] + 1} + d + v(k) \tag{2.2}$$

by considering a logistic output function, where *v(k)* denotes the sensor/measurement noise. The parameters *r*, *a*, *b*, *c*, and *d* represent the regressor mean, output coefficient, dilation, translation, and output offset of a logistic function, respectively; altogether, they determine the shape of the nonlinear output curve.

In the remainder of the dissertation, the model including state equation (2.1) and output equation (2.2) is called the *Wiener-logistic* Model. To identify the model in (2.1) and (2.2), all parameters were first assumed to be constant and estimated via a nonlinear least-squares method (Gauss-Newton algorithm) using chamber experimental data. When the indoor environmental or occupant associated conditions deviate from the nominal condition conducted in the chamber experiment, this study considered a time-varying offset parameter in the Wiener-logistic model and applied an EKF [67] to estimate the thermal sensation state and the unknown time-varying offset parameter simultaneously using occupant feedback. The estimation was achieved by treating the time-varying offset parameter as an additional state variable.

2.2 Chamber Experiment

2.2.1 Experiment Facility

The experiment was conducted in the environmental chamber located in Engineering Unit A building at Penn State University Park campus. This state-of-the-art simulation and testing facility is divided into two identical rooms and each room has its own HVAC unit which is able to simulate different indoor conditions. The HVAC system uses electric resistance heater for heating and chilled glycol/water mixture for cooling. Sophisticated measuring and data acquisition system (DAS) along with a dedicated programmable logic controller (PLC) made it an ideal facility to test different thermal control algorithms. The schematic drawing of the chamber with its basic dimensions is shown in Figure 2.1 below.

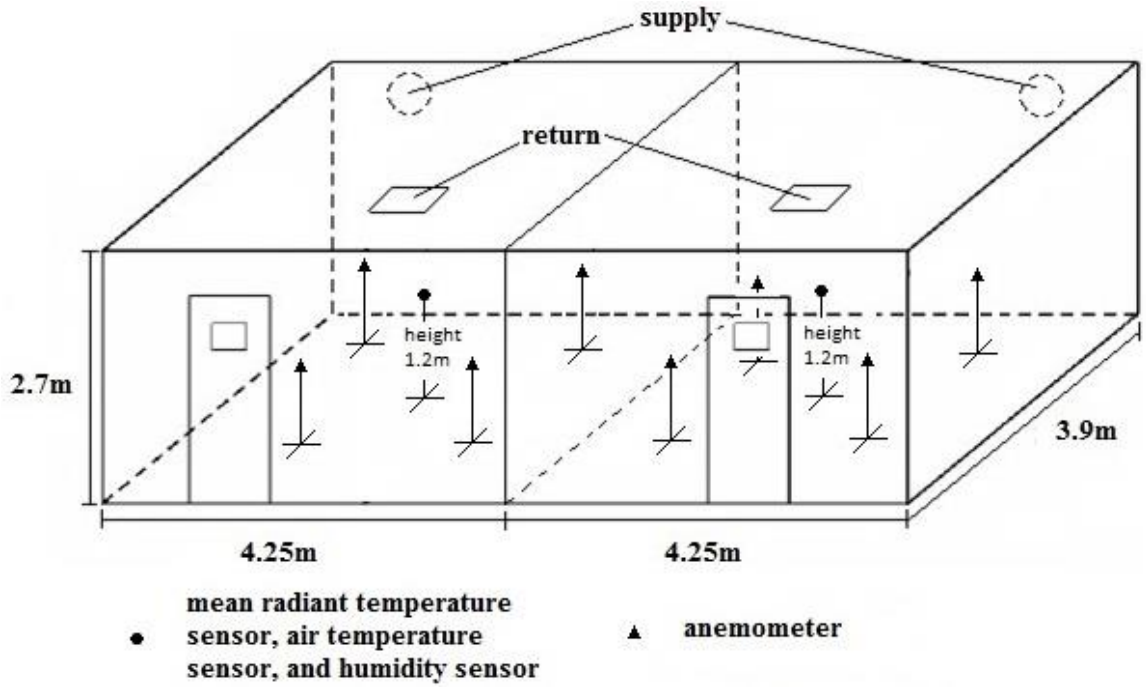

Figure 2.1. Chamber layout. The chamber is divided into two identical rooms and each room has its own HVAC unit. A HOBO U12 is mounted in the middle of each room to measure air temperature and relative humidity, and a BlackGlobe sensor is mounted at the same position for MRT. Four anemometers are installed in each room to monitor air flow velocities. Both rooms are furnished with table and chairs for occupants to use.

A HOBO U12 data logger was positioned in the middle of each room to measure air temperature and relative humidity. The temperature measurement error for the data logger is less than ±0.35 ℃ from 0 ℃ to 50 ℃, and the measurement error for the relative humidity is less than ±2.5% from10% to 90%. A BlackGlobe Temperature Sensor for Heat Stress (BlackGlobe) was mounted at the same position as the HOBO U12 data logger. The BlackGlobe thermometer measures the globe temperature and determines the MRT using the globe temperature and local velocity. The globe temperature sensor has a time delay of approximately 20 to 30 min, resulting in slightly delayed accounting of changes in MRT, mostly relevant to the data collection after the step changes in the environmental temperatures. The thermistor interchangeability error of the BlackGlobe is less than ±0.2 ℃ from 0 ℃ to 70 ℃. Several anemometers were also scattered around to monitor airflow velocities at different locations in each room. In this experiment, all environmental parameters were controlled to be the same for both rooms of the climate chamber, and both rooms were used at the same time so that there was enough space to accommodate all the participants. Therefore, the chamber can be viewed as a single virtual room and subject votes from the two rooms were not differentiated.

2.2.2 Experiment Design

The experiment was conducted in February, with outdoor temperature around 5 ℃ to 7 ℃, and outdoor humidity level around 50%. There were two sessions in the experiment and each session lasted 2.5 h. The time history of the set-point temperature of the climate chamber used in the experiment is shown in Figure 2-2. The chamber air temperature was controlled by the chamber HVAC system to follow the set point, and consequently was the MRT. In the first session, the room temperature set-point was initially set at 21 ℃ for 50 min, then raised to 30 ℃

for another 50 min, and reduced back to 21 ℃ again for the rest of the time of the session. Contrary to this "low-high-low" set-point pattern, a "high-low-high" pattern was used for temperature set points in the second session of the experiment, with the low temperature set at 23 ℃. A different low temperature was chosen in the 2nd session instead of the original 21 ℃ in the 1st session since the large internal load made it impossible for the chamber temperature to drop from 30 ℃to 21 ℃ within 50 min, even with the chamber cooling power set to its maximum.

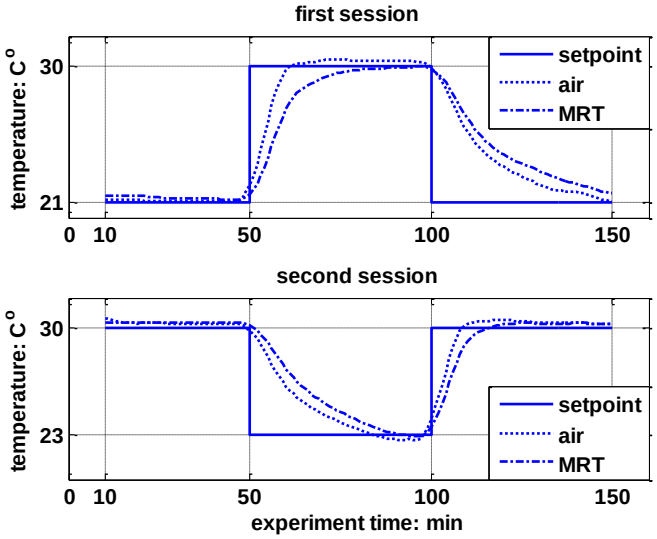

Figure 2.2. Measured and set point air temperatures and mean radiant temperatures (MRT) during the experiment.

The experiment participants were requested not to take any spicy food or caffeinated drinks immediately before the start of the experiment. During the experiment, participants were allowed to work on laptops, read, and write in their sitting positions. Nobody walked in the chamber and nobody left the chamber during the experiment. An iButton sensor was attached to each participant to measure the skin temperature at hand. All participants were asked to write down their thermal sensation votes according to the ASHRAE 7-point thermal sensation scales every 5 min during a 20 min time period immediately after the initial change of air temperature set-point, and then every 10 min for the rest of the session time. Overall, more frequent sampling

(every 5mins) was used to record the immediate sensation of participants after the chamber temperature was changed.

2.2.3 Data Collection

There were a total of 13 participants, including college and graduate students, who completed both sessions of the chamber experiment. The recruitment of participants was not conducted to achieve a specific gender ratio and the recruited participants happened to consist of 12 male and 1 female. This relatively small number of participants is acceptable for this proof-of-concept development, which is a strategy used by other thermal comfort studies [38]. Further refinement and generalization of the proposed model require an extension of the present study to include data collection effort for a larger and more diverse population of occupants. Table 2.1 lists detailed information of each participant. The weight, height, age and gender of each participant were recorded to estimate each individual's basal metabolic rate. Clothing level of each subject was also recorded with detailed description. The activity level of each participant was considered sedentary since each participant was either reading or writing in a sitting position. All environmental parameters were collected and stored in data loggers during the experiment. The measured chamber air and mean radiant temperature, relative humidity, and air velocity are shown in Figure 2.2–2.4, respectively. Since the two rooms have almost identical thermal parameters, average numbers between two rooms are used in Figure 2.2–2.4.

Table 2.1 Participant's information

ID	WEIGHT (KG)	HEIGHT (M)	AGE	GENDER	CLOTHING
1	70.3	1.7	23	M	PANTS, LONG-SLEEVE SHIRT, BOOTS
2	104.3	1.93	23	M	PANTS, LONG-SLEEVE SHIRT, SHOES
3	86.2	1.93	19	M	PANTS, SHORT-SLEEVE SHIRT, SHOES
4	97.5	1.85	22	M	PANTS, SHORT-SLEEVE SHIRT, SWEATSHIRT, SHOES
5	89.36	1.75	34	M	PANTS, LONG-SLEEVE SHIRT, SHOES
6	77.1	1.78	24	M	PANTS, LONG-SLEEVE SHIRT, SHOES
7	72.6	1.80	25	M	ATHLETIC SWEAT PANTS, SHORT-SLEEVE SHIRT, SWEATSHIRT, SHOES
8	71.7	1.85	26	M	PANTS, LONG-SLEEVE SHIRT, SHOES
9	72.1	1.70	27	M	PANTS, LONG-SLEEVE SHIRT, SHOES
10	64.7	1.75	22	M	PANTS, SHORT-SLEEVE AND LONG-SLEEVE SHIRT, SHOES
11	78	1.83	22	M	PANTS, LONG-SLEEVE SHIRT, SHOES
12	59.9	1.75	26	M	ATHLETIC SWEAT PANTS, SWEATSHIRT SHOES
13	46.3	1.55	28	F	PANTS, SHORT-SLEEVE SHIRT, SWEATSHIRT, SHOES

Figure 2.2 shows that the actual chamber temperature was more responsive to the step increase of the set point temperature than the step decrease of the set point temperature due to the capacity of the chamber HVAC system. Furthermore, the MRT followed the air temperature very closely as expected, where the visible delay of MRT is due to the time delay of the BlackGlobe temperature sensor. The humidity on the other hand showed a roughly flipped pattern of air temperature (shown in Figure 2.3) because no additional humidification was supplied.

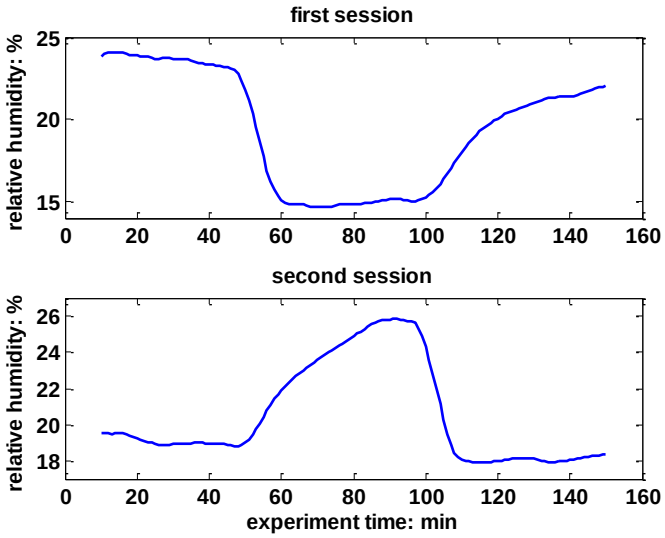

Figure 2.3. Measured relative humidity (RH) during the experiment.

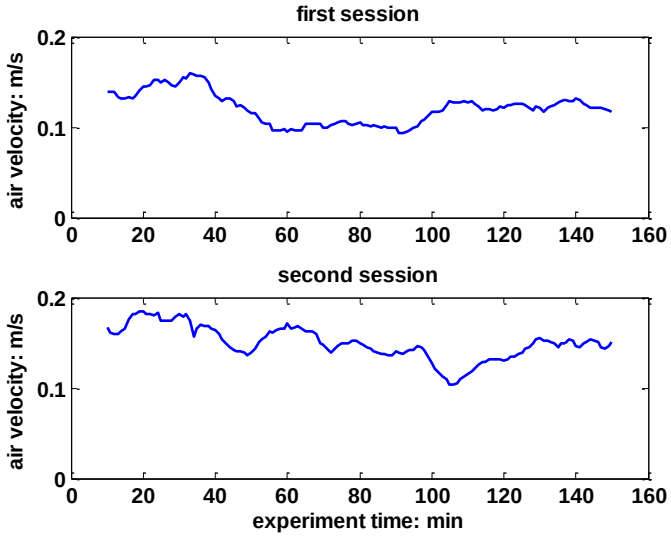

Figure 2.4. Measured air velocities during the experiment.

Figure 2.5 shows the time series of subject actual mean vote for thermal sensation along with standard deviation error bar, where the ASHRAE 7-point scales [68] were used and Figure 2.6 plots the corresponding subject votes on thermal comfort. The thermal comfort results include mean values together with standard deviation on a scale of -1 to 1, where -1, 0, and 1 correspond to very uncomfortable, just (un)comfortable, and very comfortable, respectively. The standard

deviation of subject votes on thermal comfort is relatively large, which indicates the inhomogeneity of the subject group on thermal comfort perception.

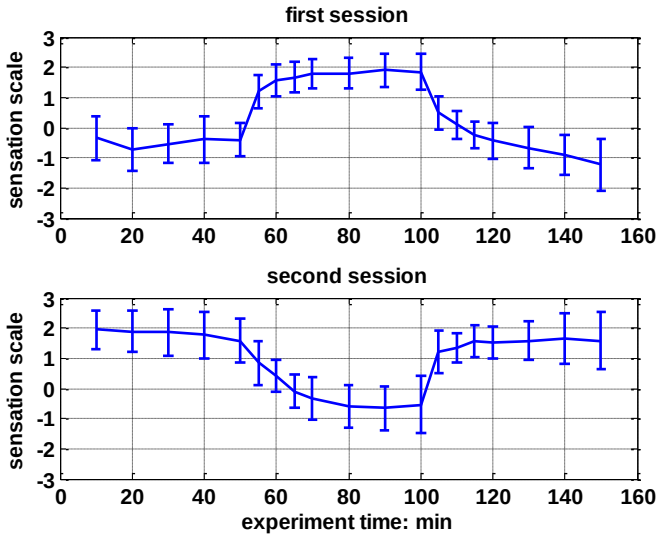

Figure 2.5. Time series of occupant actual mean vote for thermal sensation along with standard deviation error bar.

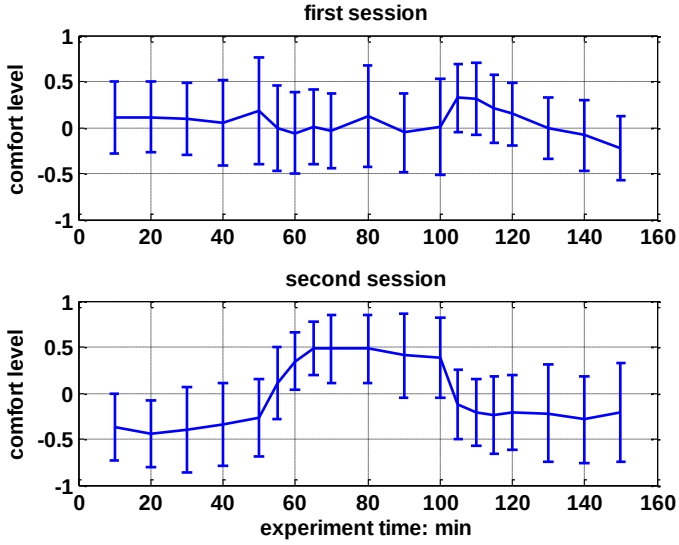

Figure 2.6. Time series of occupant votes for thermal comfort along with standard deviation error bar.

2.3 Modeling Results and Analysis

2.3.1 Thermal Sensation Model with Constant Parameters

Among the two sessions for the chamber experiment, data from one session were used as training data to estimate model parameters and data from the other session were used as validation data to evaluate the model predictions. Below we show the modeling results obtained by using the second session for training and the first session for model evaluation. Since the collected measurements from occupants were not uniformly sampled, linear interpolation was used to generate additional votes. A nonlinear least-squares (Gauss-Newton) algorithm from MATLAB was applied to the training data, and the resulting discrete-time Wiener-logistic model (with a 5-min sampling time) is given as follows,

$$x(k+1) = 0.798 \times x(k) + 0.0610 \times x(k-1) + u(k) - 0.883 \times u(k-1) + \mathrm{e(k)} \tag{2.3}$$

$$y(k) = \frac{3.033}{\exp\left[8.166 - 0.558 \times (x(k) - 7.931)\right] + 1} - 0.994 + v(k) \tag{2.4}$$

Two metrics, mean-squared error and coefficient of determination (R^2), were computed and given in Table 2.2, to quantify the goodness of fit for model prediction. Various model orders were tried for the linear state equation (2.3) and further increasing its order showed marginal improvement in goodness of fit. Figures 2.7 and 2.8 illustrate the comparison of the model prediction by the Wiener-logistic model to the subject mean vote (denoted by "measured") from the second experiment session as training data (shown in Figure 2.7) and from the first session as testing data (shown in Figure 2.8). These results show that the Wiener-logistic model prediction follows the change of subject mean vote reasonably well.

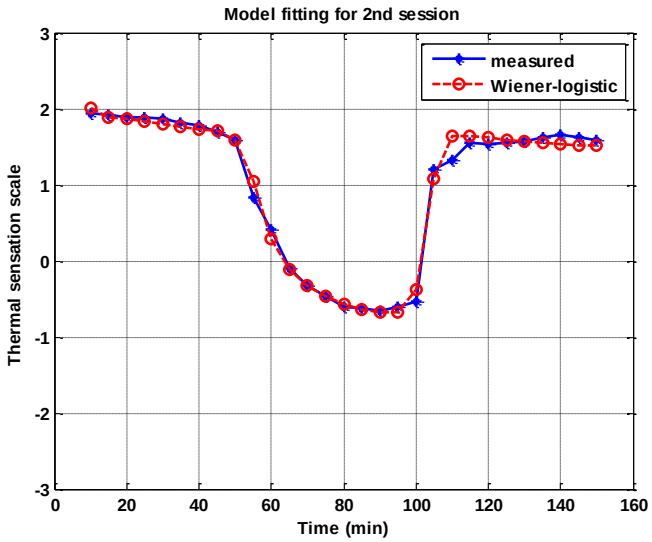

Figure 2.7. Model estimation for thermal sensation using subject mean vote from the second session as training data.

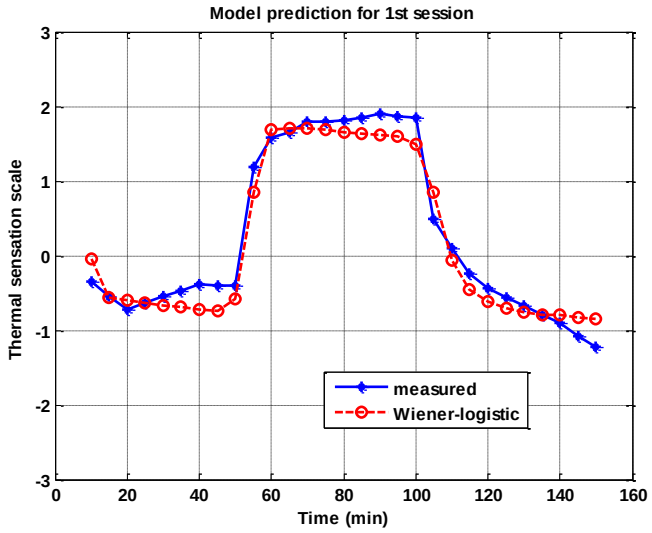

Figure 2.8. Model validation for thermal sensation using subject mean vote from the first session as testing data.

Table 2.2 Goodness of model fit and prediction in terms of Mean-squared error (MSE) and coefficient of determination (R^2)

Model	Mean-Squared Error	R-squared
Wiener-Logistic Model		
1ST Session (testing)	0.0549	0.9537
2ND Session (training)	0.0123	0.9856
Fanger's PMV Model		
1ST Session	0.6758	0.4294
2ND Session	0.2066	0.7575
modified Fiala's DTS Model (using data from 90min to 150 min)		
1ST Session	0.0771	0.9321
2ND Session	0.2354	0.6940

2.3.2 Comparison to Existing Models

This study compared the prediction performance of the Wiener-logistic model to (1) Fanger's PMV model, and (2) a modified Fiala's model for dynamic thermal sensation. Though the PMV is a static model used for prediction of thermal sensation in a steady-state environment, this study still included the comparison for possible interest of readers since PMV is often used as comfort index in indoor thermal control design [19]. Figure 2.9 shows comparison of the three models versus the time series of subject mean vote. Statistics on the goodness of fit for the Fanger's PMV model and the modified Fiala's DTS model are given in Table 2.2 as well.

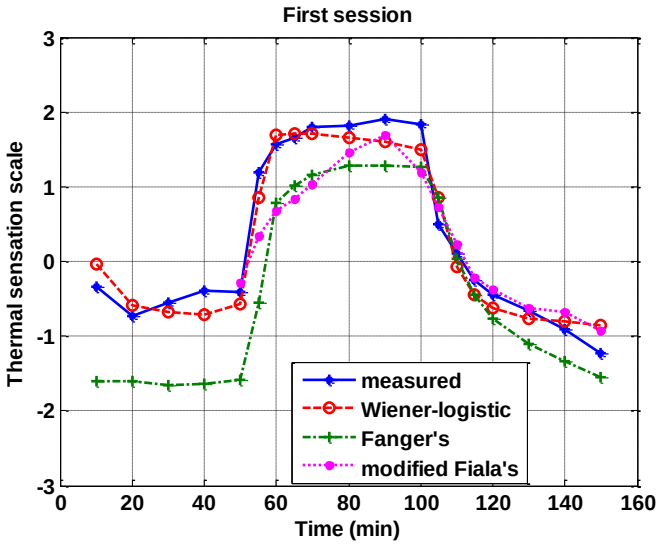

(a)

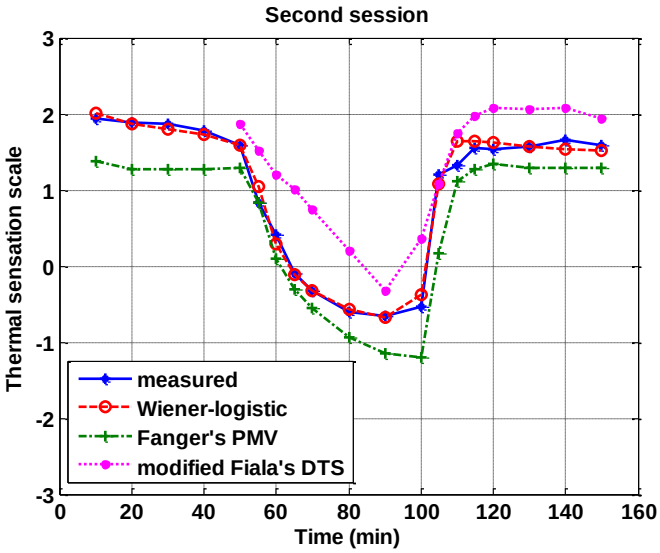

(b)

Figure 2.9. Comparisons of the Wiener-logistic, Fanger's PMV, and a modified Fiala's DTS: (a) using time series of actual mean vote from the first session; (b) using timeseries of actual mean vote from the second session.

A. Fanger' PMV Model

Fanger's PMV model used chamber environmental parameters and participants' clothing information (with a mean value of 0.71 being estimated using data from Table 2.1) to compute the prediction for thermal sensation. On one hand, Figure 2.9 shows that during transient cooling periods, the Fanger's PMV tends to have a steeper slope than the actual subject mean vote and the Wiener-logistic model prediction. On the other hand, during transient warming, the PMV tends to have a relatively flatter slope than the actual subject mean vote and the Wiener-logistic model prediction as shown in Figure 2.9(b). Though the PMV is very close to measurement results at several data points, overall the PMV underestimates the occupant thermal sensation. The subject mean vote has about 1 scale warmer sensation than the Fanger's PMV at the beginning of the first session, and a discrepancy of 0.6-0.9 scale that lasts until the thermal sensation reaches steady state. It is worth pointing out that for a mean monthly outdoor temperature of T_m= 6 ℃, the corresponding neutral temperature computed using the empirical formula by Humphreys [69] for climate-controlled buildings is $T_n = 23.9 + 0.295(T_m - 22)\ exp(-((T_m - 22)/(24\sqrt{2}))^2) = 20.12$ ℃, which agrees with the subject actual mean vote and the Wiener-logistic model prediction at the beginning of the first session where air temperature was set at 21 ℃.

B. A Modified Fiala's Model

For sedentary subjects, the Fiala's model [42], given in Appendix A, predicts the dynamic thermal sensation in terms of the mean skin temperature and its rate of change. Since only the hand skin temperature, rather than the whole-body skin temperature, was measured in our experiment, this study replaced the mean skin temperature and its derivative in the Fiala's model by the hand skin temperature and derivative, and re-estimated the model regression coefficients using experimental data. The resulting model is a modified Fiala's model, given as follows:

$$DTS_{Fiala} = 3 \times \tanh\left[0.185 \times \Delta T_{hand}^{(-)} + 0.258 \times \Delta T_{hand}^{(+)} + 3.850 \times 10^{-3} \times \frac{dT_{hand}^{(-)}}{dt} + 1.780 \times 10^{-2} \times \exp\left(\frac{-0.4814 \times t}{3600}\right) \times \frac{dT_{hand}^{(+)}}{dt_{\max}} \right] \quad (2.5)$$

where the first two terms in tanh( ) correspond to the static component, and the last two terms describe the dynamic component of the thermal sensation model. $\Delta T_{hand}^{(+)}$ and $\Delta T_{hand}^{(-)}$ denote the positive or negative deviation of local hand skin temperature from its reference value that gives the neutral thermal sensation; $dT_{hand}^{(-)}/dt$ denotes the negative rate of change of hand skin temperature, and $dT_{hand}^{(+)}/dt_{\max}$ denotes the maximum positive rate of change of hand skin temperature. The time *t* denotes the elapsed time since the occurrence of $dT_{hand}^{(+)}/dt_{\max}$. In modeling the thermal sensation during warming, $\Delta T_{hand}^{(-)}$ and $dT_{hand}^{(-)}/dt$ are set to zero, and in modeling the thermal sensation during cooling, $\Delta T_{hand}^{(+)}$ and $dT_{hand}^{(+)}/dt_{\max}$ are set to zero.

Since it took a long warm up period for the sensor to be able to measure subject hand temperature accurately, subject hand temperature measurements were not available until t = 50 min after the experiment started. Therefore, in order to have a sufficient number of data points to estimate the regression coefficients of the modified Fiala's model, this study used all data from both sessions as training data. Figure 2.9 shows that the modified Fiala's model does not do well at the beginning (50 min < *t* < 90 min) of each session, which could be due to lack of a sufficient number of data points for parameter estimation. For 90 min < *t* < 150 min, predictions of the modified Fiala's model match the observed mean vote pretty well for cooling, but they have slightly less than 0.5 scale over estimation for warming. Furthermore, Figure 2.9 shows that during the transient cooling (2nd segment of Figure 2.9(a)), the curve slope of the modified Fiala's model is closer to the curve slope of the actual subject mean vote than that of the Wiener-logistic model and the PMV. However, during the transient warming (2nd segment of Figure

2.9(b)), the curve slope of the modified Fiala's model is slightly flatter than that of the actual subject mean vote and the Wiener-logistic model. The statistics in Table 2.2 demonstrate a similar trend revealed by Figure 2.9. Besides the session-wise goodness of fit, separate metrics were calculated for the cooling segment of 1st session and the warming segment of 2nd session, respectively, noting that the session-wise fitness values could be relatively low due to an insufficient number of data points at the warming segment of 1st session and the cooling segment of 2nd session. Table 2.2 shows that for the cooling segment of 1st session, the modified Fiala's model has a very close R^2 value to that of the Wiener-logistic model for the 1st session. However, for the warming segment of 2nd session, the Wiener-logistic model has 40% higher R^2 than the modified Fiala's model.

2.3.3 Using Occupant Feedback to Improve Model Predictions

A. Time-varying Thermal Sensation Model

In the thermal sensation model (2.3–2.4), this study considered air temperature as the sole control input and explicitly modeled its effect on the occupant thermal sensation. The effects of other significant environmental input variables, such as the relative humidity and air velocity, and the effects of occupant clothing levels and metabolic rates were considered to be captured by an aggregate parameter—the offset parameter in the Wiener-logistic model. Therefore, the proposed model neither included these parameters individually nor explicitly. This study also showed through simulations that by considering a time-varying offset parameter *d* in the Wiener-logistic model (2.2) and estimating it in real time via an EKF [67], it is possible to capture the variation of occupant thermal sensation due to: Case I) the change of relative humidity, and Case II) the change of occupant clothing level. Basically, the time-varying offset parameter *d(t)* serves as a correction term for predictions of occupant thermal sensation when one or multiple un-modeled

environmental or occupant-associated inputs deviate from their nominal values being used in training datasets for model calibration. In the implementation of the EKF, the unknown time-varying offset parameter was treated as a new state variable modeled by a random process driven by an additional process noise. Then this new state variable was added to the thermal sensation state to form an augmented state and the EKF was applied to estimate the augmented state. The details of using EKF for simultaneous estimation of the state variable and unknown model coefficient (i.e., the augmented state) are given in Appendix B. Furthermore, this study also showed that a continuously changing offset parameter is not necessary. The consistency check of the EKF can automatically detect the change of environmental and/or occupant disturbance input with a statistically significant magnitude and then a new offset parameter *d* can be estimated to effectively correct the model prediction of thermal sensation. Since variations of relative humidity or occupant clothing level were not controlled in the chamber experiments, rather than using actual occupant votes, this study used the PMV with added zero mean Gaussian noise to simulate the occupant votes and referred to them as the virtual occupant's feedback. The added Gaussian noise was intended to reflect possible sensing noise between the PMV and occupant AMV. The Gaussian noise was considered to have zero mean by assuming that the PMV was not biased in predicting occupant thermal sensation. In both cases described below, the parameters (except the relative humidity and clothing level) used to run the PMV model are given as follows: air temp = 25.85 ℃, MRT =25.85 ℃, air velocity = 0.135 m/s, and activity level = 1.

Case I: Change of relative humidity level. For this case, the occupant clothing level was maintained to be 0.71. The relative humidity (RH) was set to RH = 21% for the first 24h, and changed to RH = 60% from t = 24h to t = 48h. The Gaussian noise variance in simulating the virtual occupant feedback was set to be 0.03. The process and measurement noise variances in implementing the Kalman filter were set to be 0.005 and 0.03, respectively. Figure 2.10 shows that for a constant offset parameter *d* = -1, the predicted sensation by the Wiener-logistic model is

close to the mean of virtual occupant votes at near neutral thermal sensation when RH = 21%. However, when RH increases to 60% at t = 24h, the predicted sensation is around 0.2 scale lower than the mean of virtual occupant votes. In Figure 2.11, a time-varying offset parameter *d* is considered for the Wiener-logistic model and the artificial noise variance for *d* is tuned such that the consistency of the EKF is achieved (detailed discussions are given in Section *B*). These results show that *d* increases to around -0.75 in response to the RH increase, and the resulting model prediction is able to capture the thermal sensation variation due to the increase of RH.

Case II: Change of occupant clothing level. For this case, the relative humidity was maintained at RH = 21%. The clothing level was kept at 0.71 (this was the averaged value in the chamber experiments) for the first 24h and then decreased to 0.4 from t = 24h to t = 48h. The Gaussian noise variance in simulating the virtual occupant feedback was set to be 0.01. The process and measurement noise variances in implementing the Kalman filter were set to be 0.005 and 0.01, respectively. Figure 2.12 illustrates that the Wiener-logistic model with time varying offset parameter is able to capture the effects on occupant thermal sensation due to a sudden change of occupant's clothing level at t = 24h by reducing *d* from -1 to around -1.7.

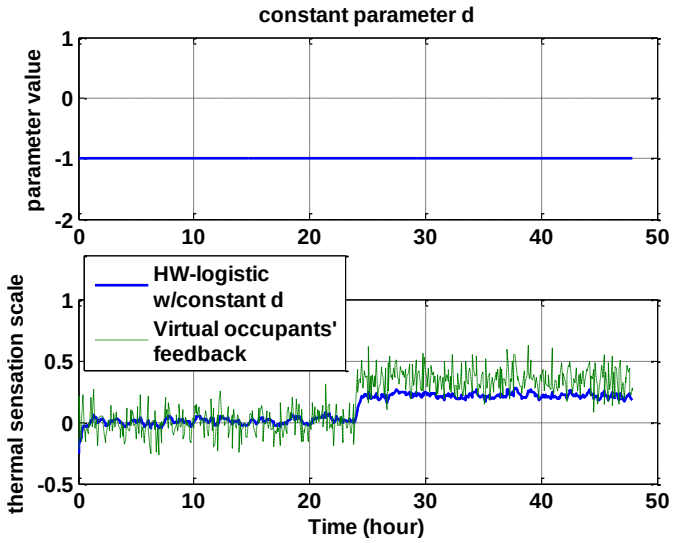

Figure 2.10. Wiener-logistic model with constant offset parameter, where the relative humidity changes from 21% to 60% at t=24h.

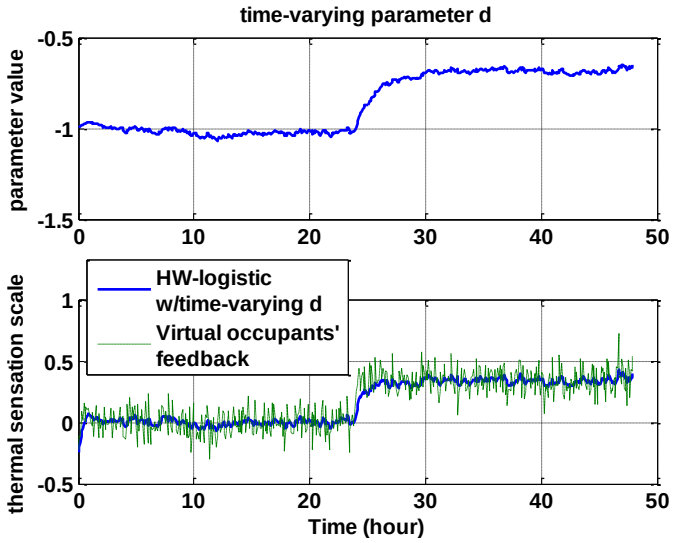

Figure 2.11. Wiener-logistic model with time-varying offset parameter, where the RH changes from 21% to 60% at t=24h.

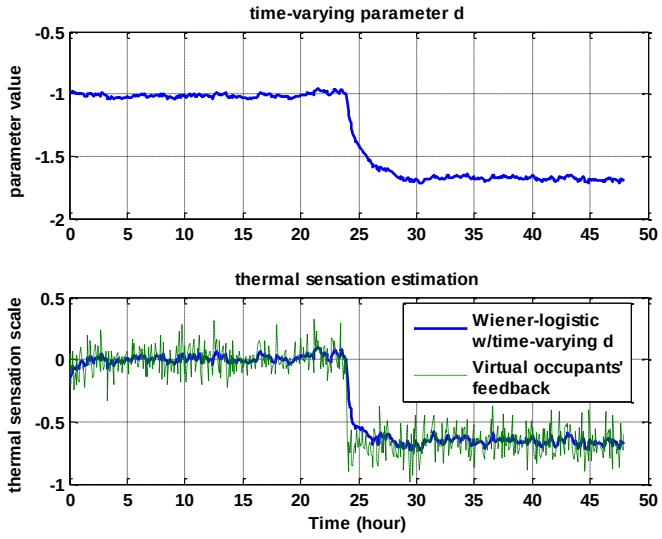

Figure 2.12. Wiener-logistic model with time-varying offset parameter, where the clothing level changes from 0.71 to 0.4 at t=24h.

B. Consistency of Kalman Filter

Capturing the thermal sensation variation due to non-negligible changes in the un-modeled environmental or occupant disturbance inputs through estimating the time-varying offset parameter *d* by EKF requires monitoring the consistency of the Kalman filter. Essentially, when such changes occur, under the original nominal offset parameter *d*, the consistency of EKF will be violated, and re-estimation of a new offset parameter *d* is needed to regain the filter consistency. The consistency of a Kalman filter can be verified by Chi-square test of whiteness of the innovation sequence. The Normalized Innovation Squared (NIS) is defined as:

$$\varepsilon_v(k) = \nu(k)' S(k)^{-1} \nu(k) \tag{2.6}$$

where the innovation ν is the difference of the measurement (corresponding to occupant feedback here) and the filter predicted measurement, and S denotes the filter calculated innovation covariance. To reduce the variability, a moving average of NIS over a sliding window of size *w* can be used and it is defined as,

$$\varepsilon_v^w(k) = \frac{1}{w} \cdot \sum_{j=k-w+1}^{k} \varepsilon_v(j) \tag{2.7}$$

where $w \times \varepsilon_v^w(k)$ is assumed to be Chi-square distributed with $w \times n_z$ degree of freedom, n_z denotes the dimension of the measurement and it is equal to 1 for the thermal sensation model.

The analysis of filter consistency for Case I is presented here, while the filter consistency check for Case II can be conducted in a similar way and thus is omitted. Consider a window size of w = 24 in (2.7), which corresponds to collecting feedback from occupants every 5 min for two hours. This study first checked the filter consistency corresponding to the Wiener-logistic model with a fixed offset parameter d = -1. Evaluation of the two-sided 99% Chi-square distribution with a degree of freedom n_z = 24 indicates that the filter is consistent if $w \times \varepsilon_v^w(k) \in [9.886,\ 45.559]$ or $\varepsilon_v^w(k) \in [0.412,\ 1.898]$, which is referred to as the 99% probability (or acceptance) region. Figure 2.13(a) shows that the filter is consistent for the first 24h, but not for the second 24h. This is confirmed by Figure 2.10 that from t = 24h to t = 48h, the predicted sensation is around 0.2 scale lower than the mean of virtual occupant votes and thus the expected value of the innovation sequence is not zero any more. Next, consider the Wiener-logistic model with a time varying parameter d whose value was estimated by an EKF (shown in Figure 2.11), Figure 2.13(b) shows that the corresponding moving average NIS is within the 99% probability bounds till t = 25.16h, when the filter consistency is lost, but the NIS comes back to the acceptance region after t = 26.15h to regain the filter consistency.

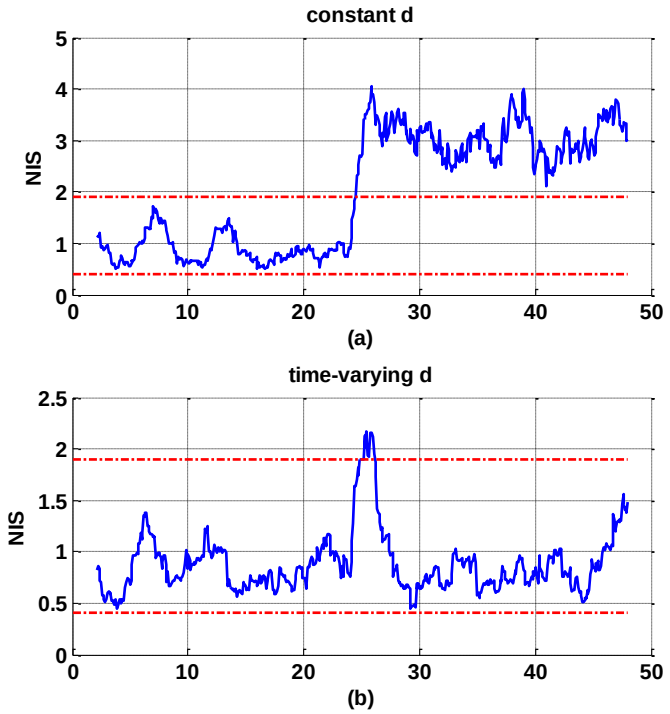

Figure 2.13. Moving average normalized innovation squared (NIS) with its 99% probability region, where the relative humidity changes from 21% to 60% at t = 24h. (a) Wiener-logistic model with constant d; (b) Wiener-logistic model with time-varying d.

A relatively simple alternative to the continuously changing offset parameter d is a piece-wise constant d, i.e., start with the Wiener-logistic model with a constant offset parameter and only re-estimate a new d when the NIS goes outside its acceptance region. Figure 2.14 shows that the moving average NIS exceeds the upper bound of its 99% probability region [0.412, 1.898] at t = 24h, which corresponds to the change of RH from 21% to 60%. Then the offset parameter d is re-estimated by EKF and a new value of d = –0.722 is obtained at t = 26.25h to regain the filter consistency. The difference between the model in Figure 2.14 and the one in Figure 2.13 is that once a new offset parameter d is obtained to regain the filter consistency, continuously updating its value via EKF is not needed until the filter consistency is lost again.

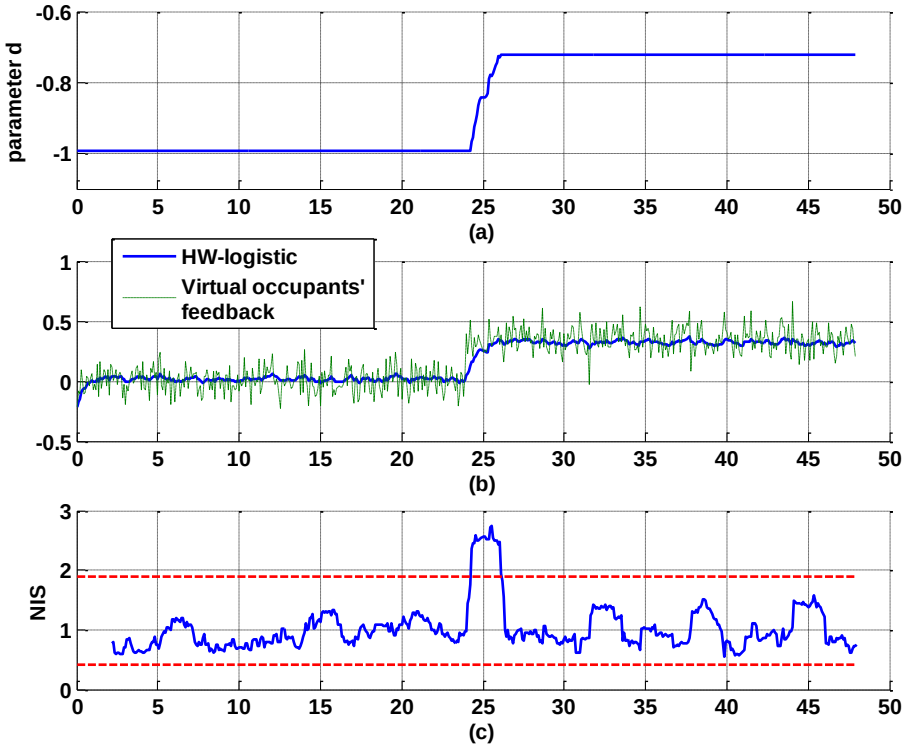

Figure 2.14. Wiener-logistic model with piece-wise constant *d*, where the relative humidity changes from 21% to 60% at *t* = 24h. (a) parameter *d*; (b) model predicted thermal sensation versus virtual occupant votes; (c) moving average normalized innovation squared (NIS).

Chapter 3

Numerical Study of MPC Design Based on Dynamic Thermal Sensation Model

Current building control algorithms are mainly rule based (if-then-else based rules) and thus the performance of a large number of buildings heavily depends on the experience of building managers. In recent years, various advanced control techniques, such as fuzzy logic control, agent-based intelligent control, neural network control, optimal control, and model predictive control have emerged in building control applications. In particular, model predictive control (see Appendix C for an introduction to model predictive control) has gained increasing popularity in utilizing passive or active thermal storage to save energy. With weather predictions and occupancy schedules, free cooling at night is used in cooling applications and night setback is adopted for heating applications. Peak-load shifting is implemented in MPC to save electricity cost by taking advantage of the time-of-day rate of electricity price. MPC is also applied to determine optimal temperature set-points at the top level of a hierarchical control, for which simple PID or on-off controllers were used for lower-level components such as fans, heating/cooling coils and thermal storage tanks. Alternatively, low level components could be directly managed by a MPC to achieve a higher level of efficiency.

While on one hand energy saving is important, on the other hand, occupant thermal comfort plays a key role in the control of HVAC systems for low-energy buildings. A large number of the existing control algorithms are designed such that the neutral temperature is achieved based on the Fanger's thermal comfort model. Alternatively, the so-called effective temperature, which is a combination of the indoor temperature and relative humidity, could be used as the index for thermal comfort [39]. Though the existing HVAC control algorithms seldom

directly optimize a PMV index (or use it as a constraint), a numerical study demonstrated that using the PMV in defining the thermal comfort constraint in a MPC could reduce energy consumption and improve thermal comfort, compared to utilizing a comfort zone from a psychrometric chart [19].

However, direct incorporation of the PMV in a MPC design for HVAC systems could pose practical implementation challenges. The calculation of PMV involves iteration, which could raise computation concerns, especially for MPC which is known to be computation intensive. Past work tried to approximate the PMV with a neural network model [11], [46]-[47] or with a linearized parameterization model [48]. In addition, most buildings typically do not have sensors to continually measure humidity, air velocity and mean radiant temperature. Even though for laboratory facilities where the aforementioned environmental sensing data are available, occupant clothing insulation and activity levels, which could vary with respect to time and vary among occupants, are seldom monitored continually and individually. Assuming a uniform and constant clothing level for occupants could cause errors in predicting occupant thermal sensations [31].

In this chapter, the MPC problem formulation uses the data-driven DTS model proposed in previous chapter. A distinctive feature of this DTS model lies in that the time-varying offset parameter of the proposed Wiener-logistic model can be estimated through an EKF using real-time occupant votes to capture the variability of thermal sensation due to environmental or occupant-associated changes. Rather than assuming that a "PMV sensor" exists [19], this study assumed that occupants act as a sensor for indoor thermal comfort and there exists a feedback channel for occupants to provide their thermal sensation votes to the controller. Field studies showed that there could be a discrepancy between Fanger's PMV and occupants' AMV [39]. Furthermore, occupants' awareness of opportunities to control their environment could affect their perceptions of thermal comfort [60]. Though under the current building environment, it

might not be practical for an individual occupant to directly control HVAC systems to achieve a personalized thermal environment, it is reasonable to assume that there is a feedback channel for occupants to communicate their thermal sensation perceptions to the controller. Replacing Fanger's PMV by such a dynamic thermal sensation model in the MPC formulation enables the proposed MPC design for HVAC systems to adapt to uncertainties and variations associated with occupants' thermal perceptions. In addition, a chance-constrained MPC was also developed using the DTS model, which provides an opportunity for the controller to adjust the probability level of violation of thermal comfort to achieve a balance between energy consumption and thermal comfort.

3.1 Building Thermal Transport Model

The thermal transport model for a single zone building was derived using a commonly used RC thermal network based on heat balance [50], [51]. For a RC thermal network, each wall or zone is abstracted as a node. Each node is then modeled as a thermal capacitance (thermal mass) with its temperature representing the state of the node. The network is formed by connecting all nodes with thermal resistors. The capacitances and resistances can be estimated based on the geometry and material properties of the building under study.

It is important to notice that the thermal network model is a simple representation of actual building environment and its mechanical system. Building network models are widely used and recently improved for their capabilities to accurately predict energy consumption in buildings [70]. These models are popular not only for their capabilities to accurately predict energy consumption in actual buildings, but also for their simplicity, allowing testing of different control algorithms prior to their deployment and further testing in more complicated scenarios [71]. In the present study, several important assumptions are made for the network model including

negligible internal radiative fluxes, which are applicable to spaces without windows and radiative cooling/heating systems, such as chilled ceiling or heating radiators [72]. Therefore, the thermal network model treats the conductive and convective heat transfer as well as thermal storage, but it neglects the radiative heat transfer. It is important to notice that this assumption also implies that the mean radiant temperature, used in thermal comfort models, is equal to the air temperature in the studied space. Our experimental study showed that this assumption is correct fora space with well-insulated walls, without windows or radiative cooling/heating systems. Furthermore, the thermal network model assumes no recirculation of the air supplied to the space, so the total amount of energy required for cooling or heating the studied space is over estimated, but the actual trends and relative differences are following performance in actual spaces. Overall, the simplifications used in the thermal network model result in heat flux values that deviate from actual systems, but represent correct trends and orders of magnitude, so they provide a good representation of an actual system to test the differences in performance of controls algorithms.

Figure 3.1 shows the RC thermal network for a single room chamber, for which the roof and floor are ignored. There are 5 nodes in the system. Node 1 represents the room air and other nodes represent the four single-layered walls of the room. Let T_i (i = 1, $\cdots$, 5) denote the temperature of the node i = 1, $\cdots$, 5, respectively. Let T_O denotes the outdoor temperature. Without loss of generality, it is assumed that wall 2 faces outside and the rest of the walls are connected to adjacent rooms (not shown in the figure) with temperature denoted by T_N.

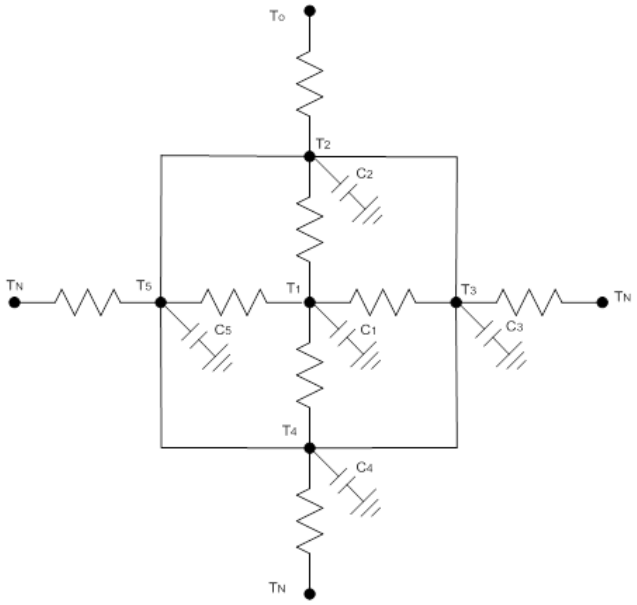

Figure 3.1. Single room thermal network model.

The capacitance of each node, C_i (i = 1, . . . , 5), depends on the lumped mass of the node and specific heat of the wall material. Each lumped thermal resistance between each pair of nodes is estimated based on different ways of heat transfer given as follows: (1) for conduction within the wall, $R_{cond}= (l_{wall})/(2k \times A_w)$, where l_{wall} denotes the thickness of the wall, k is the conduction coefficient of the wall material, and A_w is the area of the wall; (2) for convection between a wall surface and air, $R_{conv}= 1/(h \times A_w)$, where h denotes the convection coefficient. In this study, all walls are assumed to be the same, and thus the thermal resistance between each pair of nodes (i, j), R_{ij}, is assumed to be the same and it is computed as follows,

$$R_{ij} = R_{cond} + R_{conv} = \frac{l_{wall}}{2kA} + \frac{1}{hA} \tag{3.1}$$

The air change rate is set at 1ACH. The heat exchange due to ventilation can be calculated as,

$$q_{vent\_flow} = \dot{m} \times (h_{out} - h_{in}) = \dot{m} \left\{ \left[c_{pa} \times T_O + W_{out} (c_{pw} \times T_O + h_{we}) \right] - \left[c_{pa} \times T_1 + W_{in} (c_{pw} \times T_i + h_{we}) \right] \right\} \tag{3.2}$$

where q_{vent_flow} denotes the ventilation heat flow, $\dot{m}$ denotes the air mass flow rate and can be calculated based on the volume of the room and the air change rate, h_{out} denotes the outdoor specific enthalpy of moist air, h_{in} denotes the indoor specific enthalpy of moist air, c_{pa} denotes the specific heat of air, c_{pw} denotes the specific heat of water vapor, T_O denotes the outdoor temperature, T_1 denotes the indoor temperature (temperature of node 1), W_{out} denotes the outdoor humidity ratio, W_{in} denotes the indoor humidity ratio, and h_{we} denotes the evaporation heat of water at 0 ℃. It is important to note that this model assumes no recirculation, so the entire airflow rate represents outdoor airflow into the space. This is an assumption introduced to simplify the thermal network model. Humidity ratio W can be calculated as,

$$W = \frac{RH \times W_s}{1 + (1 - RH) \times W_s / 0.622} \tag{3.3}$$

where RH denotes relative humidity, W_s denotes saturation humidity ratio, which can be looked up for specific air temperatures. By (3.3), the indoor and outdoor humidity ratio W_{in} and W_{out} can be computed respectively.

Let G_{int} denote the internal gain. Then based on energy conservation, the temperature of each node, T_i, (i = 1, ⋯, 5), satisfies the following state-space model,

$$C_1 \frac{dT_1}{dt} = \frac{T_2 - T_1}{R_{21}} + \frac{T_3 - T_1}{R_{31}} + \frac{T_4 - T_1}{R_{41}} + \frac{T_5 - T_1}{R_{51}} + q_{vent\_flow} + G_{\text{int}} + u \tag{3.4}$$

$$C_2 \frac{dT_2}{dt} = \frac{T_1 - T_2}{R_{21}} + \frac{T_O - T_2}{R_{2O}} \tag{3.5}$$

$$C_3 \frac{dT_3}{dt} = \frac{T_1 - T_3}{R_{31}} + \frac{T_N - T_3}{R_{3N}} \tag{3.6}$$

$$C_4 \frac{dT_4}{dt} = \frac{T_1 - T_4}{R_{41}} + \frac{T_N - T_4}{R_{4N}} \tag{3.7}$$

$$C_5 \frac{dT_5}{dt} = \frac{T_1 - T_5}{R_{51}} + \frac{T_N - T_5}{R_{5N}} \tag{3.8}$$

where the control input u denotes the heating ($u > 0$) or cooling($u < 0$) flow.

Define $T = \begin{bmatrix} T_1 & T_2 & \dots & T_5 \end{bmatrix}^T$ (in Kelvin). Consider a constant internal gain G_{int} = 500W and a neighboring room temperature of 25 ℃. By discretization of the continuous time model with a 15 min sampling time, the resulting discrete time building thermal transport model can be written in the following compact state-space form,

$$T(t+1) = AT(t) + B_1 T_O(t) + B_2 T_N(t) + B_3[u(t) + G_{\text{int}} + q_{vent\_flow}(t)] \tag{3.9}$$

$$T_a(t+1) = CT(t+1) - 273.15 \tag{3.10}$$

where the unit of the room air temperature T_a is Celsius, and numerical values of the matrices A, B_1, B_2, B_3 and C can be calculated based on the geometry and material properties of the chamber given in Table 3.1 and their values are given as follows:

$$A = \begin{bmatrix} 0.1843 & 0.2026 & 0.2026 & 0.2026 & 0.2026 \\ 0.0051 & 0.9802 & 0.0014 & 0.0014 & 0.0014 \\ 0.0051 & 0.0014 & 0.9802 & 0.0014 & 0.0014 \\ 0.0051 & 0.0014 & 0.0014 & 0.9802 & 0.0014 \\ 0.0051 & 0.0014 & 0.0014 & 0.0014 & 0.9802 \end{bmatrix},$$

$$B_1^T = \begin{bmatrix} 0.0014 & 0.0106 & 0 & 0 & 0 \end{bmatrix},$$

$$B_2^T = \begin{bmatrix} 0.0041 & 0 & 0.0106 & 0.0106 & 0.0106 \end{bmatrix},$$

$$B_3^T = \begin{bmatrix} 0.0034 & 0 & 0 & 0 & 0 \end{bmatrix},$$

$$C = \begin{bmatrix} 1 & 0 & 0 & 0 & 0 \end{bmatrix}.$$

Table 3.1. Chamber parameters used in the building model.

	Room(air)	Walls
Density (Kg/m3)	1.16	2000
Specific heat Cp (J/Kg-K)	1007	935
Conduction coefficient k (W/m-K)		0.744
Convection coefficient h (W/m2-K)		5
Length (m)	6	
Width (m)	6	
Height (m)	3	
Air mass flow rate (kg/s)	0.139	
Thickness (m)		0.15

3.2 Control Formulation

Two types of MPC designs using the DTS were developed to minimize energy consumption while maintaining occupant thermal comfort. At each time instant *t*, the MPC solves a finite-horizon constrained minimization of energy consumption to determine the optimal heating/cooling trajectory based on the prediction of indoor conditions (from the building model) and prediction of occupants' actual mean vote (from the DTS model). Only the first step of the control trajectory is implemented at the current time instant *t* and the procedure is repeated at the next time instant. For the simulations conducted in this study, outdoor weather conditions were assumed to be known (historical data were used), based on which prediction of indoor air temperature was computed using the building thermal transport model (3.9–3.10). Due to the

considered process noise and sensor noise in the DTS model, the observed occupants' AMV is assumed to be a random variable.

In the first MPC, the thermal comfort constraint is specified in terms of the DTS model prediction for AMV and the controller assumes that the prediction is correct under certainty equivalence, i.e., the disturbance/noise is assumed to take its expected value. This MPC is referred to as Certainty Equivalence MPC, denoted as CEMPC-DTS. In the second MPC, a stochastic thermal comfort constraint is defined, which requires that the probability of AMV within a specified bound is larger than a preset number. This MPC is referred to as Chance-Constrained MPC, denoted as CCMPC-DTS. A deterministic approximation of the chance constraint was adopted in this dissertation, which leads to a tighter bound on thermal comfort than that used in CEMPC.

Performance of the CEMPC-DTS and CCMPC-DTS were compared to a MPC using Fanger's PMV as the thermal comfort index (denoted as MPC-PMV) and a rule-based PI control (denoted as RuleBased-PI) that represents the current control practice for HVAC systems. Control formulations of the three MPC designs are given in Section 3.2.1 and details on the RuleBased-PI are given in Section 3.2.2.

3.2.1 MPC Formulations

The general MPC formulation is described as follows.

Cost:

$$\min_{U_t} J_t := \sum_{k=1}^{N} [u(t+k \mid t)]^2 + \lambda \sum_{k=1}^{N} [q(t+k \mid t)] \tag{3.11}$$

This cost function is subject to the following models for building thermal transport and thermal sensation for building occupants.

Building thermal transport model:

$$T(t+k+1|t) = AT(t+k|t) + B_1T_O(t+k|t) + B_2T_N(t+k|t) + B_3[u(t+k|t) + G_{\text{int}}(t+k|t) + q_{vent\_flow}(t+k|t)] \quad (3.12)$$

$$T_a(t+k+1|t) = CT(t+k+1|t) - 273.15 \quad (3.13)$$

Thermal sensation model:

$$TS(t+k|t) = f(T_a(t+k|t), T_a(t+k-1|t), \ldots) \quad (3.14)$$

Constraint on thermal comfort:

$$y_{\min} - q(t+k|t) \le TS(t+k|t) \le y_{\max} + q(t+k|t) \quad (3.15)$$

$$q(t+k|t) \ge 0 \quad (3.16)$$

Constraint on cooling and heating power:

$$u_{\min} \le u(t+k|t) \le u_{\max} \quad (3.17)$$

where $U_t = [u(t+1|t), \cdots, u(t+N|t)]$ denotes the control input trajectory along the prediction horizon, and N denotes the length of the prediction horizon. The cost function J_t is defined as the L_2 norm of the control input $u(t+k|t)$ plus the L_1 norm of the slack variable $q(t+k|t)$ for satisfying the thermal comfort constraint. A very large number λ is chosen to heavily penalize the violation of thermal comfort. TS represents thermal sensation in a generic model (3.14), which will be substituted by different thermal comfort models in the subsequent subsections. A soft constraint (3.15) is considered for maintaining the thermal sensation within the bounds $y_{\min}$ and $y_{\max}$ using the slack variable q to avoid infeasibility in solving the resulting MPC. The control input is subject to constraint (3.17) with the maximum cooling power denoted by $u_{\min}$ ($u_{\min} < 0$) and the maximum heating power denoted by $u_{\max}$ ($u_{\max} > 0$).

A. Certainty Equivalence MPC Based on DTS Model (CEMPC-DTS)

In CEMPC-DTS, the thermal sensation equation (3.14) is computed using the DTS model under the assumption that the noise *e(t)* and *v(t)* take their respective expected values. In this study, the process noise *e(t)* and sensing noise *v(t)* are assumed to be Gaussian with zero mean, i.e., $E[e(t)]=0$ and $E[v(t)]=0$. As a result, the following thermal sensation prediction is used to substitute (3.14) in CEMPC-DTS:

$$\hat{x}(t+k+1|t)=0.798\cdot\hat{x}(t+k|t)+0.0610\cdot\hat{x}(t+k-1|t)+T_a(t+k|t)-0.883\cdot T_a(t+k-1|t) \tag{3.18}$$

$$\hat{d}(t+k|t)=\hat{d}(t+k-1|t) \tag{3.19}$$

$$\hat{y}(t+k|t)=\frac{3.033}{\exp[-0.558\cdot(\hat{x}(t+k|t)-7.931)+8.166]+1}+\hat{d}(t+k|t) \tag{3.20}$$

$$TS(t+k|t)=\hat{y}(t+k|t) \tag{3.21}$$

Note that the coefficient values in (3.18)–(3.20) correspond to a 5 min sampling time and re-discretization using a 15 min sampling time was conducted in the controller simulation.

B. Chance Constrained MPC Based on DTS Model (CCMPC-DTS)

CCMPC-DTS considers the following probabilistic (chance) constraint for thermal comfort:

$$\text{Prob}\{y_{\min}\le TS(t+k|t)\le y_{\max}\}\ge 1-\alpha \tag{3.22}$$

Where α denotes a predefined small percentage. Assuming a Gaussian distributed process/sensor noise with zero mean, the chance constraint (3.22) can be approximated by a deterministic constraint [73] as follows:

$$y_{\min}+\Delta y\le\hat{y}(t+k|t)\le y_{\max}-\Delta y \tag{3.23}$$

$$\Delta y=\beta\Omega^{1/2} \tag{3.24}$$

Where $\hat{y}(t+k|t)$ denotes the prediction for AMV given by the DTS model (3.18-3.20), $\beta=\sqrt{2}erf^{-1}(1-2\alpha)$ with erf^{-1} denoting the inverse of the standard error function

$erf(x) = \frac{2}{\sqrt{\pi}} \int_0^x e^{-u^2} du$, Ω corresponds to the measurement prediction covariance in (B-11) (which is a scalar here due to the single output variable) and it can be computed using EKF.

By further softening the constraint using the slack variable q in CCMPC-DTS, thermal constraint (3.15) is replaced by

$$(y_{\min} + \Delta y) - q(t+k \mid t) \le \hat{y}(t+k \mid t) \le (y_{\max} - \Delta y) + q(t+k \mid t) \tag{3.25}$$

Compared to the constraint used in CEMPC-DTS, the constraint in CCMPC-DTS offers two advantages: 1) a tunable probability of constraint violation α , and 2) a tighter thermal comfort bound to improve thermal comfort.

C. MPC Based on PMV Model (MPC-PMV)

In the MPC-PMV formulation, Fanger's PMV model is used to implement (3.14) for $TS(t+k \mid t)$:

$$TS(t+k \mid \mathrm{t}) = PMV(T_a(t+k \mid t), T_{mr}, RH, V_a, CLO, M) \tag{3.26}$$

Where the air temperature prediction $T_a(t+k \mid t)$ is obtained from the building model (3.12-3.13), the mean radiant temperature T_{mr} is assumed to be the same as the air temperature, and the relative humidity *RH*, air velocity V_a , occupants' clothing insulation level *CLO* and metabolic rate (activity level) *M* at time (*t*+*k*) are assumed to be known.

3.2.2 RuleBased-PI Control

In this control strategy, the thermal comfort constraint is defined by specifying heating and cooling set points, denoted by $SP_{heating}$ and $SP_{cooling}$ respectively, with a buffer to prevent short cycling. The actual values of these set points are chosen by building managers and they vary by seasons and climate regions. If the indoor temperature is low ($T_a < SP_{heating} - buffer$), a PI

control is applied to increase the indoor temperature to the heating set point $SP_{heating}$. If the indoor temperature is high ($T_a > SP_{cooling} + buffer$), a PI control is applied to cool the indoor air temperature to the cooling set point $SP_{cooling}$. The PI control with a low-pass filter used in this dissertation is given as follows:

$$u\_(k) = K_p \cdot err(k) + K_I \cdot \Delta T \cdot \sum_{i=0}^{k} err(i) \tag{3.27}$$

$$u(k) = 0.1 \cdot u\_(k) + 0.9 \cdot u(k-1) \tag{3.28}$$

Where err denotes the error between the heating set point $SP_{heating}$ (or cooling set point $SP_{cooling}$) and indoor air temperature T_a, K_p and K_I are proportional and integral gain, respectively, and ΔT is the sampling time.

3.3 Simulation Results

3.3.1 Simulation Platform

Performance of the two DTS-based MPC, CEMPC-DTS and CCMPC-DTS, was compared to the MPC-PMV and Rule-based PI through simulations. Here, the occupants' AMV is simulated using the PMV plus a random white noise w,

$$AMV(k) = PMV(k) + w(k) \tag{3.29}$$

Where the random noise w is assumed to follow a Gaussian distribution. When w has a zero mean $E[w] = 0$, we assume that the PMV is an accurate model to describe the occupants' AMV without bias. When w has a nonzero mean, i.e., $E[w] \neq 0$, we assume that the PMV is biased in evaluating AMV, noting that PMV was reported to underestimate or overestimate thermal

sensation in field surveys [39], [72]. In the remaining of this dissertation, the output of the virtual occupant model (3.29) is referred to as *virtual occupants' feedback*.

Figure 3.2 shows the block diagram for the DTS model based MPC controller (either CEMPC-DTS or CCMPC-DTS) used in simulations. It is assumed that occupants' feedback on thermal sensation is available to be used by the MPC design. At each time step of the simulation, the observed occupants' AMV is first passed to an extended Kalman Filter to estimate the state variable $\hat{x}(t+k\,|\,t)$ and the offset parameter $\hat{d}(t+k\,|\,t)$ simultaneously (details given in the Appendix B). These two parameters are then fed into the DTS model to generate the prediction of AMV $\hat{y}(t+k\,|\,t)$ along the optimization horizon. By solving the corresponding MPC optimization (CEMPC or CCMPC), the optimal heating or cooling flow is determined and then fed into the building model to compute the resulting room temperature.

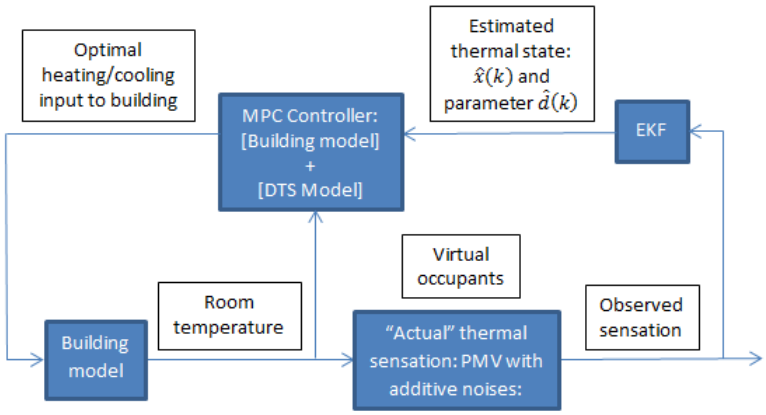

Figure 3.2. Block diagram for DTS model based MPC.

For the MPC-PMV controller, there is neither an "EKF" block nor feedback of occupants' thermal sensation to the MPC-PMV control. Among the six input variables to the PMV model, the room air temperature is predicted by the building model (3.12-3.13), the mean radiant temperature is set to be the same as the air temperature, the air velocity and occupant activity level are set to the values used in the chamber experiment described in previous chapter

(see Table 3.2), and the relative humidity and clothing insulation levels are designed to start from the nominal values given in Table 3.2 and then follow the trajectories shown in Figure 3.3 and Figure 3.4, respectively.

The simulation time step ΔT is set to be 15min. The MPC optimization horizon is chosen to be $N = 20$ sampling intervals equivalent to 5hrs. The bounds on thermal sensation are set to be $y_{\min} = -0.5$ and $y_{\max} = 0.5$. The control input is constrained by $u_{\min} = -5000$ (for 5 kilowatts max cooling power) and $u_{\max} = 5000$ (for 5 kilowatts max heating power) respectively. In the RuleBased-PI, parameters are set to be $SP_{heating} = 24$ Celsius, $SP_{cooling} = 26$ Celsius, $buffer = 1$ Celsius, $K_p = 2000$ and $K_I = 100$.

Table 3.2. Key parameters of the thermal-comfort chamber experiment.

Occupant clothing insulation	Occupant activity level	Chamber mean radiant temperature	Chamber average RH	Chamber average air velocity
0.71	1	Closely follows ambient temperature	21%	0.135m/s

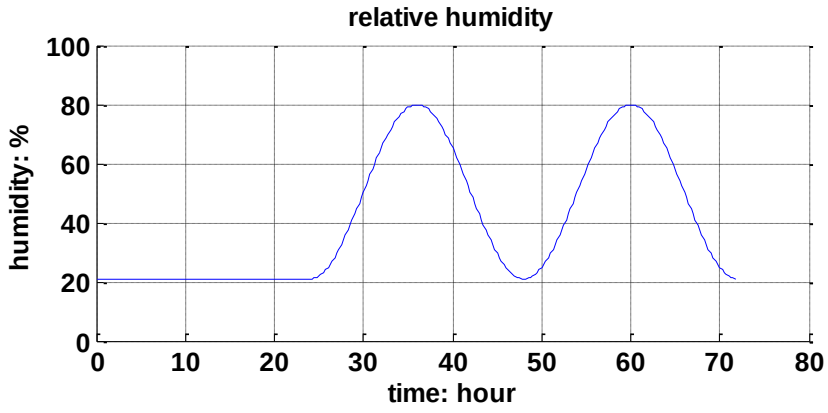

Figure 3.3. Relative humidity used in simulation.

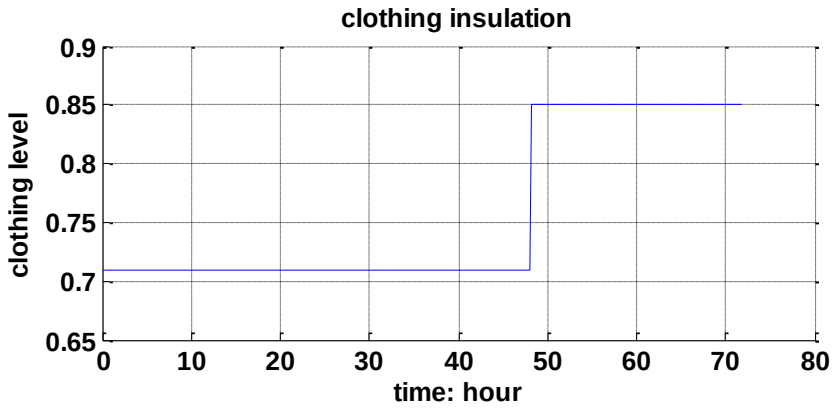

Figure 3.4. Clothing insulation level used in simulation.

3.3.2 Environmental and occupant parameters

To evaluate the control performance, simulations in this study used two different sets of outdoor weather conditions shown in Figure 3.5. In Figure 3.5, the top subplot shows the outdoor temperatures collected at State College, PA for 3 days from 03/09/2013 to 03/11/2013, and the bottom subplot shows the outdoor temperatures from 09/10/2013 to 09/12/2013. The relative humidity trajectory used in the simulations (shown in Figure 3.3) is designed to start at a nominal value of 21% in the first day followed by a sinusoidal curve ranging from 21% to 80% with a period of 24 hours for two days. The average clothing level of occupants is plotted in Figure 3.4, which is set to *CLO = 0.71* for the first two days, raised to *CLO = 0.85* at the beginning of the third day and then maintained at this value for the rest of the day. The initial values of the relative humidity and average clothing level were chosen from operating conditions of the chamber experiment [72] conducted to obtain nominal coefficients of the DTS model (2.3-2.4).

To generate the virtual occupant feedback on thermal sensation, the noise w that is added to the PMV in (3.29) is chosen to be a Gaussian noise with a standard deviation of 0.08 with three different mean values: 1) $E[w]=0$, used to simulate the scenario where there is no

discrepancy between the PMV and AMV; 2) $E[w] = 0.2$, used to simulate the scenario where the PMV underestimates the AMV, and 3) $E[w] = -0.2$, used to simulate the scenario where the PMV overestimates the AMV.

3.3.3 Performance Metrics

Three metrics are used to evaluate the control performance. The first one is total *Energy Consumption* (E), which computes the integration of control input (heating/cooling power) over time. The second one is *Violation Ratio* (VR), which is defined as the ratio of the time during which the AMV generated by the Virtual Occupants falls outside the thermal sensation bounds over the total simulation time (3 days). This metric indicates how frequently the constraint on thermal comfort is violated, but it does not provide information on how far the AMV is away from the specified bounds when the constraint is violated. The third metric, *Integration of Violation* (IOV), computes the area between the thermal sensation bound (0.5 or -0.5 depending on cooling or heating application) and the AMVs that fall outside the bound.

3.3.4 Results and Discussions

Considering two sets of weather conditions, three different expected values for the Gaussian noise w in simulating virtual occupants, and four controllers, there are a total of 24 cases being evaluated. Table 3.3 summarizes the performance statistics, which are averages of 20 simulation runs for each case. Simulation plots are presented in Figure 3.5 – Figure 3.12 for 6 different scenarios: *Scenario I* corresponds to $E[w] = 0$, *Scenario II* corresponds to $E[w] = -0.2$, and *Scenario III* corresponds to $E[w] = 0.2$, all for the time period in March; *Scenario IV*

corresponds to $E[w] = 0$, *Scenario V* corresponds to $E[w] = -0.2$, and *Scenario VI* corresponds to $E[w] = 0.2$, all for the time period in September.

A. RuleBased-PI versus MPC

Compared to the RuleBased-PI, Table 3.3 shows that in *Scenario IV* and *Scenario V*, the two deterministic MPC algorithms (MPC-PMV and CEMPC-DTS) have consistently less amount of energy consumption (used for cooling) while provide better thermal comfort (lower IOV), despite the possible bias in the PMV model. In *Scenario I* and *Scenario III*, the MPC-PMV still has a lower energy consumption (used for heating) and a lower IOV compared to the RuleBased-PI. In *Scenario I* and *Scenario II*, the CEMPC-DTS has a significantly reduced IOV (reducing IOV by 55%-75%) by using a comparable level of energy consumption (0- 7% more energy consumption), compared to the RuleBased-PI.

Figure 3.5 - Figure 3.8 shed some light on the underlying cause for energy savings with improved thermal comfort for MPC designs. The room temperature profiles given in Figure 3.5 and Figure 3.6 show that the RuleBased-PI tries to regulate the room temperature either to the heating set point at 24 Celsius in March or to the cooling set point at 26 Celsius in September, irrespective of the changes in relative humidity and occupant clothing levels. In contrast, room temperatures controlled by the three MPC designs are adjusted to adapt to the changes in RH and clothing levels. For example, in the second day the room temperatures controlled by MPCs are observed to follow a roughly flipped pattern of the humidity curve to maintain the same level of thermal sensation. In the third day, due to the increased clothing insulation level, indoor temperatures are reduced to a lower value to save energy consumption (see also Figure 3.7-Figure 3.8 for control input trajectories). Figure 3.9 and Figure 3.10 show that for all three MPC designs, AMV is closely regulated to be constant except the times when changes of RH and clothing level occur, but the AMV for the RuleBased-PI varies a lot.

For the time period in March with $E[w] = 0.2$, which implies that virtual occupants feel warmer than indicated by the PMV, extra heating provided by the RuleBased-PI and MPC-PMV leads to reduced IOV for thermal comfort constraint. The CEMPC-DTS has cut energy consumption by 8.5% compared to the Rule-Based PI, but at the expense of an increased IOV, which calls for a more stringent enforcement of the thermal comfort constraint. The corresponding CCMPC-DTS achieves a good balance between saving energy while reducing IOV compared to the RuleBased-PI. Similarly, for the time period in September with $E[w] = -0.2$, which implies that virtual occupants feel cooler than indicated by the PMV, both CEMPC-DTS and CCMPC-DTS cut down cooling power to save energy. Overall, the simulation results demonstrate that thermal-comfort based MPC designs allow the control of HVAC systems to adapt to environmental and occupant-associated changes and thus lead to reduced energy consumption and improved thermal comfort.

B. MPC-PMV versus CEMPC-DTS

Scenario I and *Scenario V* represent the cases where the PMV is assumed to be an accurate prediction for occupants' AMV ($E[w] = 0$). In both Figure 3.5(a) and Figure 3.6 it is shown that the difference between the two air temperature trajectories controlled by the MPC-PMV and CEMPC-DTS is very limited. The control input trajectories of the two controllers (shown in Figure 3.7(a) and Figure 3.8(a)) are also very close to each other except for the short periods when the changes in RH and clothing level occur. These discrepancies are mainly due to the learning error of the DTS model. Statistics from Table 3.3 also confirm this observation, with the CEMPC-DTS having a slightly higher energy consumption and IOV than the MPC-PMV.

Scenario II and *Scenario V* represent the case where PMV overestimates the AMV ($E[w] = -0.2$), i.e., the occupants feel colder/cooler than predicted by the PMV. As a result, the room temperature of the CEMPC-DTS is controlled at a higher value (close to 1 Celsius higher)

with more energy consumption in March (shown by Figure 3.5(b) and Figure 3.7(b)) and less energy consumption in September (shown by Figure 3.6(b) and Figure 3.8(b)) than the MPC-PMV to regulate the AMV at -0.5 (shown by Figure 3.9(b) and Figure 3.10(b)). Without feedback from occupants, the AMV resulted from the MPC-PMV is lower than the thermal comfort threshold of -0.5 scale.

In *Scenario III* and *Scenario VI*, occupants feel warmer than predicted ($E[w] = 0.2$) and thus less heating power is needed (*Scenario III*) and more cooling power is needed (*Scenario VI*). Case 7 of Table 3.3 shows that the CEMPC-DTS has cut the energy consumption more aggressively than desired and thus leads to a higher IOV than the MPC-PMV. This indicates that a better balance between the energy saving and thermal comfort is needed, which has been investigated in the design of the CCMPC-DTS.

For the completeness of information, Figure 3.11 and Figure 3.12 plot the offset parameter of the DTS model estimated by an EKF using occupants' feedback on thermal sensation. The variation of the offset parameter at the beginning of the first day is due to model calibration. Its variations at the second and third day show a clear adaptation to changes of the relative humidity and occupant clothing level.

Table 3.3. Performance statistics (average of 20 simulation runs).

Case Number	Weather Condition	Expected Value of Noise in Virtual Occupant	Controller	Energy(E): J	Violation Ratio(VR): %	Integration of Violation(IOV)
1	March	$E[w]=0$	RuleBased-PI	2.38e8	37.10	13.40
2			MPC-PMV	2.07e8	49.39	8.99
3			CEMPC-DTS	2.19e8	51.84	12.17
4			CCMPC-DTS	2.38e8	15.71	2.66
5		$E[w]=0.2$	RuleBased-PI	2.38e8	7.53	1.96
6			MPC-PMV	2.07e8	0.62	0.054
7			CEMPC-DTS	1.84e8	49.74	10.65
8			CCMPC-DTS	2.04e8	12.12	1.65
9		$E[w]=-0.2$	RuleBased-PI	2.38e8	61.09	43.00
10			MPC-PMV	2.07e8	99.08	57.37
11			CEMPC-DTS	2.56e8	51.93	14.53
12			CCMPC-DTS	2.74e8	18.35	4.25
13	September	$E[w]=0$	RuleBased-PI	1.96e8	41.16	22.82
14			MPC-PMV	1.82e8	49.27	9.12
15			CEMPC-DTS	1.70e8	49.39	13.81
16			CCMPC-DTS	1.86e8	19.44	3.60
17		$E[w]=0.2$	RuleBased-PI	1.96e8	71.48	55.32
18			MPC-PMV	1.82e8	99.13	57.37
19			CEMPC-DTS	2.03e8	53.65	14.43
20			CCMPC-DTS	2.25e8	20.23	3.62
21		$E[w]=-0.2$	RuleBased-PI	1.96e8	15.78	6.91
22			MPC-PMV	1.82e8	0.52	0.0291
23			CEMPC-DTS	1.37e8	42.05	11.17
24			CCMPC-DTS	1.53e8	17.43	3.26

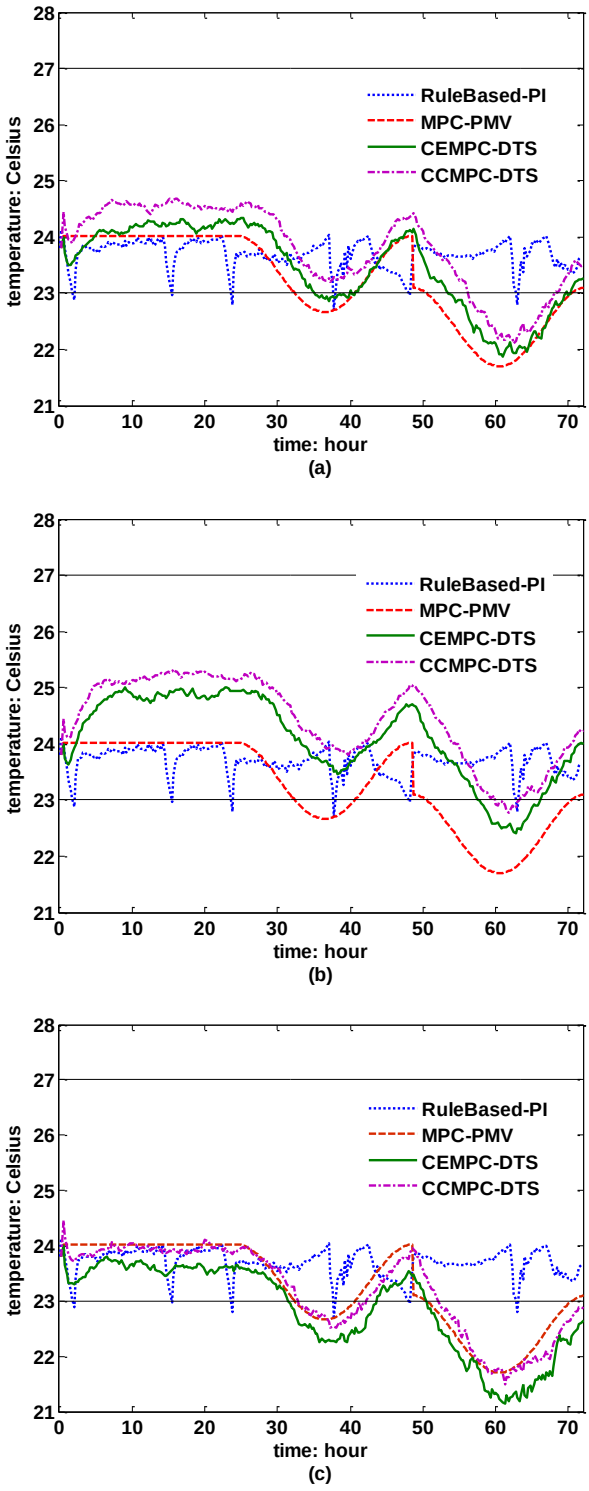

Figure 3.5. Controlled indoor air temperature. (a) Scenario I (March, $E[w]=0$). (b) Scenario II (March, $E[w]=-0.2$). (c) Scenario III (March, $E[w]=0.2$).

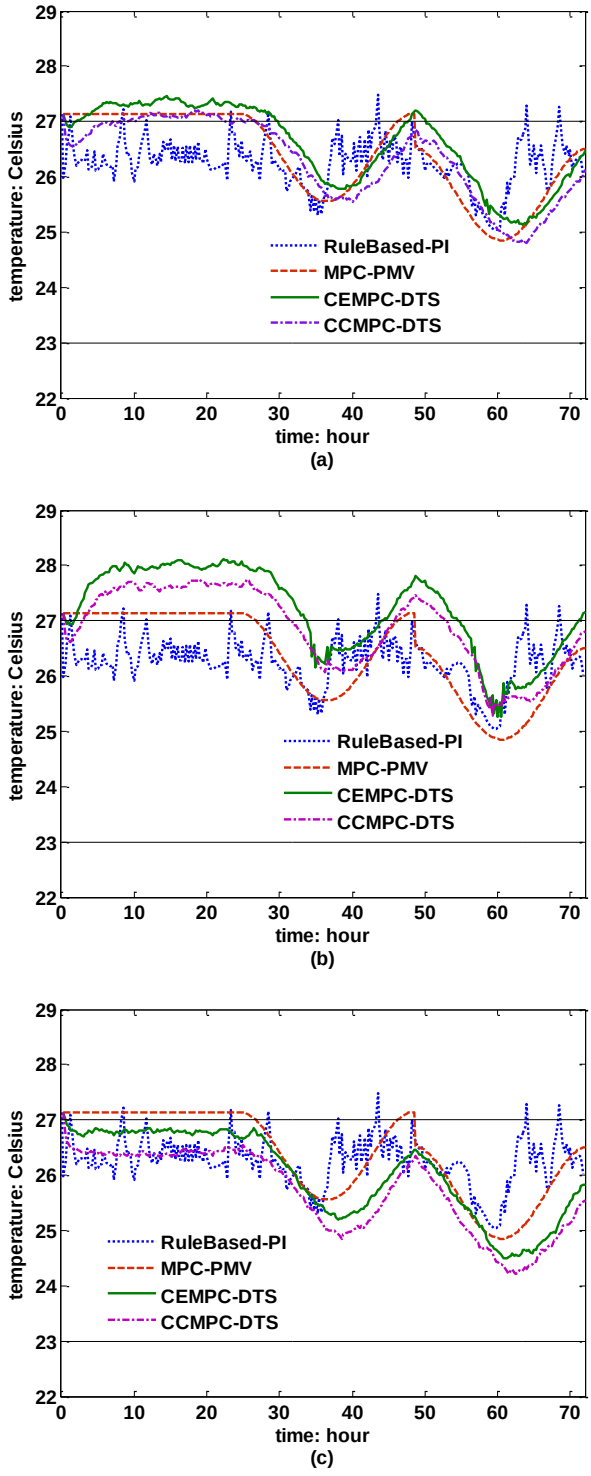

Figure 3.6. Controlled indoor air temperature. (a) Scenario IV (September, $E[w] = 0$). (b) Scenario V (September, $E[w] = -0.2$). (c) Scenario VI (September, $E[w] = 0.2$).

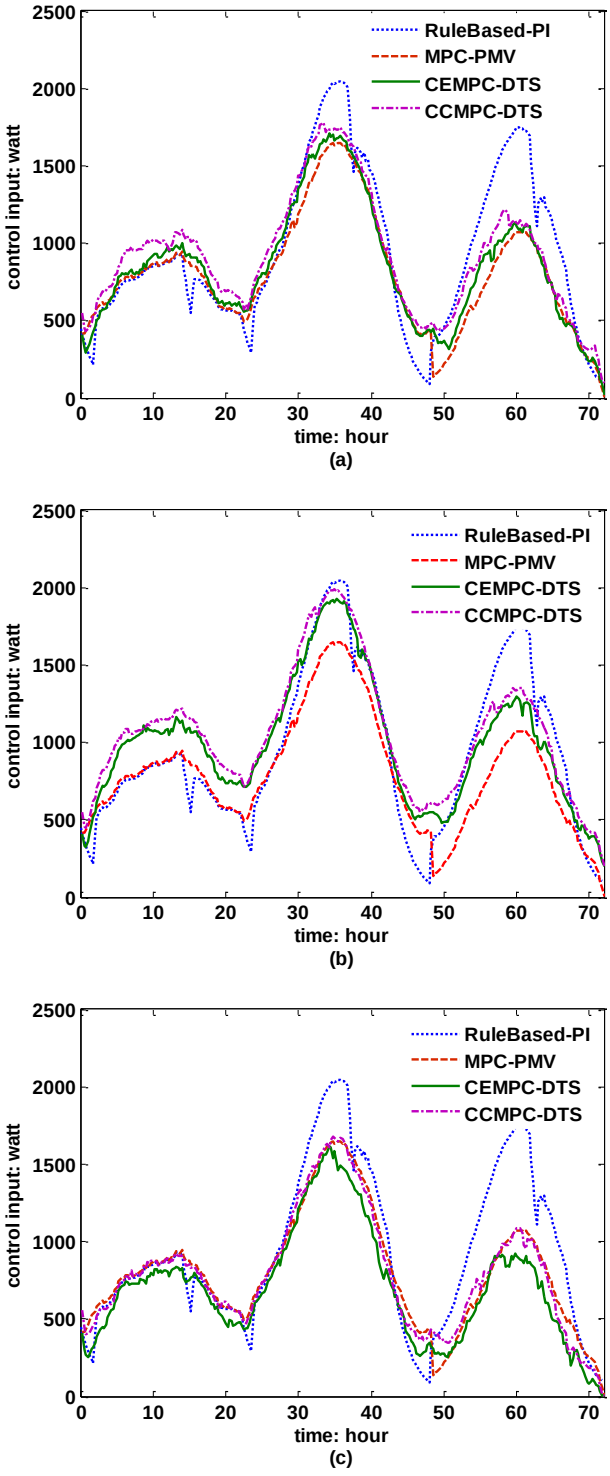

Figure 3.7. Control input. (a) Scenario I (March, $E[w] = 0$). (b) Scenario II (March, $E[w] = -0.2$). (c) Scenario III (March, $E[w] = 0.2$).

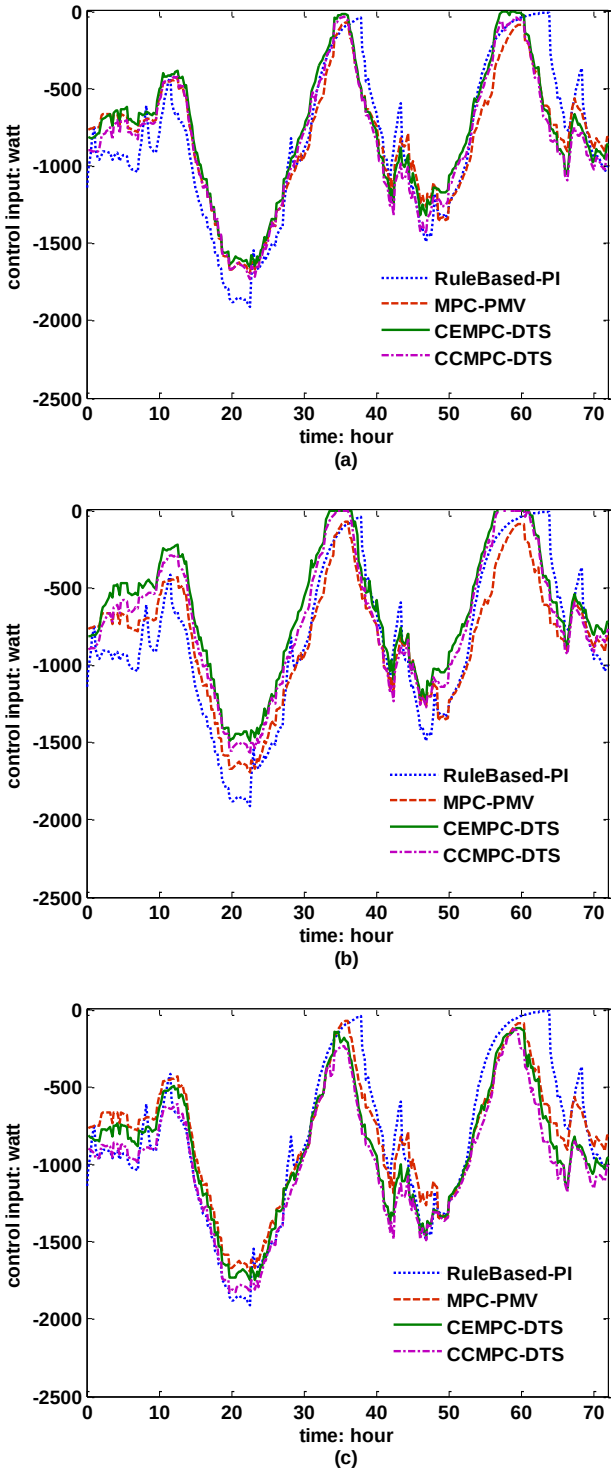

Figure 3.8. Control input. (a) Scenario IV (September, $E[w] = 0$). (b) Scenario V (September, $E[w] = -0.2$). (c) Scenario VI (September, $E[w] = 0.2$).

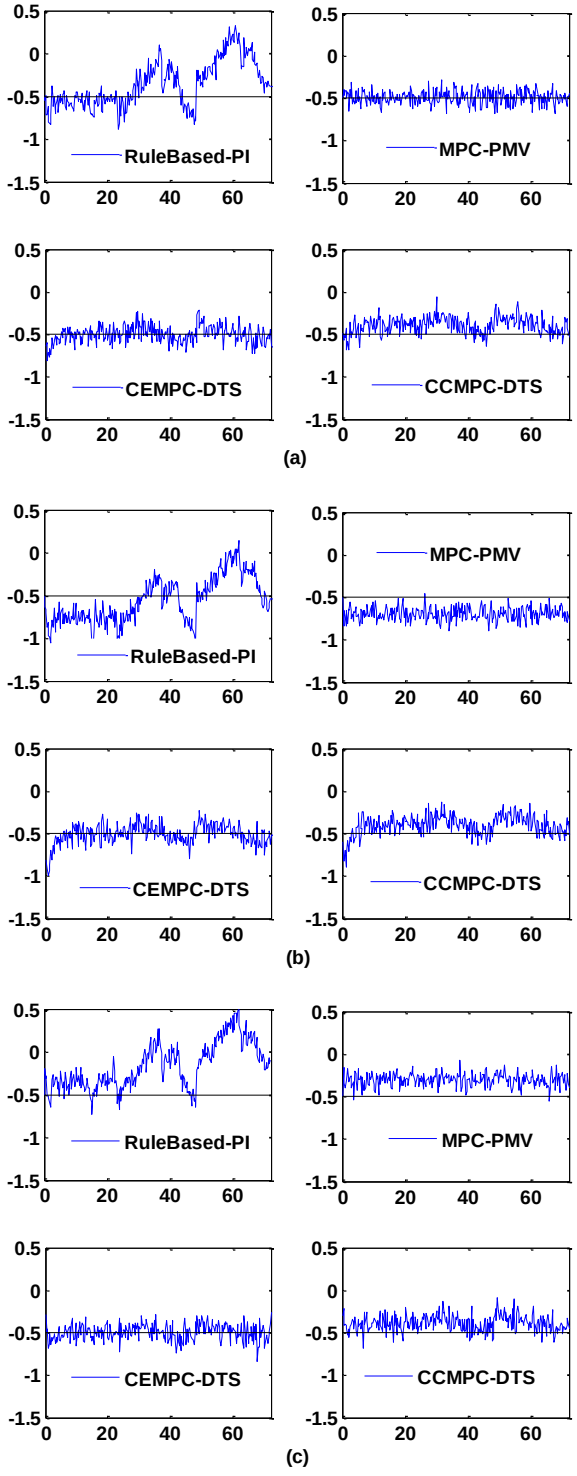

Figure 3.9. Actual mean vote (AMV) from virtual occupants. (a) Scenario I (March, $E[w] = 0$). (b) Scenario II (March, $E[w] = -0.2$). (c) Scenario III (March, $E[w] = 0.2$).

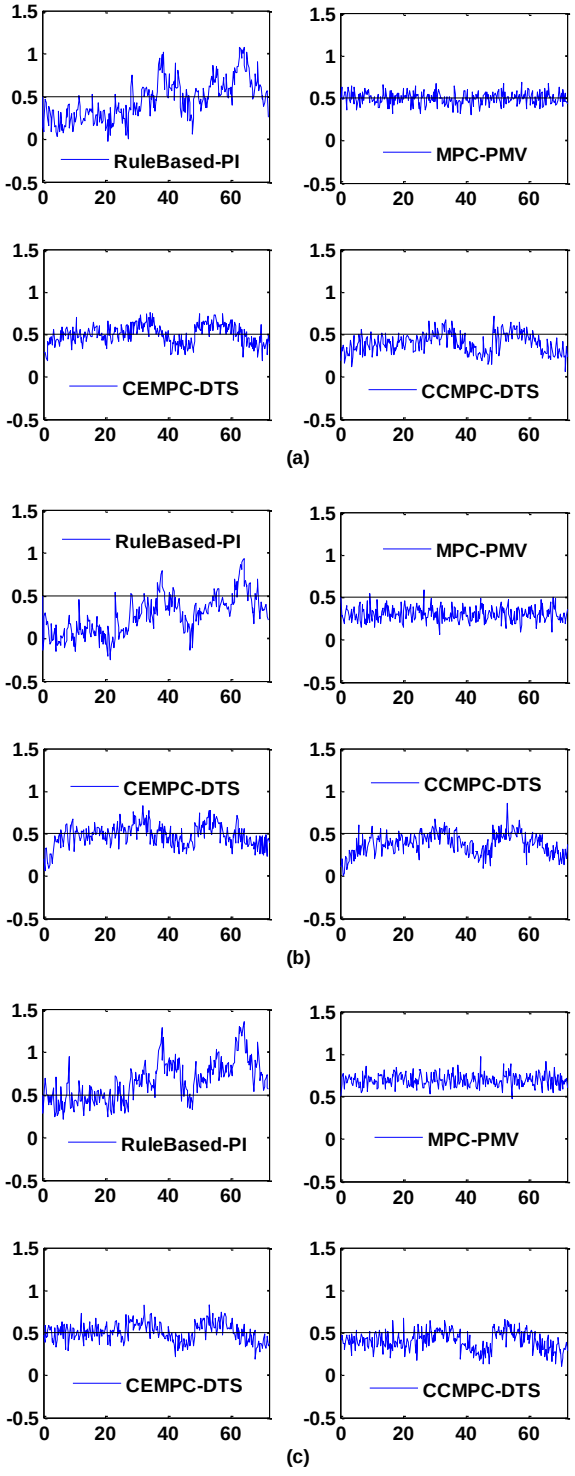

Figure 3.10. Actual mean vote (AMV) from virtual occupants. (a) Scenario IV (Sept., $E[w]=0$). (b) Scenario V (Sept., $E[w]=-0.2$). (c) Scenario VI (Sept., $E[w]=0.2$).

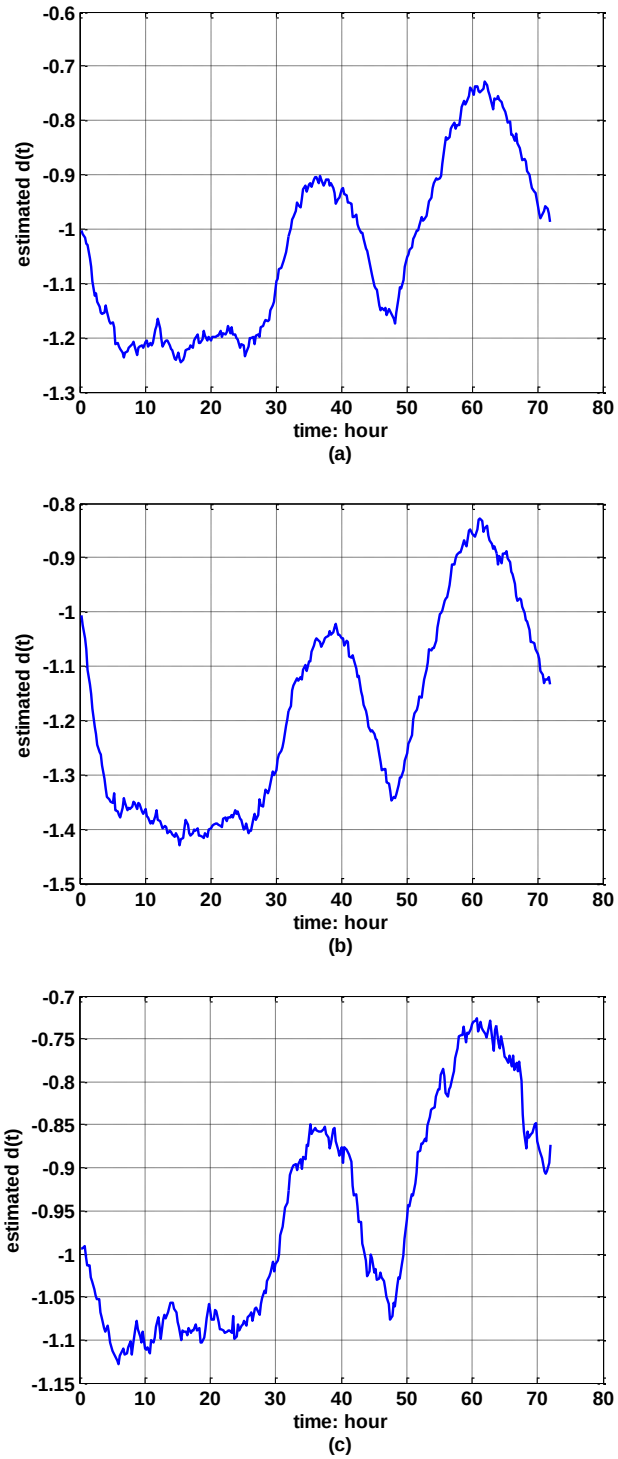

Figure 3.11. Time-varying offset parameter of the DTS model estimated by EKF. (a) Scenario I (March, $E[w] = 0$). (b) Scenario II (March, $E[w] = -0.2$). (c) Scenario III (March, $E[w] = 0.2$).

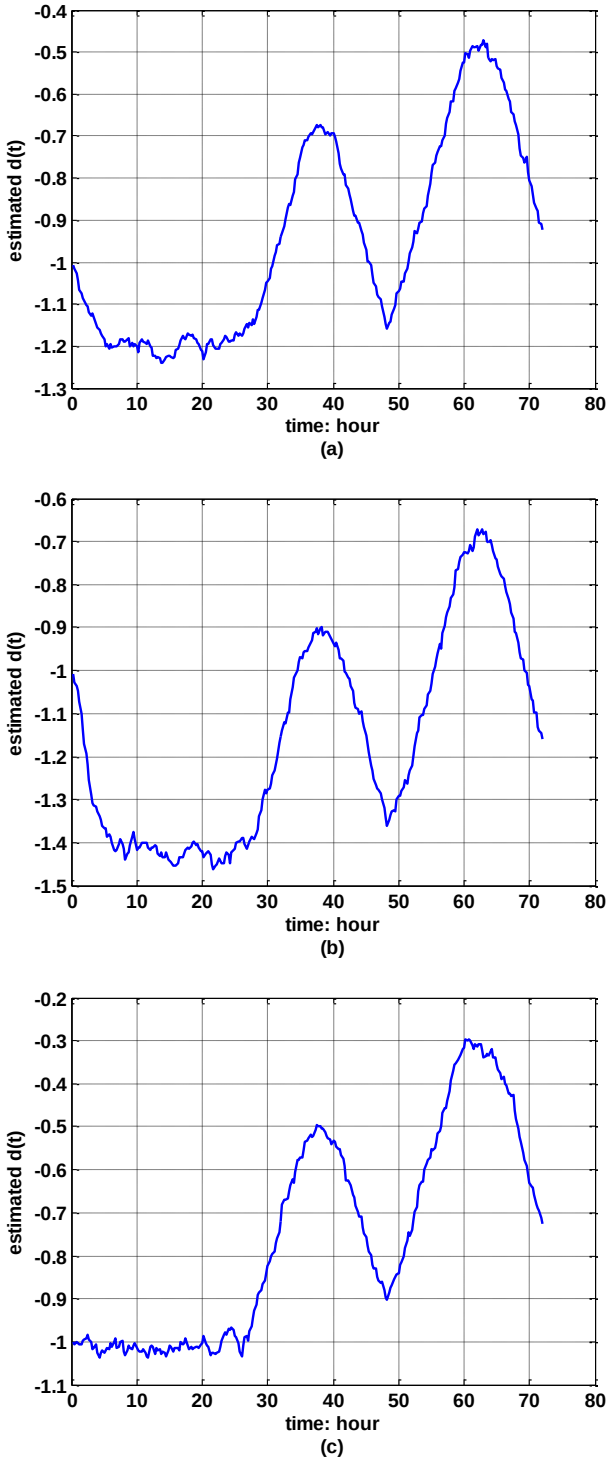

Figure 3.12. Time-varying offset parameter of the DTS model estimated by EKF. (a) Scenario IV (Sept., $E[w] = 0$). (b) Scenario V (Sept., $E[w] = -0.2$). (c) Scenario VI (Sept., $E[w] = 0.2$).

C. CEMPC-DTS versus CCMPC-DTS

Table 3.3 shows that the thermal comfort violation ratio VR is often high for the deterministic control approaches (Rulebased-PI, MPC-PMV and CEMPC-DTS), even when $E[w] = 0$. This implies that mean-vote based deterministic (or certainty-equivalent) controls are likely not able to meet the thermal comfort constraint if the variance of occupant perceptions of thermal sensation is large. The CCMPC-DTS provides an opportunity to directly specify the probability that thermal comfort constraint will be satisfied. In addition, the tighter bound on thermal comfort imposed by the deterministic approximation of the chance constraint helps to improve the thermal comfort level, though at the expense of a larger energy consumption. Table 3.3 shows that the CCMPC-DTS has the highest amount of energy consumption among all four controllers for most of the cases, but with a significantly lower VR and IOV.

D. Tuning α to achieve a balance between energy saving and thermal comfort

To investigate the tradeoff between energy saving and comfort violation, the probability α of thermal constraint violation is varied in the CCMPC-DTS to generate the Pareto frontier for energy consumption versus thermal comfort violation. Figure 3.13 shows that the RuleBased-PI is significantly farther right to the Pareto frontier for all except one case, indicating that the CCMPC-DTS can reduce energy usage and improve thermal comfort at the same time compared to the RuleBased-PI. When the PMV is an accurate prediction for the AMV ($E[w] = 0$), the energy consumption using DTS is slightly higher (3%-4% higher) than using PMV to achieve the similar level of thermal comfort. When there is a discrepancy between the PMV and AMV, thermal comfort improvement can often be achieved by the CCMPC-DTS with the same (or a

slightly higher) level of energy usage

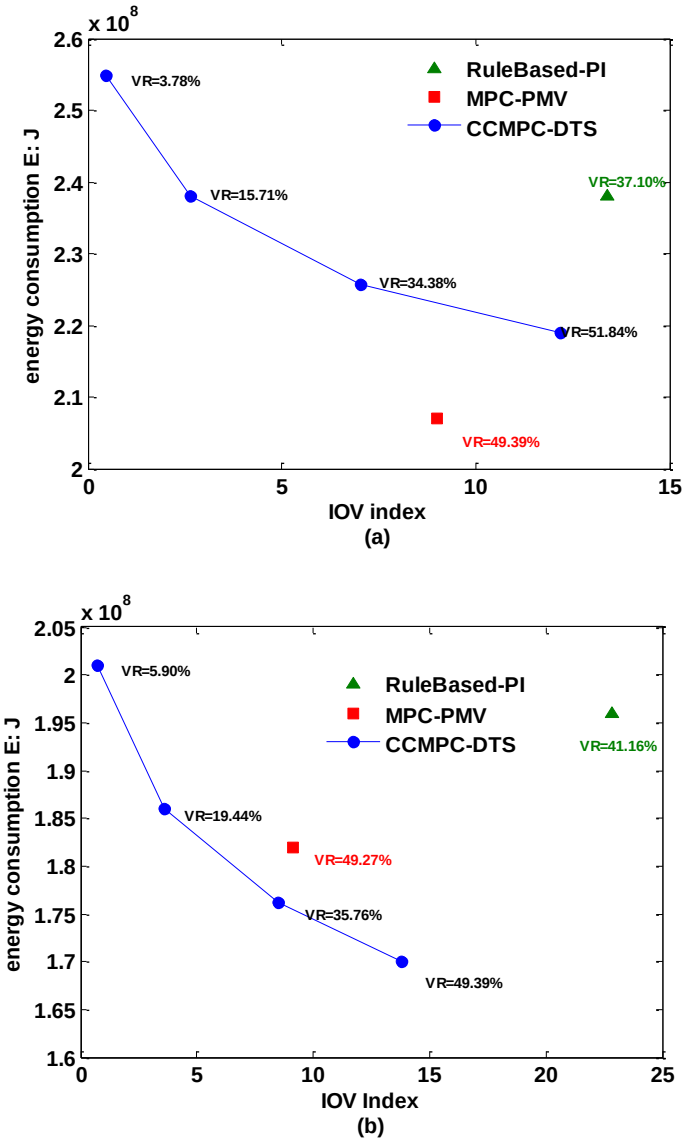

Figure 3.13. Pareto frontier of energy consumption versus thermal comfort violation. (a) March, $E[w]=0$. (b) September, $E[w]=0$.

Chapter 4

Chamber Experiment Evaluation of Occupant Feedback Based MPC

In this chapter, we present the chamber experiments used to evaluate the performance of the MPC based on the DTS model and compare its performance to the MPC based on PMV model. The experimental study not only has provided a feasibility test of implementing an occupant-feedback based MPC control but also has revealed underlying causes that allow the DTS based MPC achieve a better energy saving and thermal comfort than the PMV-based MPC.

This chapter is organized as followed. Section 4.1 describes the chamber model. A linear regression model is used to identify the chamber and the validation result is included. Section 4.2 explains the formulation of two certainty equivalence MPC designs based on DTS model and PMV model respectively. Compared with the MPC formulation in previous chapter, the MPC in chamber experiment is reformulated to take account of limitations of the actual HVAC system. Section 4.3 discusses the experiment design. Section 4.4 reports the experiment results and compares the two MPC controllers.

4.1 Chamber Model

The same chamber facility introduced in Chapter 2 was used in this experiment. Some modifications including adding a dry wall were made to the chamber after the experiment done in Chapter 2 and the locations of supply and return ducts were also changed and reflected in Figure 4.1. The schematic drawing of the chamber's HVAC system is shown in Figure 4.2. In the experiments, the supply air flow rate was kept at 325 m^3/h (with ±5% variation) and the supply

air temperature was controlled by the Allen Bradley PLC control system using a simple PI control. The dampers for outdoor air, exhaust, and recirculation in ducts were set at constant so that 10% of fresh outdoor air was mixed with return air.

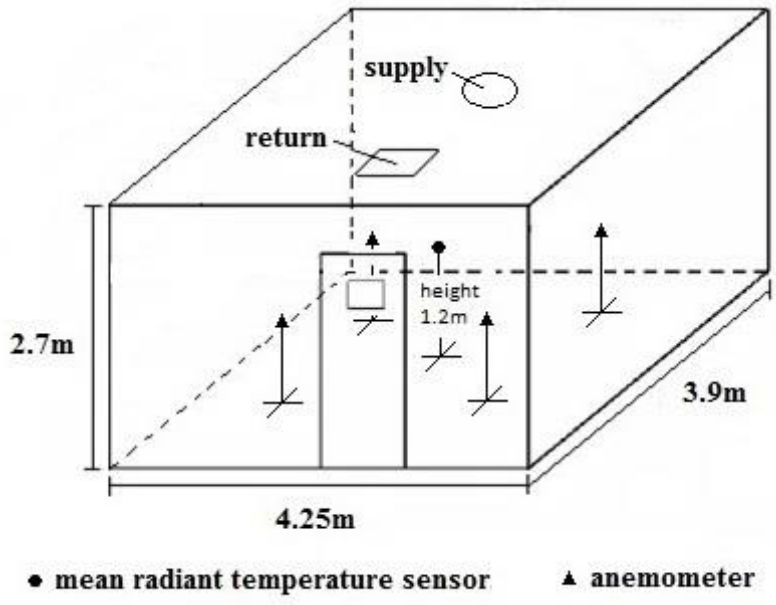

Figure 4.1. Chamber layout.

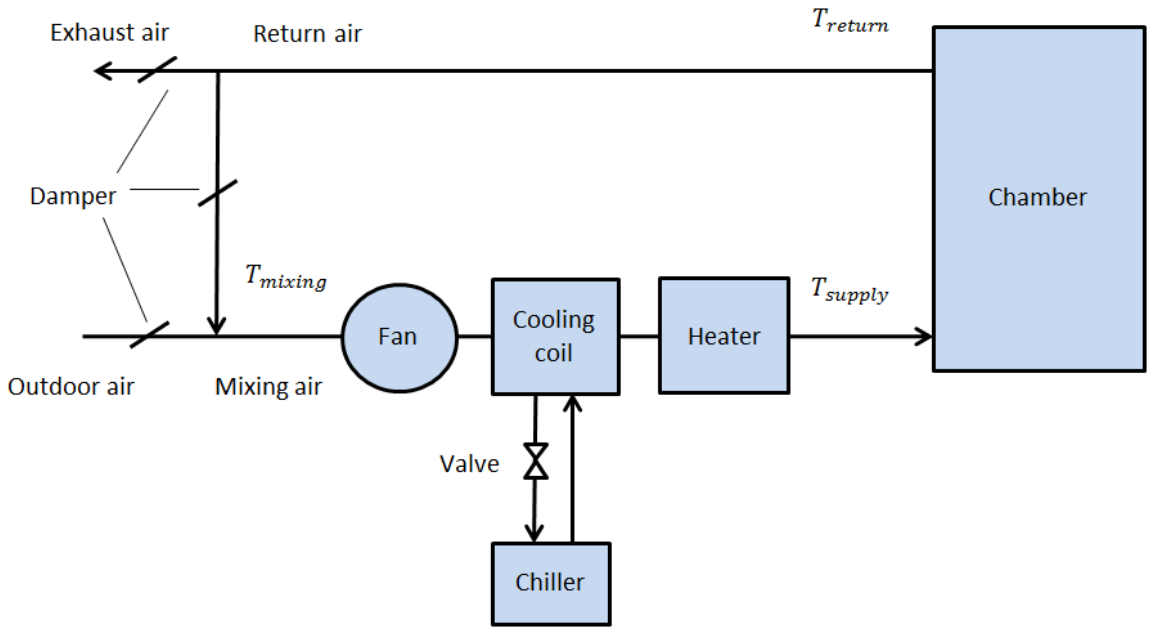

Figure 4.2. Chamber HVAC system schematic drawing.

It is possible to model the dynamic change of chamber temperature by a physical model constructed based on the energy balance principle. This study first tried to build a heat balance model on the zone air in EnergyPlus [74]. However, the resulting prediction results from such a heat balance model do not match well with measurement data on the chamber air temperature. As a result, a data-driven regression model is estimated instead, based on the collected input and output data with input variables selected based on energy balance.

The supply air temperature is chosen as the *only control input* in the chamber model. Other inputs to this model including air temperature outside the chamber and internal gains associated with occupants are considered to be known inputs (measurable). The *output* of the model is the predicted chamber temperature.

Figure 4.3 (a) shows the input/output data (training data) used for model identification. The supply air temperature initially started at 23.7 ℃, then stepped down to 13 ℃ for a little over 10 hours, raised up to 28 ℃ for another 10 hours, and finally went down to 24 ℃ for the rest of

the time. The chamber is located inside an office/classroom building and thus the temperature outside the chamber varied slightly within a small range (between 22 ℃ and 24 ℃). The internal gain associated with occupants was estimated by having one person carrying a laptop into the chamber for 6 hours when supply air temperature was maintained constant.

An autoregressive model with exogenous inputs was used to identify the chamber model. The resulting fitted model can be expressed in the following form:

$$\begin{aligned} T_{chmbr}(t+1) = {} & 0.965 \cdot T_{chmbr}(t) + 0.0286 \cdot T_{sply}(t) + 0.0523 \cdot T_{sply}(t-1) - 0.0257 \cdot T_{sply}(t-2) \\ & - 0.0315 \cdot T_{sply}(t-3) + 0.0133 \cdot T_{out}(t) + 0.0232 \cdot G_{in}(t) \end{aligned} \tag{4.1}$$

Where T_{chmbr} denotes the chamber temperature, T_{sply} denotes the supply air temperature, T_{out} denotes the temperature outside the chamber and G_{in} denotes the internal gain. The sampling time of this model is 5 min. Different orders of the model have been tried and further increase of model order does not improve model prediction performance significantly.

Figure 4.3(a) shows that the predicted chamber air temperature matches the measured chamber temperature very well, with the coefficient of determination $R^2 = 99.14\%$. Two new sets of input data were used to validate the chamber model (4.1). Figure 4.3(b) shows the model validation corresponding to a new trajectory of supply air temperature (with a flipped pattern of the one used for identification). The temperature outside the chamber was slightly lower than the one used for identification, and there was no occupant in the chamber. The predicted chamber air temperature is very close to the measurement, with $R^2 = 98.82\%$. Figure 4.3(c) shows the model validation with respect to G_{in}, with three occupants staying three hours in the chamber. The resulting error between the model predication and measurement is around 0.26℃, with $R^2 = 61\%$.

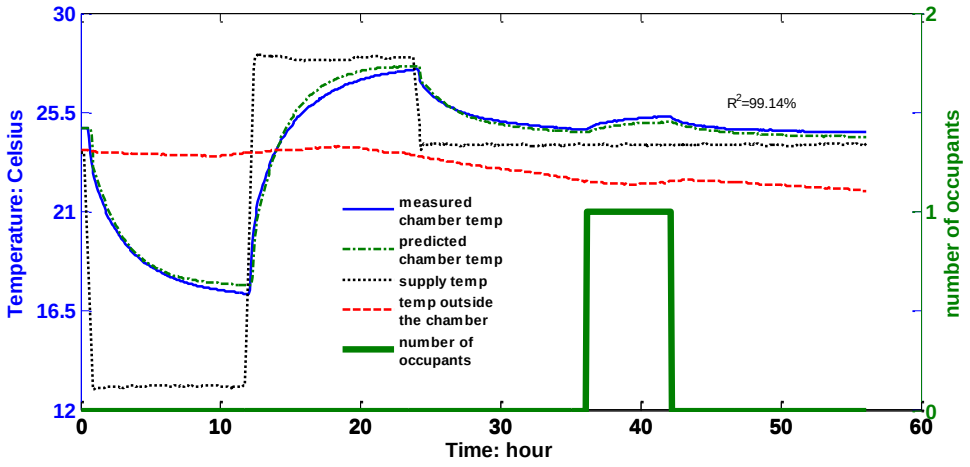

(a)

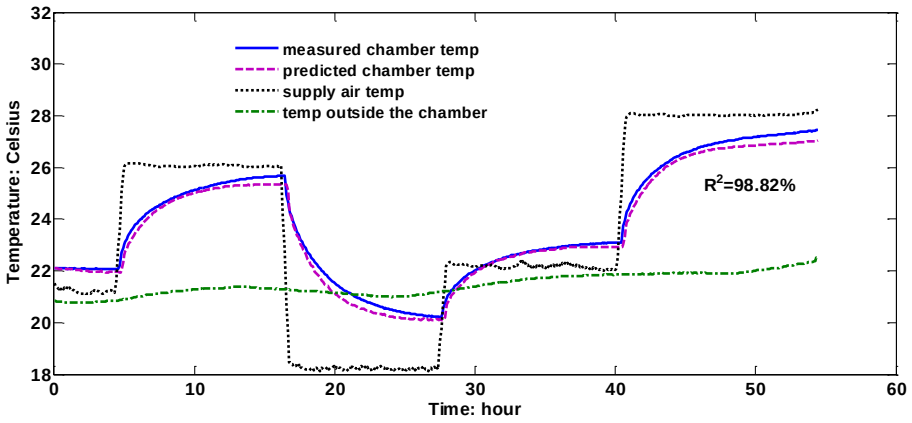

(b)

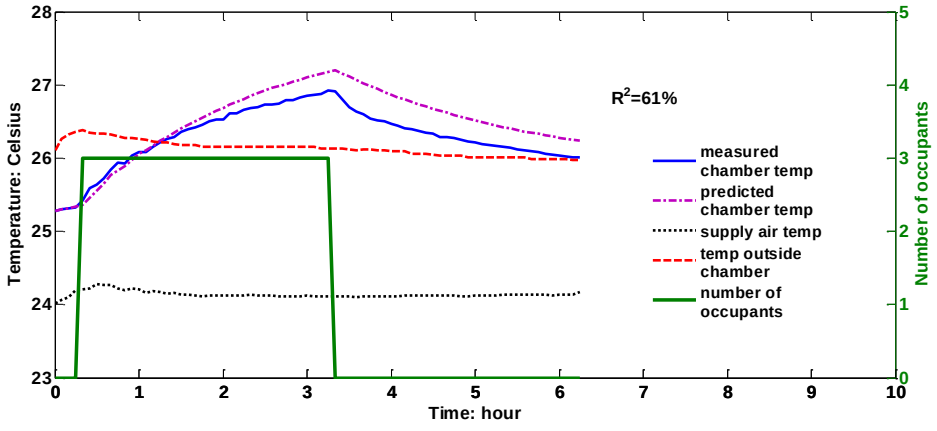

(c)

Figure 4.3. Chamber model identification and model validation. (a) predicted chamber temperature vs. measured chamber temperature under the training supply air temperature, R^2 = 99.14%; (b) model validation using a new trajectory of supply air temperature with no occupant, R^2 = 98.82%; (c) model validation using a new trajectory of number of occupants, R^2 = 61%.

4.2 Chamber Experiment MPC Formulation

Model predictive control utilizes both the chamber model and the thermal comfort model (either PMV or DTS) to calculate the optimal value of supply air temperature (which is the control input) for the chamber. The supply air temperature has an optimal value in the sense that least amount of energy will be consumed in order to maintain the chamber temperature such that occupants' thermal comfort level is within its boundary for most of the time.

The MPC is formulated as follows:

Cost:

$$\min_{\mathbf{T}_{sply}(t)} J_t := \sum_{k=1}^{N}[T_{sply}(t+k\,|\,t)-T_{chmbr}(t)]^2 + \lambda_1\sum_{k=1}^{N}[T_{sply}(t+k\,|\,t)-T_{sply}(t+k-1\,|\,t)]^2 + \lambda_2\sum_{k=1}^{N}[q(t+k\,|\,t)] \tag{4.2}$$

Subject to

Chamber model:

$$\begin{aligned} T_{chmbr}(t+k+1\,|\,t) = {} & 0.965\cdot T_{chmbr}(t+k\,|\,t) + 0.0286\cdot T_{sply}(t+k\,|\,t) + 0.0523\cdot T_{sply}(t+k-1\,|\,t) \\ & - 0.0257\cdot T_{sply}(t+k-2\,|\,t) - 0.0315\cdot T_{sply}(t+k-3\,|\,t) \\ & + 0.0133\cdot T_{out}(t+k\,|\,t) + 0.0232\cdot G_{in}(t+k\,|\,t) \end{aligned} \tag{4.3}$$

Thermal sensation model:

$$TS(t+k\,|\,t) = f(T_{chmbr}(t+k\,|\,t), T_{chmbr}(t+k-1\,|\,t), \ldots) \tag{4.4}$$

Constraints on thermal comfort:

$$y_{\min} - q(t+k\,|\,t) \le TS(t+k\,|\,t) \le y_{\max} + q(t+k\,|\,t) \tag{4.5}$$

$$q(t+k\,|\,t) \ge 0 \tag{4.6}$$

Constraints on supply air temperature:

$$T_{sply}^{\min} \le T_{sply}(t+k\,|\,t) \le T_{sply}^{\max} \tag{4.7}$$

$$-\Delta T_{sply} \le T_{sply}(t+1\,|\,t) - T_{sply}(t) \le \Delta T_{sply} \tag{4.8}$$

Where $\mathbf{T}_{sply}(t) = [T_{sply}(t+1|t), \cdots, T_{sply}(t+N|t)]$ denotes the vector of supply air temperature (vector of control input) along the prediction horizon of size N.

The cost function J_t has three components. The first component is the L_2 norm of the difference between the chamber supply air temperature and the chamber temperature. Note that the return air temperature is considered to be equal to chamber temperature. If we ignore the disturbance due to outdoor fresh air, the supply air temperature will be equal to return air temperature (or chamber air temperature) when both heater and chiller are off. Thus first part of the cost function is essentially proportional to energy consumption of the HVAC system. The second component of J_t is the L_2 norm of the difference between two consecutive control inputs, which is used to smooth the control inputs. The coefficient λ_1 was set to 100 in the experiments. The third part is the L_1 norm of the slack variable $q(t+k|t)$. The coefficient λ_2 of this term is usually set to be very large so that the slack variable can be minimized. In this study, λ_2 was set to 1000.

Depending on which thermal comfort model the MPC uses, the generic model expressed in (6) can be replaced by either PMV or DTS model. For example, in the MPC-PMV formulation, Fanger's PMV model is used:

$$TS(t+k|\mathrm{t}) = PMV(T_{chmbr}(t+k|t), T_{mr}, RH, V_a, CLO, M) \tag{4.9}$$

Where the chamber temperature $T_{chmbr}(t+k|t)$ is predicted from the chamber model (4.1); mean radiant temperature T_{mr}, relative humidity *RH* and air velocity V_a are measured by the chamber DAS; and occupants' clothing insulation level *CLO* and metabolic rate (activity level) *M* are recorded as well.

In the MPC-DTS, the thermal sensation model in (4.4) is replaced using the DTS model:

$$\hat{x}(t+k+1|t) = 0.798 \cdot \hat{x}(t+k|t) + 0.0610 \cdot \hat{x}(t+k-1|t) + T_{chmbr}(t+k|t) - 0.883 \cdot T_{chmbr}(t+k-1|t) \tag{4.10}$$

$$\hat{y}(t+k\mid t)=\frac{3.033}{\exp[-0.558\cdot(\hat{x}(t+k\mid t)-7.931)+8.166]+1}+\hat{d}(t+k\mid t) \tag{4.11}$$

$$TS(t+k\mid t)=\hat{y}(t+k\mid t) \tag{4.12}$$

Assuming that the process noise $e(k)$ and sensing noise $v(k)$ in (2.3-2.4) are Gaussian with zero mean, the above equations hold by applying expected value to (2.2-2.3).

A soft constraint (4.5) with slack variable q is formulated for maintaining the thermal sensation within the bounds $y_{\min}(=-0.7)$ and $y_{\max}(=0.7)$ to avoid infeasibility in solving the resulting MPC. Due to the limitation of the HVAC system, the control input (or supply air temperature) is bounded by $T_{sply}^{\min}=11^{o}C$ and $T_{sply}^{\max}=38^{o}C$. A constraint on the maximum allowed change of two consecutive control inputs, ΔT_{sply}, is imposed. The value of ΔT_{sply} was determined by step response of the PI control and was set to be ΔT_{sply} = 4 in this study.

4.3 Experiment Design

Chamber experiments were designed to experimentally evaluate the MPC control based on the DTS model, and to compare its performance to the PMV-based MPC. The chamber experiments with human subjects were approved by the Institutional Review Board at the Pennsylvania State University (IRB # 41077). In two consecutive weeks of June 2015, 12 experiments were conducted with each experiment lasting for 3 hours. For the 6 experiments conducted in the mornings of June 8, 9, and 10 as well as the afternoons of June 15, 16 and 17, the MPC-PMV controller was used. For the 6 experimentsconducted in the afternoons of June 8, 9, and 10 as well as the mornings of June 15, 16, and 17, the MPC-DTS controller was used. The weather conditions of the two weeks were very similar with most days rainy or cloudy, and thus

cooling applications were tested in the experiments. Histories of chamber air relative humidity and mean radiant temperature (MRT) of each individual experiment are given in the Appendix D.

For each experiment, there were 4 participants which were the maximum that can be accommodated by the chamber. There were a total of 19 participants including undergraduate, graduate students and postdoc researchers. Some of them attended just one experiment and others attended multiple experiments. During each experiment, each participant submitted a thermal sensation vote every 5 minutes. A total of 1776 votes were collected for the entire group of experiments.

During each experiment, artificial variations were introduced in the parameters that affect occupants' thermal sensations so that the MPC controller had to adjust the chamber temperature to adapt to these changing parameters. In the numerical studies conducted in [75], both occupants' clothing insulation level and indoor relative humidity were changed to follow pre-designed patterns, and then the MPC controllers reacted to such changing conditions through cooling or heating, where the MPC-PMV and MPC-DTS were compared in terms of energy consumption and occupant thermal comfort. However, it is worth pointing out that accurate control of humidity level is not easy and it is almost infeasible to repeat the same history of humidity level from one chamber experiment to another. As a result, this study only recorded the humidity and analyzed its impact on thermal comfort. The only introduced perturbation was occupants' clothing levels. During the experiments, participants were asked to wear and adjust their clothing levels specified in Table 4.1, where they started with $I_{cl} = 0.65$ for the first 80 minutes, and then increased their clothing level to $I_{cl} = 0.95$ for the rest of the time.

Table 4.1. Clothing insulation level during each experiment.

Experiment time	Estimated clo-value(I_{cl})	Typical clothes ensembles
0 – 80 min	0.65	Pants, short-sleeve shirt, and shoes (no open toe shoes)
80 – 180 min	0.95	above ensembles plus one piece of long-sleeve shirt/sweater/light jacket(or other similar level of clothes)

Figure 4.4 displays the control diagram of the chamber experiment. A two-level control architecture is applied. On the top level, based on the measurements collected from chamber DAS (or occupants' feedback), the MPC controller, which is running on a PC using *Yalmip* toolbox in *MATLAB*, calculates the optimal supply air temperature T_{sply}^{*}. On the low level, the actual supply air temperature is controlled by the heater/chiller (percentage of opening) of the HVAC system using a PI control running on the PLC to achieve T_{sply}^{*}. Since MPC-DTS and MPC-PMV use different thermal sensation models, measurements for feedback are different for each controller. For instance, the MPC-PMV receives feedback on temperatures inside and outside the chamber along with relative humidity, air velocity, mean radiant temperature and occupants' clothing insulation levels. The MPC-DTS receives temperatures inside and outside chamber as well as thermal sensation votes from participants. The real-time feedback of occupants used by the MPC-DTS was the actual mean vote of all 4 participants and this information was sent through a wireless communication channel to the PC running the MPC-DTS.

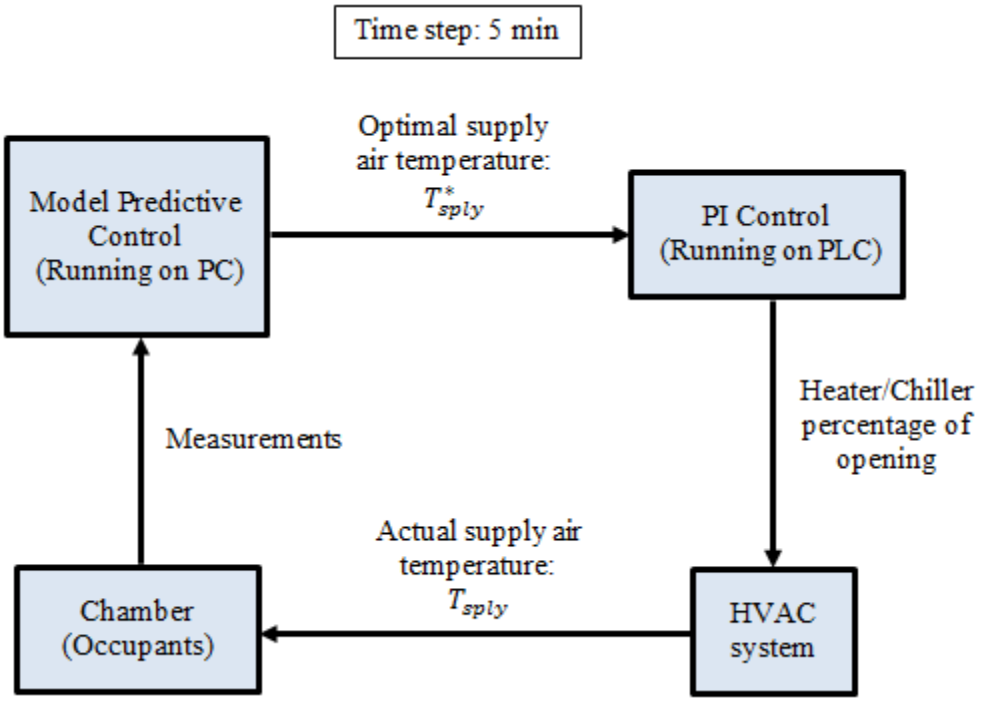

Figure 4.4. Diagram of a two-level control. On the top level, a MPC running on a PC determines the optimal supply air temperature; on the low level, a PI control running on PLC regulates the Heater/Chiller percentage of opening of the HVAC system to achieve the optimal supply air temperature. For the MPC-DTS, the MPC receives measurements of occupants (votes on thermal sensation) and for the MPC-PMV, the MPC receives measurements of chamber thermal conditions to compute PMV.

4.4 Results and Analysis

Recall that the chamber could only accommodate 4 participants at the same time. In order to compensate for the limited size of participants in each experiment, repeated experiments were conducted. Though experiments were repeated in different days, the conditions of each individual experiment shown in the Appendix D indicated that the across-experiment variations in thermal parameters such as chamber relative humidity, chamber MRT, and chamber air temperature are small. As a result, it is fair to use the average parameter values across 6 groups of experiments to evaluate each controller (MPC-PMV or MPC-DTS).

Figure 4.5 shows the average relative humidity history used in the MPC-PMV experiments versus that used in the MPC-DTS experiments (RH histories for individual experiments are given in the Appendix D). It can be observed that the two RH trajectories are very close to each other for the first 80 minutes of the experiment, where the initial increase in RH was due to the moisture brought in by the participants. There was a sudden decrease in RH at t = 80 min for the MPC-PMV, while the decrease of RH for MPC-DTS was more gradual. Note that the moisture of the chamber was mainly removed by the cooling coil. The difference in RH between the two controllers at t = 80 min were due to their reaction to the change of occupants' clothing levels at t = 80 min (more details given later), leading to different control of chiller percentage of opening. The difference of RH for the two controllers after t = 2 hour were mainly due to their respective thermal comfort models.

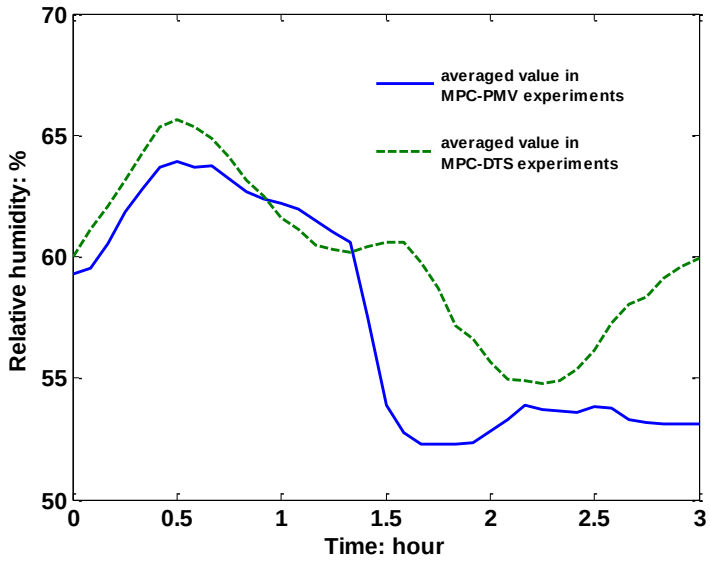

Figure 4.5. Mean history of chamber air relative humidity.

Figure 4.6 shows the mean supply air temperature history of the two MPC controllers as well as the percentage of chiller/heater openings of the HVAC system (note that the values of

heater openings are negligible due to the cooling application conducted in the experiments). The resulting chamber air temperature responses are given in Figure 4.7. Note that each curve in the figures represents the mean computed over 6 groups of experiments, and individual trajectories are given in the Appendix D. From Figure 4.6, it is observed that the errors between the optimal supply air temperatures T^{*}_{sply} calculated by the MPCs and the actual supply air temperatures provided by the HVAC system were very small. During the first 80 minutes of experiments, the mean histories of chamber temperature under the two MPCs were very close (shown in Figure 4.7), though the T_{sply} curve of the MPC-DTS had a larger oscillation ($\pm 1^{o}C$ around 24 ^{o}C) than that of the MPC-PMV (which had no overshoot) due to that the DTS model started from an bad initial value and was still in the learning period (shown in Figure 4.8).

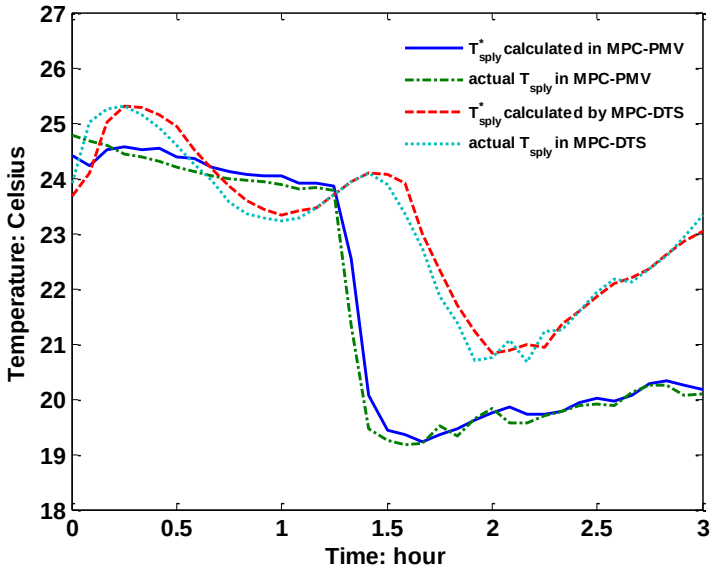

(a)

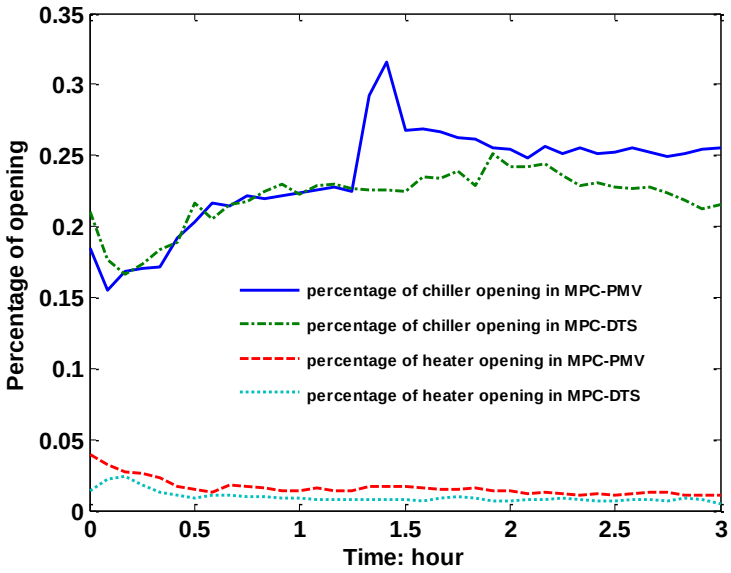

(b)

Figure 4.6. Mean history of control input. (a) Supply air temperature. (b) Chiller/heater openings.

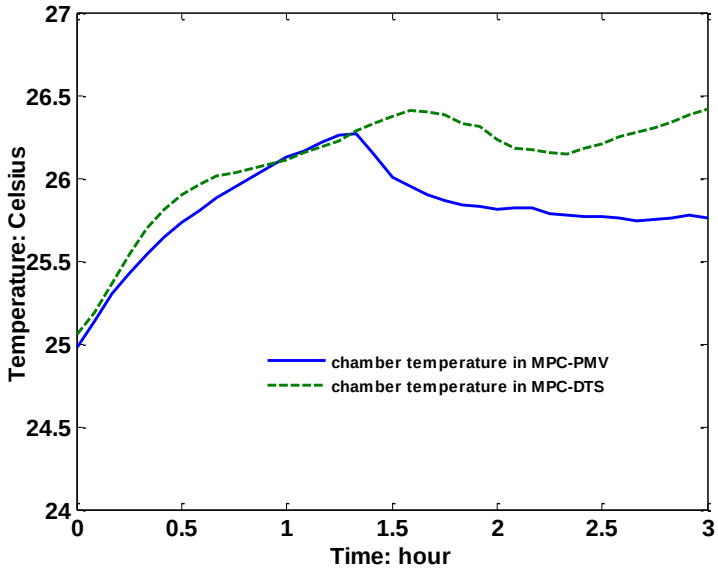

Figure 4.7. Mean chamber temperature history.

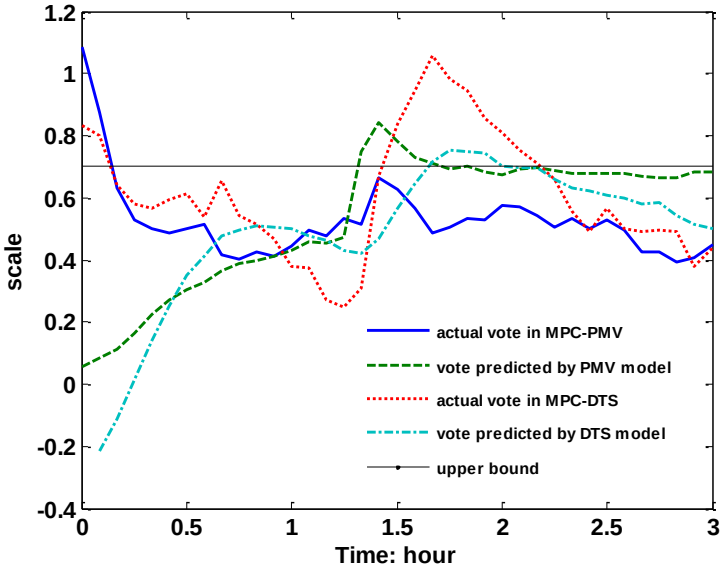

Figure 4.8. Thermal sensation votes. Under each MPC design, AMV of occupants was collected (blue solid line represents the AMV collected under MPC-PMV and red dotted line represents the AMV collected under MPC-DTS). There are errors between predictions of PMV/DTS and the corresponding AMVs.

As soon as the occupants put on an extra layer of clothing at t = 80 min, MPC-PMV quickly reduced the supply air temperature close to 19 ^{o}C so that the effect of increasing clothing insulation can be compensated by a lower chamber temperature to maintain thermal comfort. Compared to the sudden reduction of T_{sply} in MPC-PMV, there was a delay in reducing the supply air temperature in MPC-DTS and the T_{sply}'s decreasing rate was much smaller. Such different reactions of the two MPC controllers to the increase of clothing level can be explained by their respective thermal comfort models used in the MPC design. As illustrated in Figure 4.8, the PMV instantly increased with the increase of clothing level, which triggered the sudden increase of supply air temperature. In contrast, it took some time for the DTS model to adapt to participants' AMV and make corrections. The adaptive learning time of the DTS model depends on factors such as the variance of sensing noise and artificial noise introduced for offset parameter in (2.2) used in the EKF [67]. As a result, during the transient period after sudden change of thermal environment, the MPC-PMV could provide a better thermal comfort by larger energy consumption.

However, after t > 2 hr, the chiller opening under the MPC-PMV approached steady-state; in contrast, the chiller opening under the MPC-DTS started to reduce after t= 2.3 hr (with T_{sply} increasing). As a result, the chamber temperature under the MPC-DTS had been higher than that under the MPC-PMV. In the meanwhile, Figure 4.8 shows that the AMV under the MPC-DTS were under the upper bound after t = 2.3 hr, indicating that occupants' thermal comfort was maintained. The comparison of the two MPCs in this period has demonstrated that the MPC-DTS is capable of energy saving while still maintaining thermal comfort.

Since the DAS system does not have the flow measurement of the chilled glycol/water mixture, it is not possible to estimate the power consumption of chiller from water loop. A less accurate way to compare the power consumption is to look at the air side. Cooling power is

proportional to the enthalpy change of the air. In cooling application, both sensible and latent load need to be considered. Based on the supply air temperature, return air temperature and its flow rate, the sensible load can be calculated using following equation:

$$Q_s = c_p \times \dot{m} \times (T_{return} - T_{supply}) \tag{4.13}$$

Were c_p is the specific heat of air, $\dot{m}$ is the air mass flow rate, T_{return} is the return air temperature, and T_{supply} is the supply air temperature. By integrating the load over 3 hours using following equation:

$$E = \sum_{t=1}^{36} Q_s(t) \tag{4.14}$$

the averaged cooling power among 6 experiments due to sensible loads are calculated to be $3.60 \times 10^6 J$ and $4.83 \times 10^6 J$ respectively for MPC-DTS and MPC-PMV. From Figure 4.5 it is observed that more moisture was removed in MPC-PMV than in MPC-DTS experiment. Thus the latent load in larger in MPC-PMV than in MPC-DTS. Overall it can be estimated that MPC-DTS used much less energy.

The results for level of comfort can be examined from Figure 4.8. In both MPC-PMV and MPC-DTS experiments, the actual thermal sensation votes collected from participants were much higher than its model prediction at the beginning. Because some participants walked from other buildings on Campus before entering the chamber and his or her metabolic rate was higher than the metabolic rate corresponding to sedentary activity. The actual votes settled down after 15 min. During the second half of experiment, the prediction given by PMV stayed around the upper bound of comfort constraint. On the other hand, the corresponding actual vote in MPC-PMV experiment was under the upper bound. By examining the curve given by DTS model prediction, it can be seen that thermal sensation keeps climbing up from -0.2 to 0.5 at the beginning. This is due to two reasons. Firstly the chamber temperature increased during this time. Secondly the actual mean vote is higher than the model prediction so DTS model adaptively increased its offset

parameter. There is a very steep ramp in the actual votes in MPC-DTS curve from 80 min to 100 min. During this time the ramp in the vote given by DTS model is gentler. Ignoring the big gap between model prediction and actual measurement in the first half hour, actual votes from participants are consistently lower than PMV model prediction. In MPC-DTS from t = 1.42 hr to t = 2.17 hr, actual votes is out of the upper bound. During this period the DTS model was adaptively learning from the feedback from participants and it took some time for the model to catch up and correct its prediction.

Chapter 5

Conclusion and Future Work

5.1 Conclusion

In this dissertation, we developed an empirical state-space model of the Hammerstein–Wiener structure, specifically a Wiener model with logistic output function, for thermal sensation resulting of ambient temperature changes. The model takes air temperature as input, and defines mean thermal sensation as a state variable, and the occupant actual mean vote as an output. A chamber experiment provided thermal data and occupant thermal sensation votes to estimate the model coefficients. Comparison of the developed Wiener-logistic model to the classic Fanger's PMV model and a modified Fiala's model for dynamic thermal sensation was conducted. By considering a Wiener-logistic model with a time-varying offset parameter estimated by an Extended Kalman Filter using occupant feed-back, this study also showed that when indoor environmental or occupant associated conditions deviate from the nominal condition conducted in the chamber experiment, the consistency check of the EKF can automatically detect the changes, and re-estimation of the offset parameter can effectively correct the model predictions of thermal sensation.

Furthermore, two model predictive control strategies using the developed data-driven DTS model were developed as complementary design tools to the PMV-based MPC control for optimizing indoor thermal comfort and energy saving. The proposed chance-constrained MPC was designed to allow specifying the probability of violation of thermal comfort constraint, in order to achieve a balance between energy saving and thermal comfort. Simulation results

demonstrated that when the PMV model provides an accurate prediction for occupants' AMV, the DTS-based MPC designs are able to achieve a similar level of thermal comfort and energy consumption without the sensor data and computation required by the PMV. When there is a discrepancy between the PMV and AMV, the proposed DTS model based MPC designs could potentially outperform the PMV-based MPC by providing a better indoor thermal comfort. The DTS model based MPC algorithms developed in this study assume that there is a feedback channel for occupants to communicate their thermal perceptions to the control system, which is lacking in the current building control systems.

Lastly, experimental evaluation of the proposed DTS based MPC design algorithms in a chamber environment was conducted. The designed controller directly utilized information received from occupants in the real time control. To the best of our knowledge, it is the first study that included occupant feedback in HVAC control system. The MPC based on PMV model was also tested. It was shown that less cooling was used in MPC-DTS than in MPC-PMV. The thermal comfort was maintained well by both controllers. It is observed that actual mean vote from participants was below the upper bound in MPC-PMV. Actual mean vote in MPC-DTS was also within the constraint most of the time except for the period during which the DTS model has to learning from occupants about the change induced by the added clothing insulation. The experiment results demonstrated that the DTS-based MPC using occupant feedback provides the opportunity to significantly save energy consumption while maintain occupant thermal comfort.

5.2 Future Work

The chamber experiment in Chapter 2 had a relatively small number of human subjects. In addition, the participants were primarily young male, corresponding to the same boundary condition as Fanger's comfort studies with young subjects. Thus when the model is applied to a

different group and size of human subjects, it could possibly lead to numerical errors in the developed model parameters. Experiments with larger number of participants are needed. Even though this can be mitigated by allowing the offset parameter of the proposed model to be time varying and thus the model can be updated for any new applications by an EKF using new additional data whenever they are available. Overall, the developed data-driven state-space model of thermal sensation provides ample opportunities for improvements with additional data sets as all data-driven models do.

Similarly, the experiments conducted in Chapter 4 were short of participants. In order to test out MPC-DTS's ability to adjust its control input based on real time feedback given by occupants, disturbance was injected to thermal comfort by changing participants' clothing level. Since the experiments were conducted in the summer, only cooling application was tested. Although the data collected with the limited amount of participants clearly demonstrated that including occupants in control design could potentially reduce energy consumption without sacrificing comfort, a long term experiment with larger number of participants is desired in order to further compare the MPC-DTS with MPC-PMV and evaluate their energy consumptions.

Bibliography

[1] D. Al-Homoud, S. Mohammad, Performance characteristics and practical applications of common building thermal insulation materials, Building and Environment 40 (2005) 353-366.

[2] A.M. Papadopoulos, State of the art in thermal insulation materials and aims for future developments, Energy and Buildings 37 (2005) 77-86.

[3] B. Andersson, W. Place, R. Kammerud, M.P. Scofield, The impact of building orientation on residential heating and cooling, Energy and Buildings 8 (1985) 205-224.

[4] J. Figueiredo, J. Martins, Energy production system management–renewable energy power supply integration with building automation system, Energy Conversion and Management 51 (2010) 1120-1126.

[5] O.T. Masoso, L.J. Grobler, The dark side of occupants' behaviour on building energy use, Energy and Buildings 42 (2010) 173-177.

[6] J. Ouyang, K. Hokao, Energy-saving potential by improving occupants' behavior in urban residential sector in Hangzhou City, China, Energy and Buildings 41 (2009) 711-720.

[7] J.E. Braun, Reducing energy costs and peak electrical demand through optimal control of building thermal storage, ASHRAE transactions 96 (1990) 876-888.

[8] J.E. Braun, Load control using building thermal mass, Journal of Solar Energy Engineering, 125 (2003) 292-301.

[9] J. Singh, N. Singh, J.K. Sharma, Fuzzy modeling and control of HVAC systems-A review, Journal of Scientific and Industrial Research 65 (2006) 470-476.

[10] A.I. Dounis, D.E. Manolakis, Design of a fuzzy system for living space thermal-comfort regulation, Applied Energy 69 (2001) 119-144.

[11] J. Liang, R. Du, Thermal comfort control based on neural network for HVAC application, in: Proc. of IEEE Conference on Control Applications, Toronto, Canada, 2005.

[12] J.W. Moon, J.J. Kim, ANN-based thermal control models for residential buildings, Building and Environment 45 (2010) 1612-1625.

[13] K. Dalamagkidis, D. Kolokotsa, K. Kalaitzakis, G.S. Stavrakakis, Reinforcement learning for energy conservation and comfort in buildings, Building and environment 42 (2007) 2686-2698.

[14] B. Qiao, K. Liu, C. Guy, A multi-agent system for building control, in: Proc. of the IEEE/WIC/ACM international conference on Intelligent Agent Technology, Hong Kong, China 2006.

[15] A.I. Dounis, C. Caraiscos, Advanced control systems engineering for energy and comfort management in a building environment—A review, Renewable and Sustainable Energy Reviews 13 (2009) 1246-1261.

[16] S. Soyguder, M. Karakose, H. Alli, Design and simulation of self-tuning PID-type fuzzy adaptive control for an expert HVAC system, Expert Systems with Applications 36 (2009) 4566-4573.

[17] E.F. Camacho, C.B. Alba, Model predictive control, Springer, London, 2004.

[18] M. Kummert, P. Andr é, J. Nicolas, Optimal heating control in a passive solar commercial building, Solar Energy, 69 (2001) 103-116.

[19] R.Z. Freire, G.H. Oliveira, N. Mendes, Predictive controllers for thermal comfort optimization and energy savings, Energy and buildings, 40 (2008) 1353-1365.

[20] M. Kummert, P. André, Simulation of a model-based optimal controller for heating systems under realistic hypothesis, in: Proceedings of the 9th International Building Performance Simulation Association Conference, Montreal, Canada, 2005.

[21] G.P Henze, D.E. Kalz, S. Liu, C. Felsmann, Experimental analysis of model-based predictive optimal control for active and passive building thermal storage inventory, HVAC&R Research, 11 (2005) 189-213.

[22] Y. Ma, A. Kelman, A. Daly, F. Borrelli, Predictive control for energy efficient buildings with thermal storage: Modeling, stimulation, and experiments, IEEE control systems magazine, 32 (2012) 44-64.

[23] M. Gwerder, J. Tödtli, Predictive control for integrated room automation, in: 8th REHVA World Congress Clima, Lausanne, Switzerland, 2005.

[24] J. Ma, S. Member, F. Yang, Z. Li, S. J. Qin, A Renewable Energy Integration Application in a MicroGrid Based on Model Predictive Control, Power Energy Soc. Gen. Meet. IEEE, (2012) 1-6.

[25] J. A. Momoh, F. Zhang, and W. Gao, Optimizing Renewable Energy Control for Building using Model Predictive Control, In North American Power Symposium (NAPS) , IEEE (2014) 1-6.

[26] S. Prívara, J. Široký, L. Ferkl, J. Cigler, Model predictive control of a building heating system: The first experience, Energy and Buildings, 43 (2011) 564-572.

[27] A. Aswani, N. Master, J. Taneja, D. Culler, C. Tomlin, Reducing transient and steady state electricity consumption in hvac using learning-based model-predictive control, Proceedings of the IEEE, 100 (2010) 240-253.

[28] Y. Ma, F. Borrelli, B. Hencey, B. Coffey, S. Bengea, P. Haves, Model predictive control for the operation of building cooling systems, IEEE Transactions on Control Systems Technology, 20 (2012) 796-803.

[29] P.M. Ferreira, S.M. Silva, A.E. Ruano, Energy savings in HVAC systems using discrete model-based predictive control, in: Proc. of The 2012 International Joint Conference on Neural Networks, Brisbane, Australia, 2012.

[30] P.O. Fanger, Thermal Comfort, McGraw-Hill Inc., New York, 1970.

[31] M. Castilla, J.D. Álvarez, M. Berenguel, F. Rodríguez, J.L. Guzmán, M. Pérez, A comparison of thermal comfort predictive control strategies, Energy and Buildings, 43 (2011) 2737-2746.

[32] F. Oldewurtel, C.N. Jones, M. Morari, A tractable approximation of chance constrained stochastic MPC based on affine disturbance feedback, in: Proc. of 47th IEEE Conference on Decision and Control, Cancun, Mexico, 2008.

[33] Y. Ma, B. Francesco, Fast stochastic predictive control for building temperature regulation, in: Proc. of American Control Conference, Montreal, Canada, 2012.

[34] R.J. De Dear, K.G. Leow, S.C. Foo, Thermal comfort in the humid tropics: field experiments in air-conditioned and naturally ventilated buildings in Singapore, International Journal of Biometeorology, 34 (1991) 259-265.

[35] J. Busch, A tale of two populations: thermal comfort in air-conditioned and naturally ventilated offices in Thailand, Energy and Buildings 18 (1992) 235-249.

[36] G. Schiller, A comparison of measured and predicted comfort in office buildings, ASHRAE Transactions, 96 (1990) 609-622.

[37] N. Wong, S. Khoo, Thermal comfort in classrooms in the tropics, Energy and Buildings 35 (2003) 337-351.

[38] G. Brager, R.J. De Dear, Thermal adaptation in the built environment: a literature review, Energy and Buildings, 27 (1998) 83-96.

[39] J. Van Hoof, Forty years of Fanger's model of thermal comfort: comfort for all?, Indoor Air 18 (2008) 182-201.

[40] R.J. De Dear, G. Brager, Developing an adaptive model of thermal comfort and preference, ASHRAE Transactions 104 (1998) 145-167.

[41] P.O. Fanger, J. Toftum, Extension of the PMV model to non-air-conditioned buildings in warm climates, Energy and Buildings 34 (2002) 533-536.

[42] D. Fiala, K, Lomas, M. Stohrer, First principles modeling of thermal sensation responses in steady-state and transient conditions, ASHRAE Transactions, 109 (2003) 179-186.

[43] R.J. De Dear, P.O. Fanger, Thermal sensations resulting from sudden ambient temperature changes, Indoor Air 3 (1993) 181-192.

[44] H. Zhang, E. Arens, C. Huizenga, Thermal sensation and comfort models for non-uniform and transient environments: Part I: Local sensation of individual body parts, Building and Environment 45 (2010) 380-388.

[45] F. Oldewurtel, A. Parisio, C.N. Jones, D. Gyalistras, M. Gwerder, V. Stauch, M. Morari, Use of model predictive control and weather forecasts for energy efficient building climate control, Energy and Buildings, 45 (2012) 15-27.

[46] P.M. Ferrira, A.E. Ruano, S. Silva, E.Z.E. Conceicao, Neural networks based predictive control for thermal comfort and energy savings in public buildings, Energy and Buildings 55 (2012) 238-251.

[47] S. Atthajariyakul, T. Leephakpreeda, Neural computing thermal comfort index for HVAC systems, Energy Conversion and Management 46 (2005) 2553-2565.

[48] C.C. Federspiel, H. Asada, User-adaptable comfort control for HVAC systems, Journal of dynamic systems, measurement, and control 116 (1994) 474-486.

[49] A. Foucquier, S. Robert, F. Suard, L. Stéphan, A. Jay, State of the art in building modelling and energy performances prediction: A review, Renewable and Sustainable Energy Reviews 23 (2013) 272-288.

[50] G. Fraisse, C. Viardot, O. Lafabrie, G. Achard, Development of a simplified and accurate building model based on electrical analogy, Energy and buildings 34 (2002) 1017-1031.

[51] B. Bueno, L. Norford, G. Pigeon, R. Britter, A resistance-capacitance network model for the analysis of the interactions between the energy performance of buildings and the urban climate, Building and Environment 54 (2012) 116-125.

[52] S. Liu, G.P. Henze, Impact of Modeling Accuracy on Predictive Optimal Control of Active and Passive Building Thermal Storage Inventory, ASHRAE transactions, 110 (2004) 151.

[53] C. Liao, P. Barooah, An integrated approach to occupancy modeling and estimation in commercial buildings, in: Proc. of American Control Conference, Baltimore, Maryland, 2010.

[54] T.H. Chen, T.Y. Chen, Z.X. Chen, An intelligent people-flow counting method for passing through a gate, in: Proc. of IEEE Conference on Robotics, Automation and Mechatronics, Bangkok, Thailand, 2006.

[55] S. Meyn, A. Surana, Y. Lin, S.M. Oggianu, S. Narayanan, T.A. Frewen, A sensor-utility-network method for estimation of occupancy in buildings, in: Proc. of 48th IEEE Conference on Decision and Control, Shanghai, China, 2009.

[56] F. Oldewurtel, A. Parisio, C.N. Jones, M. Morari, D. Gyalistras, M. Gwerder, K. Wirth, Energy efficient building climate control using stochastic model predictive control and weather predictions, in: Proc. of American Control Conference, Baltimore, Maryland, 2010.

[57] M. Maasoumy, A. Sangiovanni-Vincentelli, Optimal control of building hvac systems in the presence of imperfect predictions, in: Proc. of Dynamic Systems and Control Conference, Fort Lauderdale, Florida, 2012.

[58] A. Prékopa, Stochastic programming, Springer, 1995.

[59] M. Paciuk, The role of personal control of the environment in thermal comfort and satisfaction at the workplace, Ph.D. thesis, University of Wisconsin-Milwaukee, 1989.

[60] J. Toftum, Central automatic control or distributed occupant control for better indoor environment quality in the future, Building and environment 45 (2010) 23-28.

[61] A. Leaman, B. Bordass, Productivity in buildings: the 'killer' variables, Building Research & Information 27 (1999) 4-20.

[62] S. Barlow, D. Fiala, Occupant comfort in UK offices—How adaptive comfort theories might influence future low energy office refurbishment strategies, Energy and Buildings 39 (2007) 837-846.

[63] T. Moore, D.J. Carter, A.I. Slater, Long-term patterns of use of occupant controlled office lighting, Lighting Research and Technology, 35 (2003) 43-57.

[64] J.A. Jakubiec, C.F. Reinhart, The 'adaptive zone'–A concept for assessing discomfort glare throughout daylit spaces, Lighting Research and Technology, 44 (2012) 149-170.

[65] C.S. Park, G. Augenbroe, N. Sadegh, M. Thitisawat, T. Messadi, Occupant responsive optimal control of smart façade systems, in: Proc. of 8th International Building Performance Simulation Association Conference, Eindhoven, Netherlands, 2003.

[66] A. Guillemin, Using genetic algorithms to take into account user wishes in an advanced building control system, Ph.D. thesis, Ecole Polytechnique Fédérale de Lausanne, 2003.

[67] Y. Bar-Shalom, X. Li, T. Kirubarajan, Estimation with Applications to Tracking and Navigation, John Wiley & Sons, New York, 2001.

[68] ASHRAE, ASHRAE standard, standard 55-2013, in: Thermal Environmental Conditions for Human Occupancy, 2013.

[69] M. Humphreys, Outdoor temperatures and comfort indoors, Building Research and Practice, 6 (1978) 92-92.

[70] J.D. Bynum, D.E. Claridge, J.M. Curtin, Development and testing of an Automated Building Commissioning Analysis Tool (ABCAT), Energy Build. 55(2012) 607-617.

[71] S. Goyal, P. Barooah, A method for model-reduction of non-linear thermal dynamics of multi-zone buildings, Energy Build. 47 (2012) 332-340.

[72] X. Chen, Q. Wang, J. Srebric, A data-driven state-space model of indoor thermal sensation using occupant feedback for low-energy buildings, Energy Build. 91 (2015) 187-198.

[73] A. Prékopa, Stochastic Programming, Springer, 1995.

[74] DOE, US, Energyplus engineering reference, The Reference to EnergyPlus Calculations, 2014.

[75] X. Chen, Q. Wang, J. Srebric, Model Predictive Control for Indoor Thermal Comfort and Energy Optimization Using Occupant Feedback, Energy and Buildings, 102 (2015) 357–369.

Appendix A

Fiala's Dynamic Thermal Sensation Model

Fiala's model for predicting dynamic thermal sensation for sedentary subjects, in terms of the 7-point ASHRAE scale from -3 to +3, is given as follows:

$$DTS = 3 \cdot \tanh[0.3 \cdot \Delta T_{sk,m}^{(-)} + 1.08 \cdot \Delta T_{sk,m}^{(+)} + 0.11 \cdot \frac{dT_{sk,m}^{(-)}}{dt} + 1.91 \cdot \exp(\frac{-0.681 \cdot t}{3600}) \cdot \frac{dT_{sk,m}^{(+)}}{dt_{\max}}] \quad \text{(A.1)}$$

where $\Delta T_{sk,m}^{(-)}$ and $\Delta T_{sk,m}^{(+)}$ denote the negative and positive deviation of the mean skin temperature from its reference temperature corresponding to neutral thermal sensation; $dT_{sk,m}^{(-)}/dt$ and $dT_{sk,m}^{(+)}/dt$ denote the negative and positive time derivative of the mean skin temperature, respectively. The dynamic component of this model for skin cooling, represented by $0.11 \cdot dT_{sk,m}^{(-)}/dt$, is modeled differently from skin warming, which is described by the maximum positive rate of change of skin temperature, $dT_{sk,m}^{(+)}/dt_{\max}$, multiplying an exponentially decaying coefficient $\exp(-0.681 \cdot t/3600)$, where *t* denotes the time elapsed since the occurrence of $dT_{sk,m}^{(+)}/dt_{\max}$.

Appendix B

An Extended Kalman Filter for Estimating Thermal Sensation State and Time-varying Offset Parameter Simultaneously

Consider the Wiener-logistic dynamic thermal sensation model (2.3-2.4),

$$x(k+1) = f_1 x(k) + f_2 x(k-1) + g_1 T_a(k) + g_2 T_a(k-1) + e(k) \tag{B.1}$$

$$y(k) = \frac{a}{\exp\left[-c - b\cdot(x(k)-r)\right]+1} + d + v(k) \tag{B.2}$$

where the model coefficients $f_1, f_2, g_1, g_2, a, b, c, r$ are constant and defined accordingly. We assume that the offset parameter d is slowly time-varying and modeled as a (discrete time) wiener process as follows:

$$d(k+1) = d(k) + e_d(k) \tag{B.3}$$

where the parameter process noise e_d is assumed to have zero mean and nonzero variance Q_d.

Define an augmented state variable $x_A(k)$ consisting of the original state variable $x(k)$, $x(k-1)$, and the time-varying parameter $d(k)$,

$$x_A = \begin{bmatrix} x_{A_1} \\ x_{A_2} \end{bmatrix},\ x_{A_1} = \begin{bmatrix} x_{A_1}^1 \\ x_{A_1}^2 \end{bmatrix} \triangleq \begin{bmatrix} x(k) \\ x(k-1) \end{bmatrix},\ x_{A_2}(k) \triangleq d(k) \tag{B.4}$$

Then the original thermal sensation model (B.1 and B.2) together with the parameter model (B.3) can be rewritten as follows,

$$\begin{aligned} x_A(k+1) &= F x_A(k) + G \circ T_a(k) + \varepsilon(k) \\ y(k) &= h(x_A(k)) + v(k) \end{aligned} \tag{B.5}$$

where,

$$G \circ T_a(k) = \begin{bmatrix} g_1 T_a(k) + g_2 T_a(k-1) & 0 & 0 \end{bmatrix}^T,$$

$$\varepsilon(k) = \begin{bmatrix} e(k) & 0 & e_d(k) \end{bmatrix}^T,$$

$$F = \begin{bmatrix} f_1 & f_2 & 0 \\ 1 & 0 & 0 \\ 0 & 0 & 1 \end{bmatrix} \tag{B.6}$$

and the output nonlinear function satisfies,

$$h(x_A(k)) = \frac{a}{\exp(-c - b(x_{A_1}^1(k) - r)) + 1} + x_{A_2}(k).$$

The process noise $\varepsilon(k)$ and sensor noise $v(k)$ are assumed to be white noise and satisfy the following,

$$\begin{aligned} &E[\varepsilon(k)] = 0, E[\varepsilon(k)\varepsilon^T(k')] = Q(k)\delta_{kk'} \\ &E[v(k)] = 0, E[v(k)v^T(k')] = R(k)\delta_{kk'} \end{aligned} \tag{B.7}$$

It is assumed that the initial estimate $\hat{x}_A(0|0)$ is uncorrelated with the process noise and sensor noise sequences. Assume that one has the estimate $\hat{x}_A(\mathrm{k}|\mathrm{k}) = \mathrm{E}[x_A(k)|Z^k]$ at time *k*, with the associate covariance matrix $P(k|k)$, where Z^k denotes the statistics obtained at time *k*.

The predicted state at time *k*+1 based on time *k* is obtained as follows,

$$\hat{x}_A(k+1|k) = F\hat{x}_A(k|k) + G \circ T_a(k) \tag{B.8}$$

The state prediction covariance is updated as

$$P(k+1|k) = FP(k|k)F^T + Q(k) \tag{B.9}$$

The predicted measurement for the 2nd-order Kalman filter is given by,

$$\hat{\mathrm{y}}(\mathrm{k+1}|\mathrm{k}) = h(\hat{x}_A(\mathrm{k+1}|\mathrm{k})) + \frac{1}{2}tr\left[h_{x_A x_A}(\mathrm{k+1})P(\mathrm{k+1}|\mathrm{k})\right] \tag{B.10}$$

and the measurement prediction covariance matrix is updated as

$$S(\mathrm{k+1}) = h_{x_A}(\mathrm{k+1})\,\mathrm{P(k+1)}h_{x_A}^T(\mathrm{k+1}) + \frac{1}{2}tr\left[h_{x_A x_A}(\mathrm{k+1})P(\mathrm{k+1}|\mathrm{k})h_{x_A x_A}(\mathrm{k+1})P(\mathrm{k+1}|\mathrm{k})\right] + R(\mathrm{k+1}) \tag{B.11}$$

where h_{x_A} and $h_{x_A x_A}$ denote the Jacobian and Hessian of the nonlinear function *h*, respectively,

$$h_{x_A}(\mathrm{k+1}) = [\nabla_{x_A} h(x_A)]^T \,|_{x_A=\hat{x}_A(\mathrm{k+1|k})},$$
$$h_{x_A x_A}(\mathrm{k+1}) = [\nabla_{x_A} \nabla^T_{x_A} h\ (x_A)]\,|_{x_A=\hat{x}_A(\mathrm{k+1|k})} \tag{B.12}$$

Appendix C

Introduction to Model Predictive Control

Model Predictive Control (MPC) is an advanced control method that has been used as process control in chemical plants and refineries. MPC is implemented as a discrete time controller. One great advantage of MPC is that it provides a systematic approach to control multivariable dynamic system and deals with the constraints explicitly in its problem formulation.

At each time step, based on measurements of current states, MPC uses the dynamic model of the system to predict the evolution of the states and outputs into the future. MPC then solves an optimization problem which is formulated based on the prediction. The solution of the optimization problem is a serial of control inputs along the prediction horizon. Only the first control input in this serial is implemented. In the next time step, the whole process is repeated.

The following example shown in Figure C.1 demonstrates the principles of MPC. In this example, the dynamic system described in (C.1-C.2) is controlled to track the reference input r.

$$x(t+1) = f(x(t), u(t)) \tag{C.1}$$

$$y(t) = g(x(t), u(t)) \tag{C.2}$$

Where x denotes the state vector of dynamic system, u denotes control input, and y denotes the output. At time *t*, the state of the system is sampled and MPC solves the following optimization problem.

Cost:

$$\min_{u(t),\ldots,u(t+N-1)} J_t := \sum_{k=1}^{N} [y(t+k \mid t) - r(t)]^2 \tag{C.3}$$

Subject to:

$$x(t+k+1 \mid t) = f(x(t+k \mid t), u(t+k \mid t)) \tag{C.4}$$

$$y(t+k\,|\,t) = g(x(t+k\,|\,t), u(t+k\,|\,t)) \tag{C.5}$$

$$y_{\min} \le y(t+k\,|\,t) \le y_{\max} \tag{C.6}$$

$$y_{\min} \le u(t+k\,|\,t) \le y_{\max} \tag{C.7}$$

An online computation is used to explore trajectories of state evolution and the optimal sequence of control inputs along the prediction horizon of size N is calculated as $U^*(t) = [u(t), u(t+1), .., u(t+N-1)]$ in order to minimize the error between the output and the reference input r. Only the first element in vector $U^*(t)$ is implemented. Then the system states at next instance are sampled again the calculation of optimization problem is repeated. The prediction horizon keeps being shifted forward.

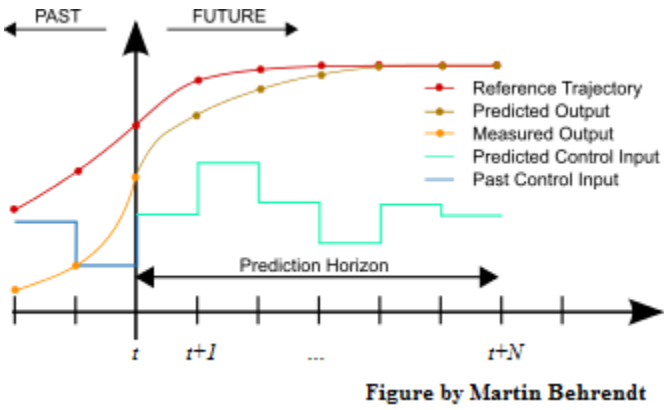

Figure C.1. Example of MPC. This figure is taken from following website: https://commons.wikimedia.org/wiki/File%3AMPC_scheme_basic.svg

Appendix D

Thermal Parameters, Input and Output in Individual Chamber Experiment

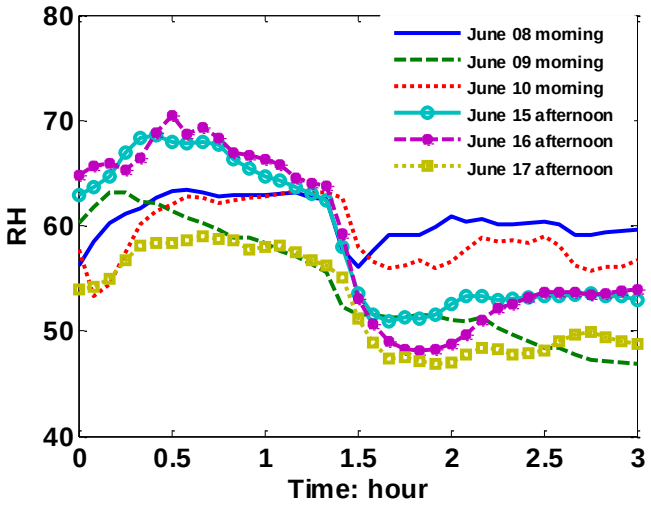

(a)

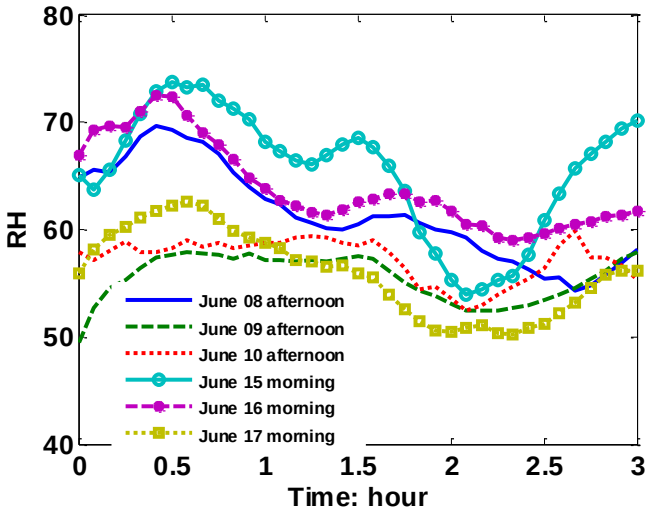

(b)

Figure D.1. Indoor relative humidity (%) histories of individual experiments. (a) Individual RH used in MPC-PMV. (b) Individual RH used in MPC-DTS.

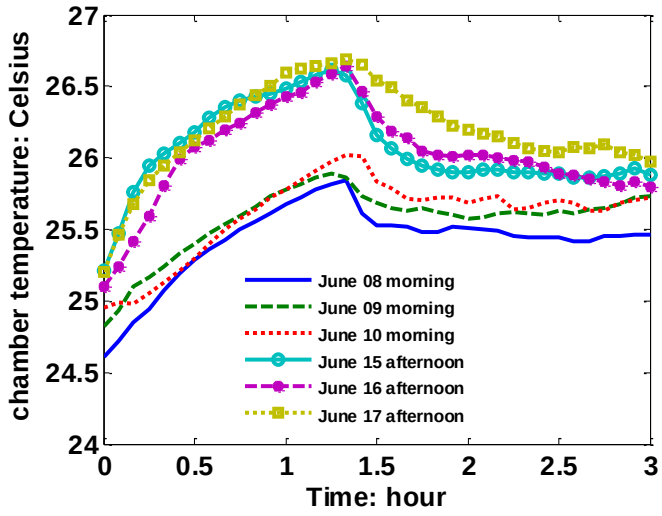

(a)

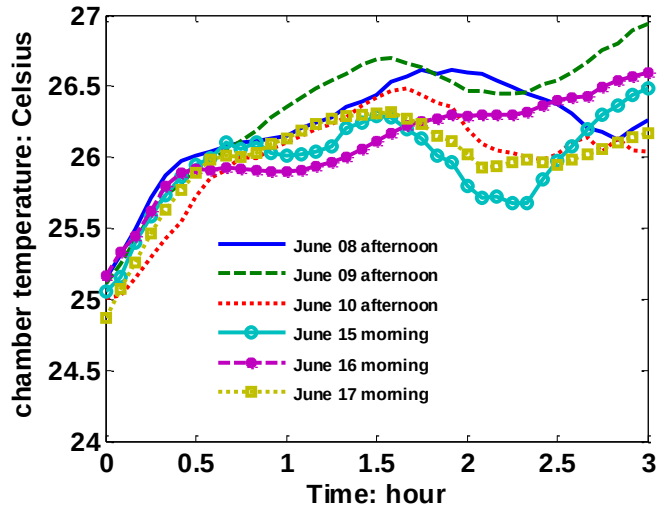

(b)

Figure D.2. Chamber temperature histories of individual experiments. (a) Chamber temperature in MPC-PMV. (b) Chamber temperature in MPC-DTS.

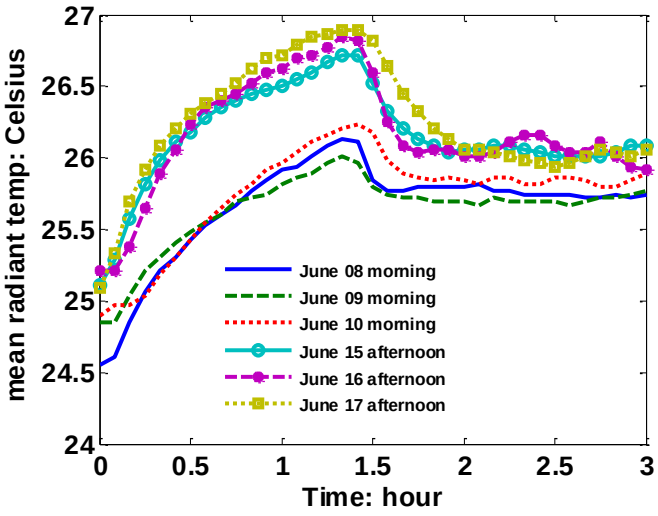

(a)

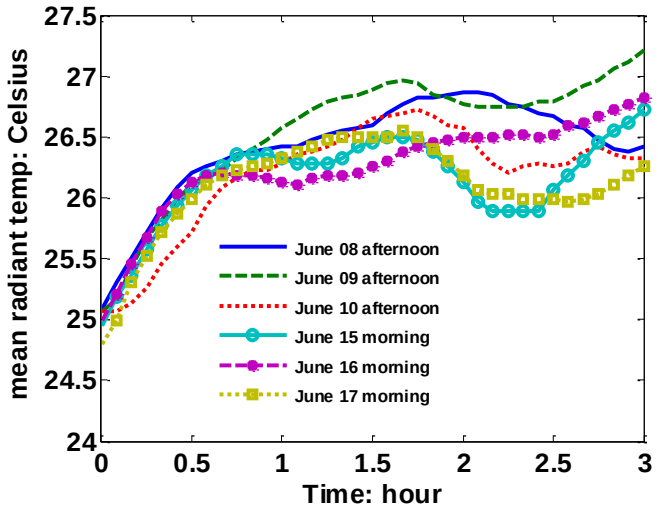

(b)

Figure D.3. Chamber mean radiant temperature histories in individual experiments. (a). MRT in MPC-PMV. (b). MRT in MPC-DTS.

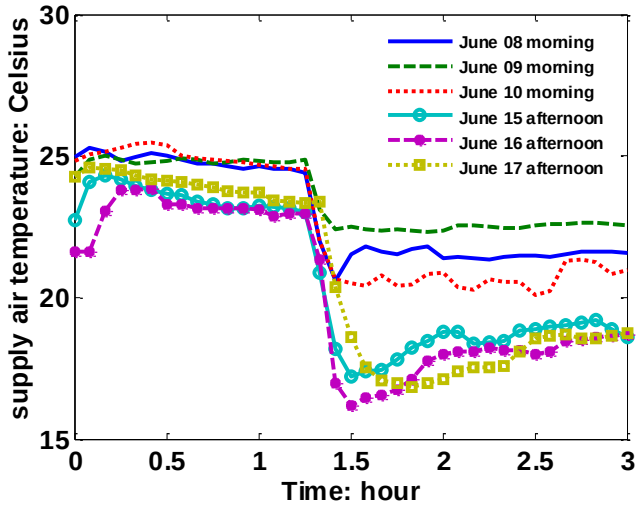

(a)

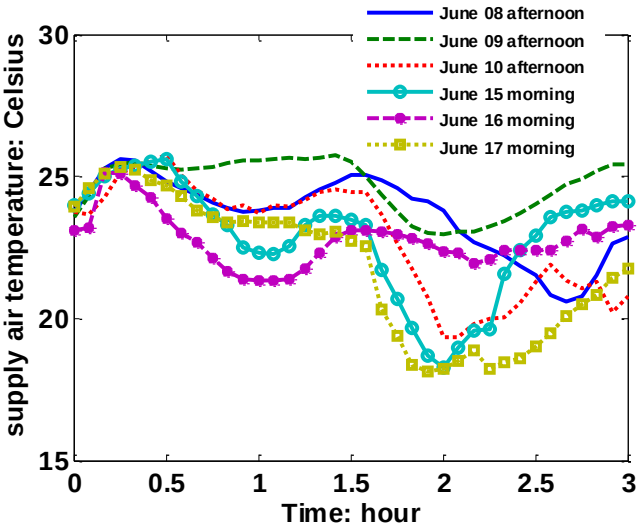

(b)

Figure D.4. Supply air temperature of individual experiments. (a). Supply air temperature under MPC-PMV. (b) Supply air temperature under MPC-DTS.

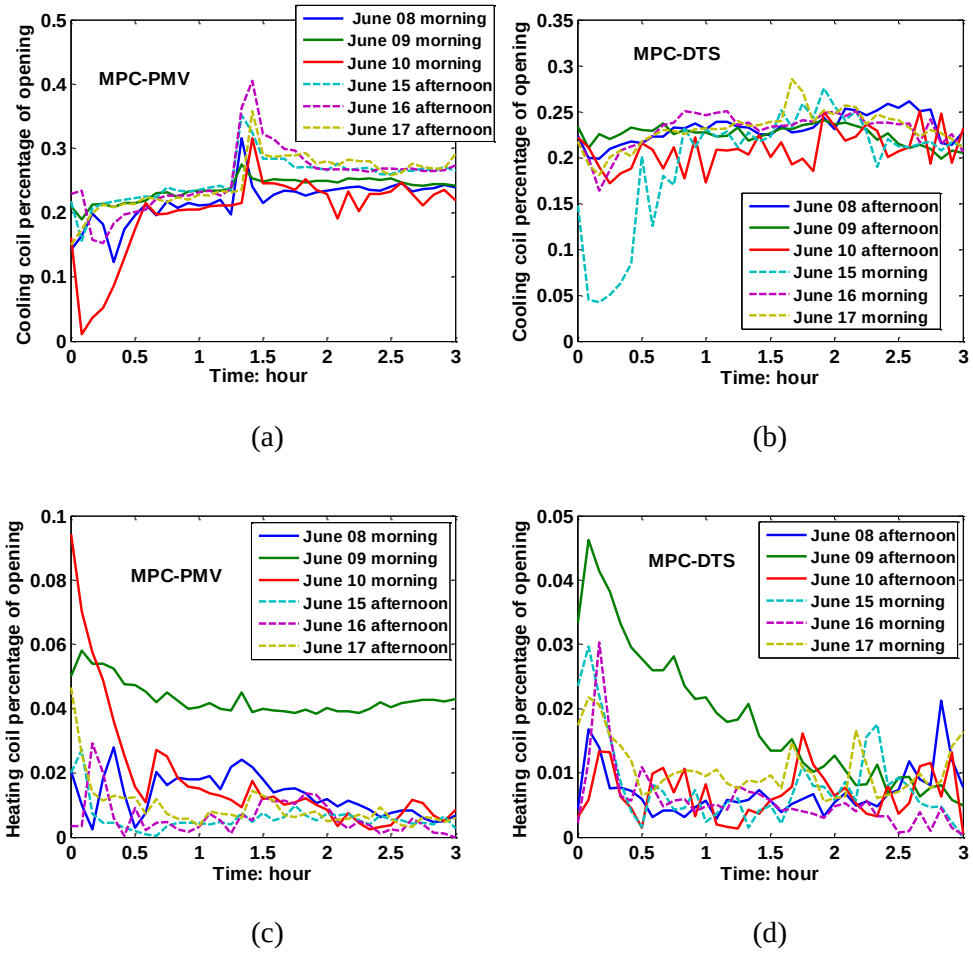

Figure D.5. Heating/Cooling coil percentage of opening. (a) Cooling under MPC-PMV. (b) Cooling under MPC-DTS. (c) Heating under MPC-PMV. (d) Heating under MPC-DTS.

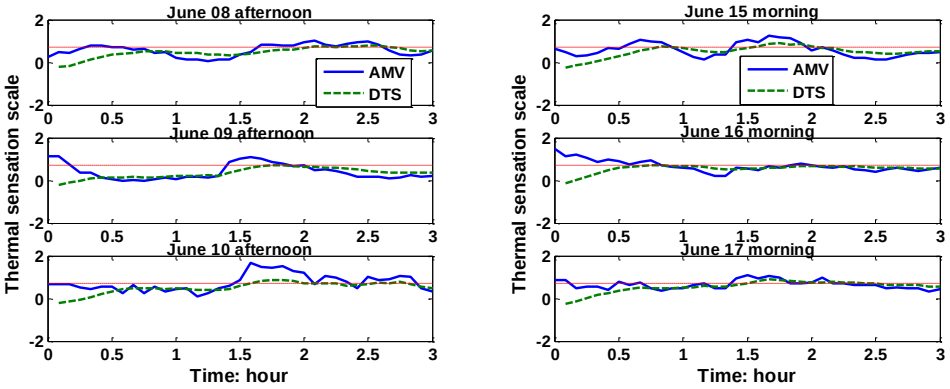

Figure D.6. AMV vs. DTS prediction under the MPC-DTS.

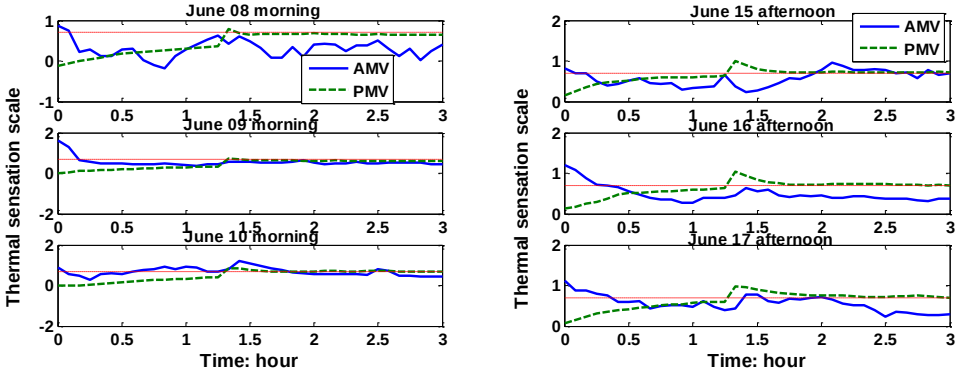

Figure D.7. AMV vs. PMV under the MPC-PMV.

VITA

Xiao Chen

Xiao Chen received his B.Sc. degree in Mechanical Engineering in 2007 from Zhejiang University, China and his M.Sc. degree in Mechanical Engineering in 2010 from Stony Brook University, New York. In 2011, he was enrolled in the graduate program in Mechanical Engineering at the Pennsylvania State University and began to pursue his PhD degree. His research interests include dynamic system modeling, system identification and model predictive control.